



Wind-induced vibration of structural cables

M. Jafari · F. Hou · A. Abdelkefi 

Received: 16 April 2019 / Accepted: 14 February 2020 / Published online: 17 March 2020
© Springer Nature B.V. 2020

Abstract The wind-induced vibration of cables has been widely studied over the past decades because of cables' many applications in cable-stayed, suspension, and tied-arched bridges, and power transmission lines. They have been mostly investigated through research conducted on rigid model cables with a finite length and circular cross-sectional geometry that represents a section model of a long cable. These models have been considered accurate because the behavior of flow over a cable and circular cylinder is similar, although there are structural differences between them. Cables usually experience small- to large-amplitude vibration due to wind loads that causes fatigue failure and poses a significant threat to the safety and serviceability of these structures. Although this paper mainly focuses on reviewing the past studies about different types of wind-induced cable vibration, some general information related to circular cylinders has been briefly reported for better understanding of the flow over cables. This paper incorporates an extensive review based on the existing papers about different sources of wind-induced cable vibration consisting of vortex-induced vibration, rain-wind-induced vibration,

dry galloping, ice galloping, and wake galloping. Furthermore, this paper explains the mechanism, vibration source, and a mitigation solution for each type based on the past studies using wind tunnel experiments, computational fluid dynamics, field measurements, or analytical approaches. This review helps to better understand the aerodynamics and fluid–structure interactions of cables with or without ice/rain on the surface, while static and dynamic wind loads act on the structure.

Keywords Vortex-induced vibration (VIV) · Rain-wind-induced vibration (RWIV) · Ice galloping (IG) · Dry galloping (DG) · Wake galloping (WG)

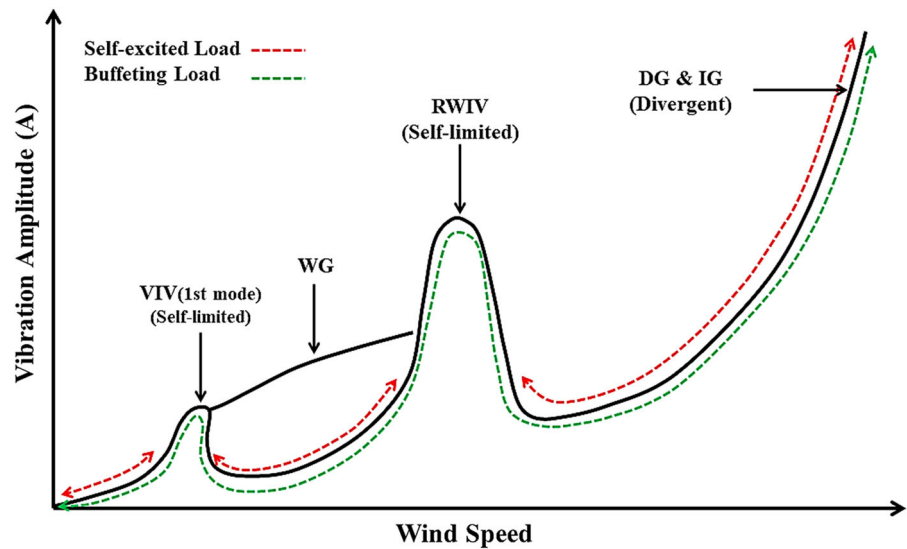
1 Introduction

Over the past decades, horizontally or vertically spanned cables have been studied using different methods, such as wind tunnel experiments, field measurements, numerical simulations, and analytical approaches. Such extensive research has been conducted on cables because of their various engineering applications including cable-stayed and suspension bridges, power transmission lines, and suspension roofs. Long cables that have smooth or grooved surfaces are prone to large-amplitude wind-induced vibration due to their low inherent structural damping. Wind-induced vibration can cause catastrophic failure for not only cables, but for the structures supported by them as well. These mechanisms involve complex aeroelastic inter-

M. Jafari · F. Hou
Aerospace Engineering Department, Iowa State University,
Ames, IA 50011, USA

A. Abdelkefi (✉)
Department of Mechanical and Aerospace Engineering,
New Mexico State University, Las Cruces, NM 88003,
USA
e-mail: abdu@nmsu.edu

Fig. 1 Wind-induced cable response due to wind loads



actions that depend on the spatial orientation, geometry, surface-characteristics, and dynamic/structural properties of cables. In general, static and dynamic wind loads that act on cables or other structures are classified into three types: vortex shedding, buffeting, and self-excited loads. Furthermore, other factors such as arrangement, rain fall, and ice accretion on the cable surface change the aerodynamic and aeroelastic loads. As a result, various aeroelastic phenomena arise including vortex-induced vibration (VIV), rain-wind-induced vibration (RWIV), dry galloping (DG), ice galloping (IG), and wake galloping (WG). The past literature has been reviewed in this paper in order to determine the mechanisms and effective parameters, and to obtain results of these vibration sources for smooth cables and power transmission lines. Apart from all other significant factors, variation in aerodynamic damping is the common source between all vibration types that makes cables vulnerable to wind loads. Figure 1 schematically shows the cable response for different vibration sources and wind loads versus wind speed changes. As shown in Fig. 1, VIV and RWIV have limited-amplitude vibration, while DG and IG can cause divergent motion. However, all vibration sources need to be considered in the design procedure of cable-supported structures to prevent any type of motion-induced vibration.

Different vibration sources that may happen for cables are briefly explained as follows:

Vortex-induced vibration (VIV) This type of vibration is caused by the vortices that alternatively separate

from each side of a cylinder. The Strouhal number determines the frequency of vortex shedding, and it indicates that there is a range of wind speed in which the vortex shedding frequency is near the natural frequency of structures; a large-amplitude vibration could occur. VIV is supposed to take place at the reduced velocity that is the reciprocal of the Strouhal number. However, field measurements showed that VIV of cables on cable-stayed bridges occurs at higher reduced velocities than the reciprocal of the Strouhal number. In addition, the amplitude of VIV at higher reduced velocity is usually larger than that of the conventional Karman vortex-induced vibration. According to the definition of Strouhal number, the cables on cable-stayed bridges could experience different modes of VIV simultaneously, since the wind speed varies along the height of the model. This phenomenon has been verified both from wind tunnel test and field measurement.

Rain-wind-induced vibration (RWIV) This type of vibration usually happens on windy and rainy days, which is why it is called rain-wind-induced vibration. RWIV is characterized by a large amplitude and low frequency in addition to a restricted velocity. It poses a significant threat to cable-stayed bridges and has been observed on many bridges across the world. Although the underlying mechanism of RWIV has not yet been discovered, there is a consensus among research communities that the upper rivulet formed on a cable's surface on windy and rainy days plays an important role in the occurrence of RWIV. As a result, the majority

of experimental studies on RWIV have been focused on the upper rivulet on cables, either using artificial rivulets or a spraying water system. Numerical models of RWIV usually adopt a two-degree-of-freedom (DOF) or a three-DOF model, depending on whether the motion of the cable in the horizontal direction is considered or not. Quasi-steady theory is usually employed to express the aerodynamic loads, of which the aerodynamic properties such as lift and drag coefficient are identified from experiments.

Dry galloping (DG) This instability is the most challenging vibration source because it normally happens at high wind speed and special conditions that makes it more difficult to capture with the wind tunnel test or numerical simulations. During the past years, two different mechanisms have been found to explain the dry-cable galloping. The first explanation is the unsteady galloping, which can be studied using dynamic loads and occurs when there is an axial flow behind the yaw and/or inclined cable mitigating the Karman vortex shedding [1]. As a result, the cable shows the unsteady response with non-stationary amplitude. The second explanation is conventional galloping or divergent-type galloping and can be explained by quasi-steady theory. Classical galloping is another name for this type since it is described by classical quasi-steady theory. The aerodynamic static forces are calculated, and aerodynamic damping is calculated to capture this type of galloping based on developed 3DOF quasisteady equations.

Ice galloping (IG) This type of galloping occurs when there is an ice accretion on the cable surface (windward) that creates the aerodynamic instability due to the asymmetric cross-sectional geometry. The shape of accumulated ice, which is dependent on weather condition, temperature, and wind speed, is either crescent or triangular shaped. Ice galloping that is a low-frequency vibration can cause large-amplitude vibration and has been widely reported for power transmission lines, but it can happen for smooth cables with ice accretion as well. This phenomenon has been mostly studied with an analytical approach to determine the instability conditions of ice-induced galloping. There are difficulties when simulating ice for dynamic testing in an icing wind tunnel. Therefore, ice galloping has been investigated by conducting dynamic tests with artificial ice or performing static tests in an icing wind tunnel.

Wake galloping (WG) This phenomenon for cables has been seen less than other types because it occurs when the cables are very close to each other, as in bundled power transmission lines. When two cables are placed parallel and close to each other, vortex shedding generated by the upstream cable can induce the second one due to the interaction between them. Wake galloping can be seen for cables with different arrangements, such as tandem (more common), staggered, and side by side. The critical range of space ratios $L^* = L/D$, where L is the distance between the center of two parallel cables and D is the cable diameter, for tandem smooth cables and conductors is typically 4–6 [2], and 10–20 [3], respectively. Although wake galloping and wake-induced vibration of circular cylinders have been widely observed, they have been investigated for cables specially conductor types in only a few studies due to its low occurrence chance for structural cables.

Some of the past reported cases that observed the cable vibration for bridges due to wind loads are summarized in Table 1. It should be noted that no specific damage has been reported for dry-cable galloping of bridges, based on the existing literature. In this paper, the wind-induced vibration of cables with smooth or grooved surfaces (power transmission line or conductor) has been reviewed. The focus of the review is cables, although necessary information related to circular cylinders is mentioned due to the similarity of the flow behavior around both structures. The paper presents existing knowledge from basic explanations to advanced achievements on cable vibration. The past studies use different approaches, which then help other scholars design mitigation devices with the purpose of suppressing cable vibration.

2 Properties of yawed/inclined cable or circular cylinder

Velocity of incoming flow can be divided into a mean velocity (U) in direction of X , and three fluctuating components of u' , v' , and w' associated with directions of X , Y , and Z , respectively. For a circular cylinder, yaw and inclination angles can be defined based on the direction of incoming flow, as shown in Fig. 2. The past studies [1, 25] have indicated that the aerodynamic behavior of a non-inclined ($\alpha = 0^\circ$) cable (circular cylinder) is equivalent to an inclined cable, based on the definition of equivalent yaw angle (β^*). There-

Table 1 Observed different types of wind-induced cable vibration for bridges

Bridge	Country	Year	References
<i>VIV</i>			
Evripos	Greece	–	Virlogeux [4]
Fred Hartman	Texas, USA	–	Zuo et al. [5]
Gjemnessund Bridge	Norway	–	Hjorth-Hansen and Strømmen [6]
Ikuchi Bridge	Japan	1991	Fujino et al. [7]
Kurushima Bridge	Japan	1999	Fujino et al. [7]
Akinada Bridge	Japan	2000	Fujino et al. [7]
Haneda Sky Arch	Japan	1993	Fujino et al. [7]
<i>RWIV</i>			
Kohlbrand	Germany	1974	Ruscheweyh and Hirsch [8]
Brotonne	France	1977	Wianecki [9]
Meiko-Nishi	Japan	1984	Hikami [10], Hikami and Shiraishi [11]
Farø	Denmark	1985	Langsø and Larsen [12]
Tempozan	Japan	1986	Miyasaka et al. [13], Oshima and Nanjo [14]
Aratsu	Japan	1988	Yoshimura et al. [15]
Ben Ahin	Belgium	1988	Lilien et al. [16], Cremer et al. [17]
Burlington	Vermont, USA	1990s	Virlogeux [4]
Glebe Island	Australia	1990s	Virlogeux [4]
Nanpu	China	1992	Fujino et al. [7]
Yangpu	China	1995	Gu [18]
Erasmus	Holland	1996	Geurts et al. [19]
Øresund	Denmark/Sweden	2001	Larsen and Lafreniere [20]
Cochrane	Alabama, USA	2002–2004	Irwin [21], Irwin et al. [22]
<i>IG</i>			
Øresund	Denmark/Sweden	2004	Larsen and Lafreniere [20]
<i>WG</i>			
Yobuko	Japan	1989	Narita and Yokoyama [23], Yoshimura et al. [15]
Akashi	Japan	1998	Toriumi et al. [24]
Ikara Bridge	Japan	1996	Fujino et al. [7]
Chichibu Park Bridge	Japan	1994	Fujino et al. [7]

fore, aerodynamic properties of inclined cables can be approximately calculated from the zero-inclination yawed case. The definitions of inclination angle (α), actual yaw angle (β), and equivalent yaw angle (β^*) are shown in Fig. 2b and (c). Equation (1) relates actual yaw angle and inclination angle to the equivalent yaw angle.

$$\beta^* = \sin^{-1}(\sin \beta \cos \alpha) \quad (1)$$

Some of the most important non-dimensional numbers that will be discussed later are mentioned in Table 2. These parameters describe the behavior of fluid flow over a structure in static conditions and the motion

of a bluff body in dynamic conditions. The length of a cable is usually considered enough to neglect the edge effect when the aspect ratio (L/D) is more than 10 [27]. The Reynolds number (Re), the ratio of inertial force to the viscous force, is a dimensionless number to describe the state of flow, e.g., laminar/uniform and turbulent flow. The reduced velocity (RV) and reduced frequency (K), which are related to each other, are usually used to define the unsteadiness of the problem or motion of model. The Scruton number (Sc) is a non-dimensional parameter to describe the flow-induced vibration of structures. The Strouhal number (St) is a dimensionless number to define the oscillating flow mechanisms and

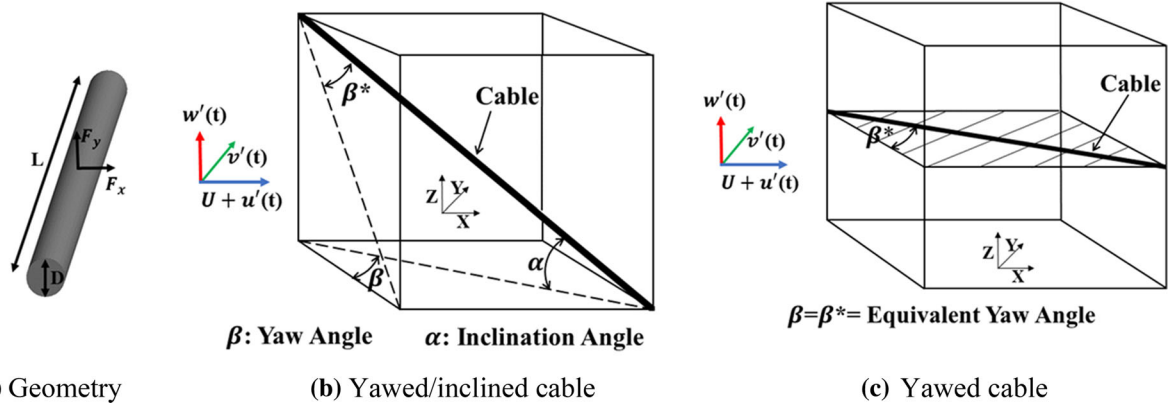


Fig. 2 Definition of actual yaw angle and equivalent yaw angle [26]

Table 2 Common dimensionless numbers in wind-induced cable vibration

Non-dimensional number	Definition	Variable	Description
Reynolds number	$Re = \frac{\rho U D}{\mu}$	D	Diameter (m)
		L	Length (m)
Reduced velocity	$RV = \frac{U}{nD}$	U	Mean wind speed (m/s)
		ρ	Fluid density (kg/m ³)
Reduced frequency	$K = \frac{\omega D}{U} = \frac{2\pi}{RV}$	μ	Dynamic viscosity of fluid (kg/m s)
		m	Mass per unit length (kg/m)
Scruton number	$Sc = \frac{m\zeta}{\rho D^2}$	ζ	Mechanical damping ratio
		n	Natural frequency (Hz)
Strouhal number	$St = \frac{f_s D}{U}$	ω	Angular/circular frequency (rad/s)
		F_x	Drag force (N)
Drag coefficient	$C_D = \frac{F_x}{0.5\rho U^2 DL}$	F_y	Lift force (N)
		P	Pressure (Pa)
Lift coefficient	$C_L = \frac{F_y}{0.5\rho U^2 DL}$	P_{st}	Static pressure (Pa)
		M	Mass (kg)
Pressure coefficient	$C_P = \frac{P - P_{st}}{0.5\rho U^2}$		

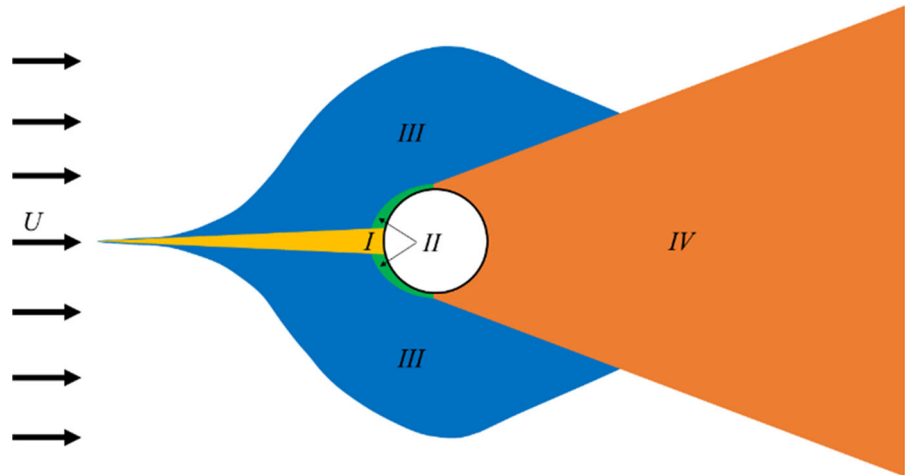
the “lock-in” velocity. Two main aerodynamic forces of drag and lift are the projected components of total force acting on a structure due to incoming flow. The direction of the drag force is defined as parallel to the relative velocity (U_{rel}), and the direction of the lift force is perpendicular to the drag force. Two original sources of drag force applying to a structure are skin friction and pressure distribution. The contribution of skin friction is the more significant source of drag for streamline bodies, whereas pressure is the main source of drag for bluff bodies due to the large separation area. Pressure coefficient (C_P) is another dimensionless number

describing the pressure distribution around a structure. The normalized drag and lift (C_D and C_L) forces can be extracted from the pressure coefficient by integrating force around the structure and projecting them in drag and lift directions.

3 Aerodynamic characteristics of circular cylinders

Aerodynamics of streamline bodies, e.g., airfoils, and bluff bodies, e.g., circular cylinders, have been stud-

Fig. 3 Main regions to describe the flow over a circular cylinder [38]



ied by many researchers as a fundamental subject of fluid mechanics in aerospace, mechanical, and civil engineering. Studying the flow behavior over a circular cylinder has received remarkable attention by researchers in the past due to many applications for this structure, e.g., offshore risers, bridge piers, periscopes, chimneys, towers, masts, stays, cables, antennae, and wires [28]. Flow over a circular cylinder has been studied from low to high Reynolds numbers with different techniques such as experimental wind tunnel tests using a particle image velocimetry (PIV) system [29–32] and point measurement, or numerical methods using computational fluid dynamics [33–36]. Aerodynamic and aeroelastic characteristics of a circular cylinder or cable are mainly a function of Reynolds number and reduced velocity in static and dynamic conditions, respectively. Furthermore, the aerodynamic properties of this structure depend on some other effective parameters, such as surface roughness (smooth or rough), upstream flow condition (uniform or turbulent), and position of the cylinder with respect to incoming flow (normal or yawed). Flow over circular cylinders has been widely studied in the past, and the following sections briefly review some of the most effective parameters on the aerodynamics of this structure. Flow regime around a circular cylinder can be generally described in four regions (see Fig. 3). These regions are summarized as follows [37]:

- (I) One narrow region of retarded flow.
- (II) Two boundary layers attached to the surface of the cylinder.

- (III) Two sidewise regions of displaced and accelerated flow.
- (IV) One wide region downstream of the separated flow called “wake.”

Drag and lift coefficients including mean and fluctuation components are primarily a function of Reynolds number, as illustrated in Fig. 4. This figure shows that the mean drag coefficient generally reduces by increasing the Reynolds number except in the critical region, while the mean lift coefficient is mostly zero due to symmetric geometry. Flow regime classifications and their effects on aerodynamic coefficients are displayed in Fig. 3 and are briefly summarized in Table 3.

The fluctuating lift coefficient, which is usually measured from recording the surface pressure, is plotted for different Reynolds numbers in Fig. 5. This fluctuating load component is used in design of specific applications [27].

Another important parameter is the pressure coefficient. This characteristic describes the pressure distribution around a structure and is calculated by measuring the surface pressure of a model. Figure 6a displays the mean pressure coefficient of a smooth circular cylinder in uniform flow at different Reynolds numbers; and Fig. 6b shows the fluctuating pressure coefficient from $\theta = 0^\circ$ to 180° at different Reynolds numbers. As shown in Fig. 6a, the variation of Reynolds number changes the location of the minimum pressure coefficient, base pressure, and reverse pressure. Figure 6b indicates the reduction of fluctuating pressure as the Reynolds number increases.

Fig. 4 Aerodynamic coefficients (mean and fluctuating) of a circular cylinder [39]

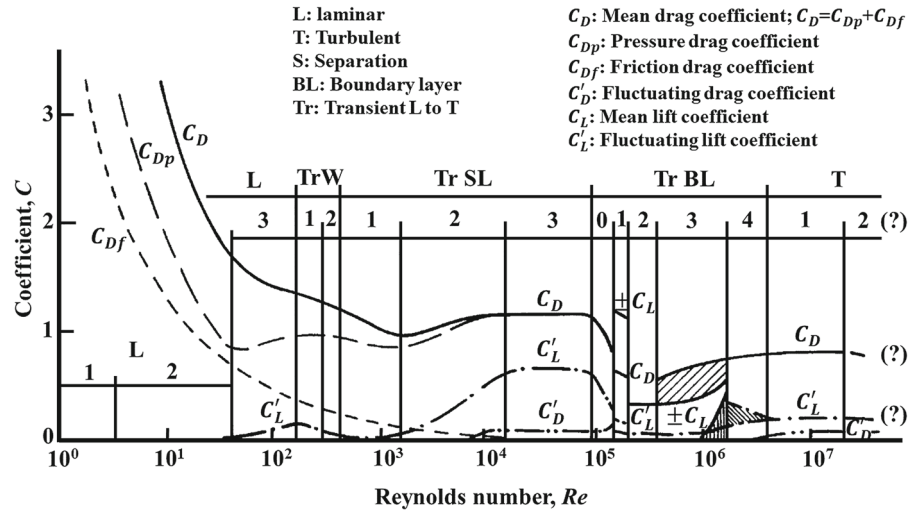


Table 3 Description of flow regime over a circular cylinder explained in Fig. 4 [37]

State	Name	Regime	Reynolds number
Laminar	L1	No separation	$0 < Re < 4-5$
	L2	Closed wake	$4-5 < Re < 30-48$
	L3	Periodic wake	$30-48 < Re < 180-200$
Transition in wake	TrW1	Far-wake	$180-200 < Re < 220-250$
	TrW2	Near-wake	$220-250 < Re < 350-400$
Transition in shear layers	TrSL1	Lower	$350-400 < Re < 1-2k$
	TrSL2	Intermediate	$1-2k < Re < 20-40k$
	TrSL3	Upper	$20-40k < Re < 100-200k$
Transition in boundary layers	TrBL0	Pre-critical	$100-200k < Re < 300-340k$
	TrBL1	Single bubble	$300-340k < Re < 380-400k$
	TrBL2	Two-bubble	$380-400k < Re < 500k - 1M$
	TrBL3	Supercritical	$500k - 1M < Re < 3.5-6M$
	TrBL4	Post-critical	$3.5-6M < Re < ?(not\ known)$
Fully turbulent	T	Invariable	$(Not\ known)? < Re < \infty$
		Ultimate	

Strouhal number is another important non-dimensional characteristic defining the “lock-in” velocity, and the frequency of vortex shedding is the same as the natural frequency of the structure. Figure 7 displays the Strouhal number of a circular cylinder at different Reynolds numbers. This figure highlights a huge jump for smooth surfaces at the critical range of Reynolds numbers [28]. In Table 4, the useful empirical equations are mentioned to calculate the Strouhal number and fluctuating lift coefficient (C'_L) at different ranges of Reynolds numbers. Moreover, in Table 5, a summary

of the aerodynamic coefficients of circular cylinders at different regimes is shown.

3.1 Effect of roughness

The past studies showed that the surface roughness shifts the critical range of Reynolds numbers to lower values for a circular cylinder, which means a drag reduction or an increase in Strouhal number at the critical range occurs in lower Reynolds numbers. Fig-

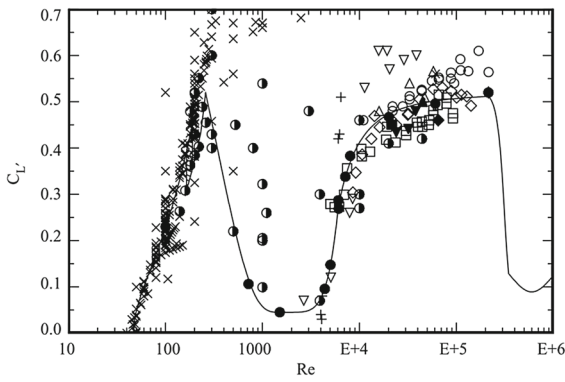


Fig. 5 Fluctuating lift coefficient of a circular cylinder at different Reynolds number; open square, Keefe [40]; plus sign, Leehey and Hanson [41]; filled triangle, Sonnevile [42], open triangle, Mohr [43]; inverted open triangle, Moeller and Leehey [44]; shaded square, Gartshore [45]; open diamond, Szepessy and Bearman [46]; open circle, West and Apelt [47]; filled diamond, Sakamoto and Haniu [48]; multiplication sign, filled circle, and half-filled circle Norberg [49]

ure 8 indicates the Strouhal number for specific surface roughness (k/D), which confirms shifting the critical Reynolds number to lower value. Moreover, it shows that the critical range of Reynolds numbers becomes shorter as surface roughness increases, and the maximum peak of the Strouhal number reduces with increasing roughness. Consequently, the surface roughness is an effective parameter to change the frequency of vortex shedding, especially in the critical range for mitigation or postponing the vortex-induced vibration.

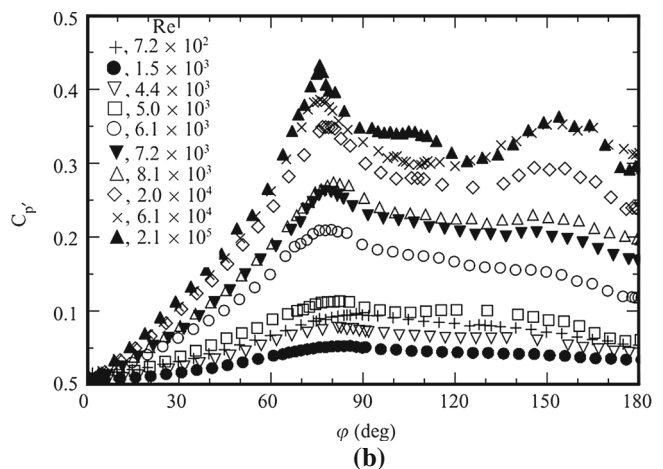
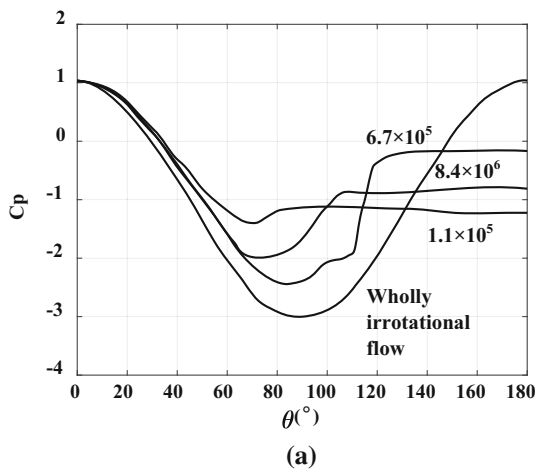


Fig. 6 Pressure coefficient distribution of a circular cylinder (a) Mean pressure coefficient, replotted from [50]. (b) Fluctuating pressure coefficient [51]

Figure 9 shows the effect of roughness on the mean drag coefficient of a circular cylinder and proves that critical Reynolds number happens at lower values for surfaces with greater roughness. According to the results, changing the surface roughness has the most effects on critical range, but the lowest effect on the subcritical regime due to high boundary layer thickness [38]. Furthermore, the drag reduction is less for surfaces with more roughness, and this feature can be used to reduce the drag at high Reynolds numbers by polishing the surface.

3.2 Effect of turbulence

Although most of the past experimental wind tunnel tests have been performed in uniform flow, few experimental and numerical studies have demonstrated the effect of turbulent intensity on the aerodynamics of circular cylinders. According to the literature, the mean drag coefficient reduces in the subcritical region by increasing the turbulent intensity, while the drag coefficient increases in the critical region by increasing the turbulent intensity. To display the influence of turbulent intensity on the pressure distribution over a circular cylinder, the mean pressure coefficient is plotted in Fig. 10 for a uniform flow and turbulent flow at similar Reynolds numbers. This figure indicates that turbulent flow increases three important values of the mean pressure coefficient, namely base pressure, maximum pressure coefficient, and location of adverse pressure.

Fig. 7 Strouhal number as a function of the Reynolds number for a circular cylinder [52]

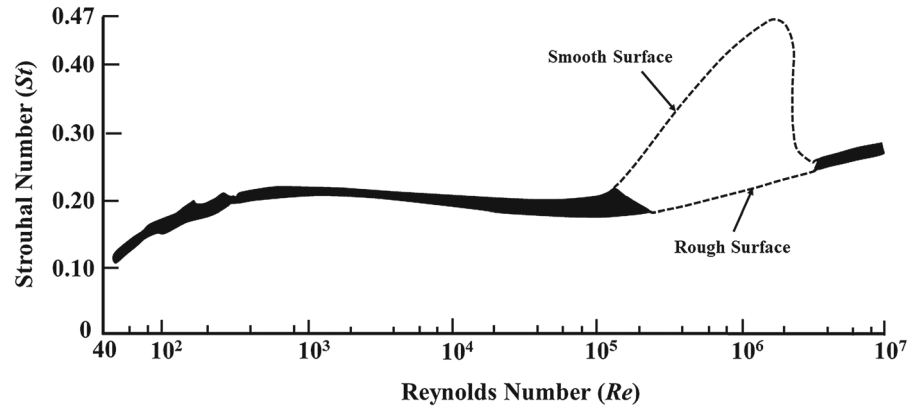


Table 4 Summary of empirical equations to predict the Strouhal number and fluctuating lift coefficient [49]

Re	$St \cong$	Re	$C'_L \cong$
47–190	$0.2663 - 1.019/\sqrt{Re}$	47–190	$[(Re - 47)/47]/30 + ((Re - 47)/47)^2/90]^{0.5}$
165–260	$-0.089 + 22.9/Re + 7.8 \times 10^{-4} \times Re$	165–230	$0.43 \times (Re/230)$
260–325	0.2016	230–260	$0.78 \times (Re/260) - 0.26$
325– 1.6×10^3	$0.2139 - 4.0/Re$	260– 1.6×10^3	$0.045 + 1.05 \times (1 - Re/1.6 \times 10^3)^{4.5}$
$1.6 \times 10^3 - 1.5 \times 10^5$	$0.1853 + .0261 \times \exp(-0.9 \times (\log(Re/1.6 \times 10^3))^{2.3})$	$1.6 \times 10^3 - 5.4 \times 10^3$	$0.045 + 3.0 \times (\log(Re/1.6 \times 10^3))^{4.6}$
$1.5 \times 10^5 - 3.4 \times 10^5$	$0.1848 + 8.6 \times 10^{-4} \times (Re/1.5 \times 10^5)^{4.6}$	$5.4 \times 10^3 - 2.2 \times 10^5$	$0.52 - 0.06 \times (\log(Re/1.6 \times 10^3))^{-2.6}$
		$2.2 \times 10^5 - 3.4 \times 10^5$	$0.09 + 0.43 \times \exp[-10^5 \times (Re/10^6)^{10}]$

3.3 Effect of yaw angle

Since circular cylinders are usually normal to the incoming flow, the aerodynamics of a yawed and/or an inclined cylinder have not been sufficiently explored in the past. Studies showed that an axial flow is generated along the spanwise direction behind the yawed cylinder, which interferes with vortex shedding in the wake of the cylinder. Hence, the yaw and/or inclination angle has significant effects on the circular cylinder that can change the aerodynamics of this structure. For instance, Fig. 11 indicates that the mean drag coefficient of a yawed circular cylinder is reduced as the yaw angle increases and it reveals the independency of the normal drag coefficient to the yaw angle at low Reynolds numbers (independence principle). Therefore, studying yawed and/or inclined circular cylinders or cables

can be an interesting topic to discover the objects' aerodynamic features as the wind direction changes.

4 Wind loads

Wind loads that act on a structure can be generally classified as static and dynamic loads for the purpose of analysis. Dynamic loads are important because they can cause structural fatigue or failure over long or short periods. The dynamic loads are defined either in frequency or time domain. While equations of motion of a structure under wind loads can be written for all three degrees of freedom of a structure, two lateral and one torsional directions, only along-wind and across-wind motions are considered important for a cable without ice or rain because the torsional motion is negligible compared to the others. External wind loads on a cable

Table 5 Summary of aerodynamic coefficient of circular cylinder at different regimes [38] original data from [49,53–57]

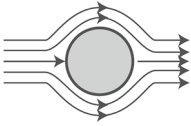
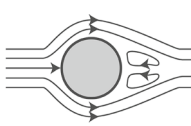
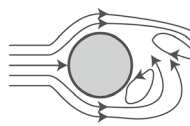
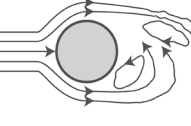
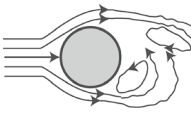
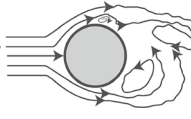
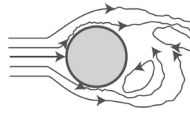
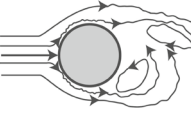
Regime	No separation	Pair of stationary vortex	Laminar vortex shedding	Turbulent vortex shedding
Re range	$0 < Re < 5$	$5 < Re < 40$	$40 < Re < 200$	$200 < Re < 300$
C_D	$4 < C_D < +\infty$	$2.1 < C_D < 4$	$1.5 < C_D < 2.1$	$1.3 < C_D < 1.5$
C_L	0	0	0	0
St	–	–	$0.1 < St < 0.2$	$St \cong 0.2$
$C_{D,rms}$	–	–	$0 < C_{D,rms} < 0.04$	$0.04 < C_{D,rms} < 0.05$
$C_{L,rms}$	–	–	$0 < C_{L,rms} < 0.4$	$0.4 < C_{L,rms} < 0.5$
Spectrum of C_L	–	–	Single narrow peak	Single narrow peak
Streamline view				
Regime	Subcritical	Critical	Upper transition	Post-critical
Re range	$3 < Re < 3 \times 10^5$	$3 \times 10^5 < Re < 3.5 \times 10^5$	$3.5 \times 10^5 < Re < 4.5 \times 10^5$	$4.5 \times 10^5 < Re < 4.5 \times 10^5 < \infty$
C_D	$1.2 < C_D < 1.3$	$0.3 < C_D < 1.2$	$0.3 < C_D < 0.5$	$0.5 < C_D$
C_L	0	$\cong 1.3$	0	0
St	$St \cong 0.2$	$0.2 < St < 0.45$	$0.25 < St < 0.45$	$St < 0.25$
$C_{D,rms}$	$0.05 < C_{D,rms} < 0.07$	$0.07 < C_{D,rms} < 0.03$	$0.03 < C_{D,rms} < 0.04$	$C_{D,rms} < 0.04$
$C_{L,rms}$	$0.09 < C_{L,rms} < 0.5$	$0.04 < C_{L,rms} < 0.09$	$0.02 < C_{L,rms} < 0.04$	$C_{L,rms} < 0.02$
Spectrum of C_L	Single narrow peak	Random with 1 peak	Random with 2/1 peaks	Single narrow peak
Streamline view				

Fig. 8 Effect of surface roughness on the Strouhal number of a circular cylinder [58]

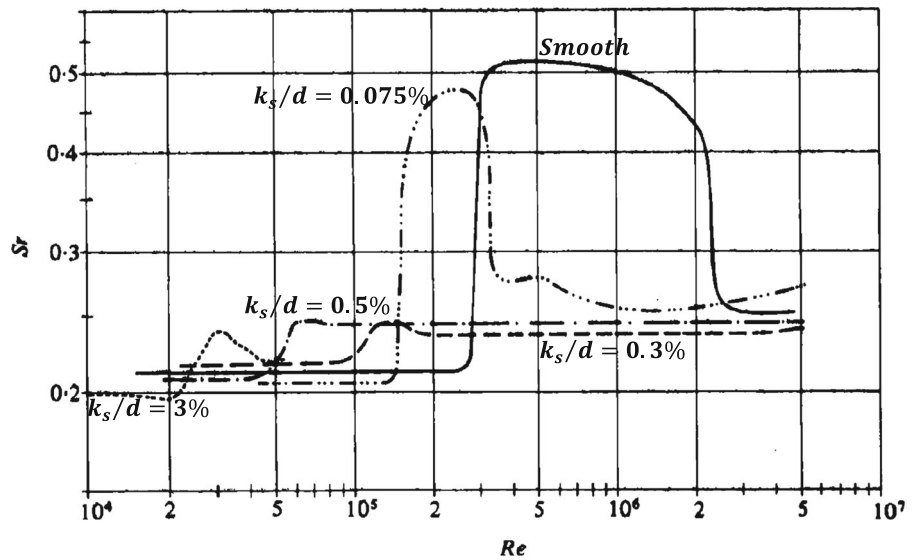


Fig. 9 Effect of surface roughness on mean drag coefficient of a circular cylinder [58]

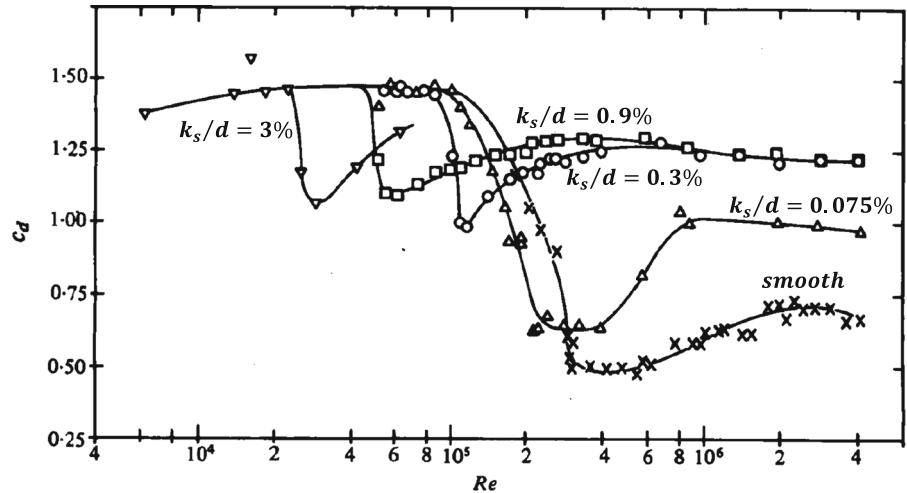
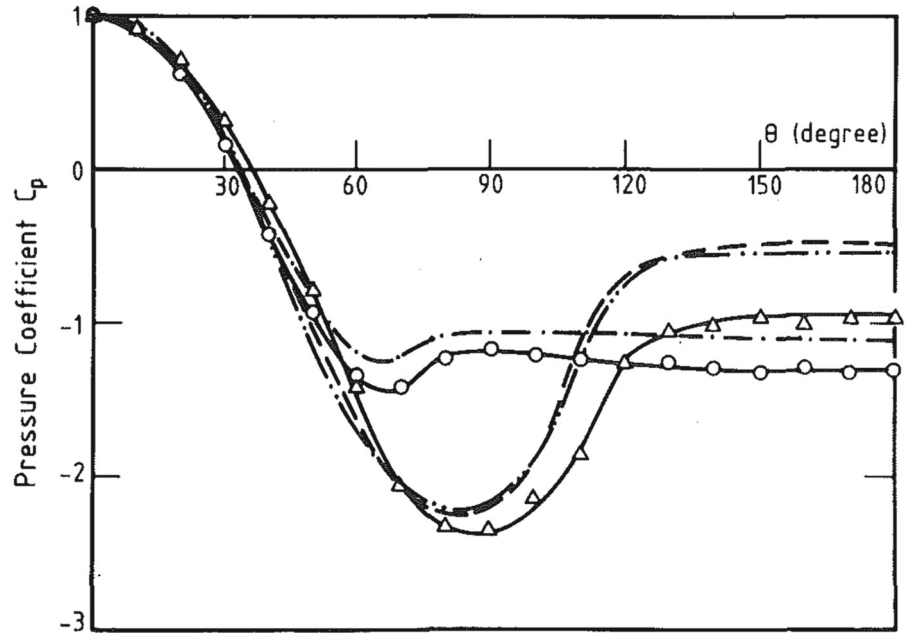


Fig. 10 Effect of turbulent flow on the mean pressure coefficient of a circular cylinder; open circle, $Re = 1.21 \times 10^5$, smooth (Kwok [59]); open triangle, $Re = 1.24 \times 10^5$, $\sigma_u/U = 0.088$ (Kwok [59]); dashed line with single dot, $Re = 1.20 \times 10^5$, smooth (Wong [60]); dashed line, $Re = 1.11 \times 10^5$, $\sigma_u/U = 0.129$ (Batham [61]); dashed line with double dots, $Re = 1.25 \times 10^5$, $\sigma_u/U = 0.036$ (Sadeh and Saharon [62])



can be divided into vortex shedding, buffeting, and self-excited loads, as presented in Fig. 12.

Figure 13 shows the dynamic wind loads and velocity components for a circular section of a cable. The equations of motion for across-wind, or vertical (h), and along-wind, or lateral (p), motions can be written as follows:

$$m(\ddot{h} + 2\omega_h \zeta_h \dot{h} + \omega_h^2 h) = F_{ae}^h = F_{se}^h + F_b^h + F_{vs}^h \quad (2)$$

$$m(\ddot{p} + 2\omega_p \zeta_p \dot{p} + \omega_p^2 p) = F_{ae}^p = F_{se}^p + F_b^p \quad (3)$$

where m is the mass per unit length, h and p denote the vertical and lateral displacements, ω_h and ω_p represent

the natural frequencies, ζ_h and ζ_p are the total damping ratios, and F_{se} , F_b , and F_{vs} are self-excited, buffeting, and vortex shedding-induced loads per unit length of a cable; U represents the mean wind speed, while $u(t)$ and $w(t)$ are along-wind and across-wind turbulence components, normal to the cable axis. Different system identification methods can be applied to extract the parameters of each of the above wind load components using a section model of a yawed cable. These wind loads and the extraction methods are described in ‘‘Appendix’’.

Fig. 11 Effect of yaw angle on the Strouhal number of a circular cylinder [63]

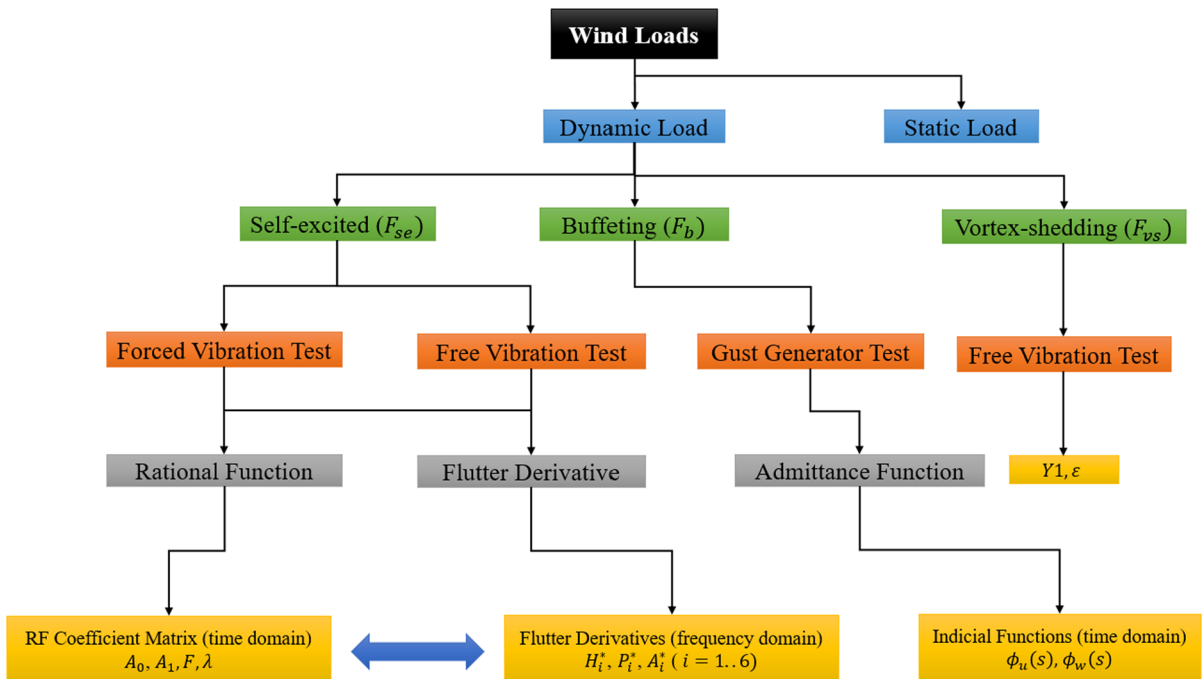
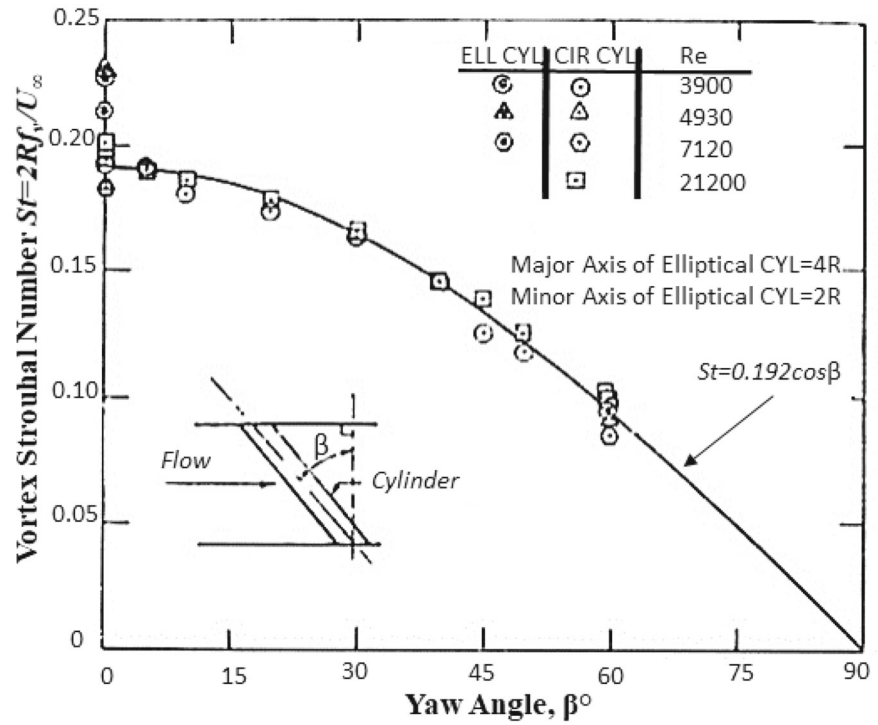


Fig. 12 Flowchart of wind loads and extraction methods

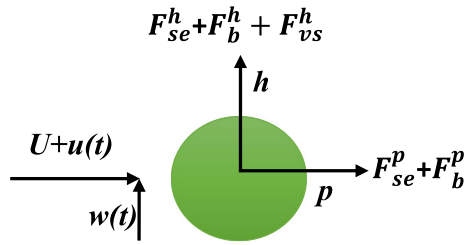


Fig. 13 Schematic view of dynamic wind loads and velocity components over a smooth cable

5 Wind-induced vibration

5.1 Vortex-induced vibration (VIV)

Vortices can be generated and then separated from either side of a bluff body in a periodic way when air flows past it, resulting in an oscillating force that is perpendicular to both the flow and the structure. The vibration of structures caused by such kind of oscillating force is called vortex-induced vibration (VIV). The frequency of the oscillating force is characterized by a non-dimensional number, namely Strouhal number, which is defined as $St = \frac{fD}{U}$, where f is the frequency of the oscillating force, D is the dimension of the structure which for cables is normally taken as the diameter, and U is the wind speed. It has been revealed by Lienhard [52] that the Strouhal number of cylinders remains as a constant value approximately equal to 0.2 over a large range of Reynolds numbers. The effect of Reynolds number on Strouhal number is given in Sect. 2. The amplitude of vortex-induced vibration on structures is associated with the force that is generated due to vortex shedding. A comprehensive study of VIV on cylinders carried out by Feng [64] analyzed both amplitude and frequency responses in the cross-flow direction. It can be seen from Fig. 14 that initially, the frequency of the vortex shedding (f) follows a straight line relationship with reduced velocity. The slope of this line is 0.198, which is approximately equal to the Strouhal number of the cylinder. After reaching the natural frequency of the structure, there is a range of wind speeds in which the frequency of the oscillating force is equal to the natural frequency of the cable, and, hence a large-amplitude vibration can be observed because of the resonance. This range is defined as the lock-in or synchronization region, of which the wind speed can be calculated using the definition of Strouhal number.

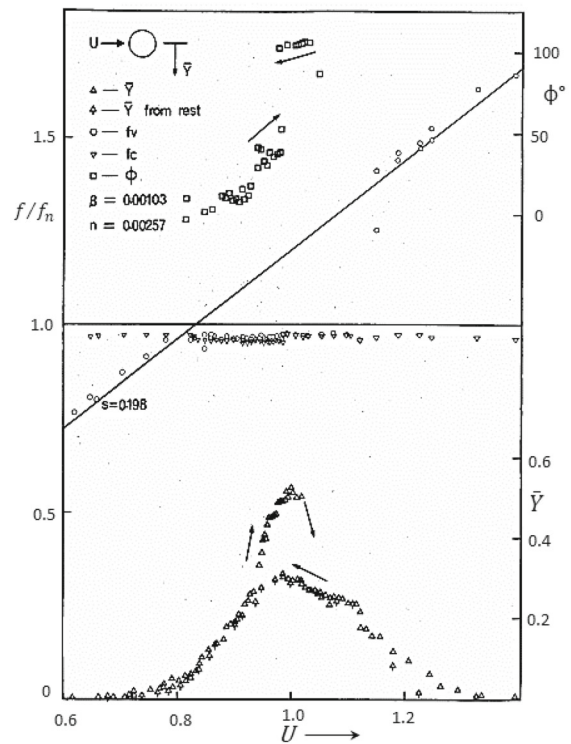


Fig. 14 Response of a cylinder oscillating in cross-wind direction [64]

Since vortex shedding is capable of producing a large-amplitude vibration and therefore imposing a significant threat to cables, numerous investigations have been carried out using either numerical simulations, experimental tests, or field measurements for the purpose of unveiling the underlying mechanism of vortex-induced vibration on cables. Among all the properties of vortex-induced vibration, amplitude serves as the major concern because large-amplitude vibration could lead to structure failure. An experimental study by Wootton [65] showed the dependence of amplitude upon the structure damping ratio. It was observed that the amplitude decreases with the increase in the Scruton number in the lock-in region. A nonlinear empirical model proposed by Simiu and Scanlan [66] to formulate the vortex shedding force acting on cylinders relates the damping ratio of the structure to the steady-state amplitude. The equation that can be employed to predict the steady-state amplitude of VIV on cylinders is given by:

$$y_0 = 2 \left[\frac{2m\xi K - \rho D^2 Y_1}{-\rho \varepsilon Y_1} \right]^{1/2} \tag{4}$$

where y_0 denotes the steady-state amplitude, m is the mass per unit length, ξ represents the damping ratio, K is the reduced frequency, ρ is the air density, D denotes the diameter of the structure, and ε and Y_1 are the parameters of the nonlinear model which can be identified from the wind tunnel test. A detailed derivation for the nonlinear empirical model of vortex shedding force is given in Sect. 7.1.1.

In addition to the damping ratio, the yaw angle also plays an important role in the vortex-induced vibration on cylinders. Among all the methodologies related to VIV on yawed cylinders, the independence principle (IP), which is the application of the component of velocity normal to the cylinder axis, is the most widely used. However, studies related to the vortex shedding on inclined cylinders yielded conflicting results, particularly corresponding to the critical yaw angle beyond which the IP is not valid. Surrt and Surry [67] performed a wind tunnel test of an inclined cylinder whose yaw angle ranged from 0° to 55° . It was found that the Strouhal number obtained from the IP remained as a constant up to the yaw angles of 40° to 50° . Van Atta [68] measured the Strouhal number of an inclined cylinder and validated that IP is effective when the yaw angle is smaller than 35° . Willden and Guerbi [69] proved that the Strouhal number of a yawed cylinder follows the IP until the yaw angle reaches 40° , therefore, the critical range of yaw angle in which the Independence Principle fails is between 40° and 60° . However, an experiment related to the formation of a vortex on a stationary inclined cylinder concluded that the application of the IP is not valid as the results showed that the frequency of vortex shedding of yawed cylinders is larger than the one predicted from IP. Moreover, the angle and length of the vortex as well as the base pressure are all smaller than those of a vertical cylinder that has the same velocity component normal to the axis [70]. Lucor and Karniadakis [71] investigated the drag coefficient of an inclined cylinder by using direct numerical simulation (DNS) and demonstrated that the IP is invalid when the yaw angle falls into the region between -70° and -60° . A similar numerical simulation using DNS method carried out by Zhao et al. [72] found that both the Strouhal number and drag coefficient agree very well with IP when the yaw angle is $\alpha \leq 30^\circ$, though the RMS of the lift coefficient is smaller than the value calculated from IP.

Another important factor that has a significant effect on the VIV of cylinders is surface roughness. Imperfec-

tion of cables caused by ice accretion or water rivulets, which is usually the case for stayed cables of bridge, can result in a notable change on the aerodynamics of cables and hence influence the vortex-induced vibration. Buresti [73] carried out a research to explore the influence of surface roughness on flow regimes of a cylinder. The effect of surface roughness on VIV has been confirmed, for example, critical regime, which is characterized by the absence of regular vortex shedding, could be significantly reduced or even disappear for the highly roughed cylinders. Besides, the boundaries between different flow regimes were found to be a function of the surface roughness. Furthermore, Diana et al. [74] increased the surface roughness of a cylinder to reproduce post-critical flow conditions, where the correlation of vortex shedding along the cable can be controlled. Górski et al. [75] performed an experimental test to examine the effect of accretion of ice on an inclined cable. It was observed that an asymmetric and irregularly iced cross section with rounded edges of the ice ribs on the bottom and a quasi-circular shape on its upper side of the cable model was generated during the test. The Strouhal number was changed, and its dependence upon the Reynolds number can be determined by the angle of inclination. Trush et al. [76] conducted a wind tunnel test on the VIV of rough cables and observed that the peak amplitude may increase or decrease depending on the location where the ice is formed. In particular, the amplitude may be amplified if the ice is accreted on the leeward (backside) surface of the cable. Besides, they have found that VIV on ice accreted bridge cables can be weakened by increasing the turbulence intensity of the incoming flow. The aforementioned studies are summarized in Table 6.

Apart from numerical simulation or experimental tests, field measurement serves as another important way to study vortex-induced vibration on cables. Matsumoto et al. [78] found from field observation that wind-induced vibration on stayed cables usually occurs at reduced velocities $U/fD = 20, 40, 60, 80$ and so on, instead of the reciprocal of Strouhal number. In order to explain the mechanism of this phenomenon, a series of experiments was conducted and it was concluded that such a mechanism can be attributed to the fluid interaction between Karman vortex and axial vortex traveling along the axis of the cable. In addition, 3D characteristics of vortex shedding have been observed, which are extensively dependent on the end conditions as well as the yaw angle of the cable.

Table 6 Numerical and experimental tests of VIV on cables

References	Re	α°	β°	D (mm)	L (m)	Test type
Surratt and Surry [67]	4.5k–63k	0	0–55	23.11	–	WT
Van Atta [68]	< 80	0	0–90	3.175	–	WT
Buresti [73]	26k–280k	0	0	33–118	0.78	WT
Diana et al. [74]	> 100k	0	0	720	3.3	WT
Górski et al. [75]	24k–165k	30	60	160	–	WT
Trush et al. [76]	65k–120k	0	0	200	0.8	WT
Evangelinos et al. [77]	1k	0	–60 and –70	D	22D	NS
Zhao et al. [72]	1k	0	0–60	D	9.6D	NS

WT wind tunnel test, NS numerical simulation

Moreover, Matsumoto et al. [79] performed a field test using a full-scale cable, and they have observed that vortex-induced vibrations at higher reduced velocities are able to keep their amplitude constant for a long time when compared to the conventional Karman vortex-induced vibration, which only occur for a short time period. Therefore, it was suggested that the vortex-induced vibration can be divided into two different types, namely Karman vortex-induced vibration and vortex-induced vibration occurring at high reduced velocities. Further field observations conducted by Zuo and Jones [80] led to a similar conclusion, that is, the large-amplitude vibration of cables results from a type of vortex shedding mechanism that is different from traditional Karman vortex shedding. Besides, they found one of the characteristics for classical Karman vortex-induced vibration to be that the amplitude of such vibration is usually less than 20% of the cable's diameter and typically occurs in smooth flow at low wind speed. To gain more insights into the mechanism of such unclassical vortex shedding, Zuo and Jones [81] continued their research by testing a yawed and inclined cylinder in a wind tunnel. They proposed that this type of vortex shedding is due to the inherent nature of a stayed cable's inclination, which enables the formation of a three-dimensional vortex and makes it distinct from Karman vortex. Additionally, a mechanism of the translation from classical Karman vortex-induced vibration to vortex-induced vibration at high reduced velocities was discovered, which was believed to be related to a type of low-amplitude cable vibration observed in the field. Matsumoto et al. [79] examined the parameters that control these two types of vortex-induced vibration using wind tunnel tests. They found that parameters

such as water rivulets, wind turbulence intensity, and pressure field are able to influence the characteristics of vortex-induced vibration and control the occurrence of two different types of vortices. It has also been observed that the formation of vortices on the upstream side and downstream side is different due to the existence of yaw angle.

According to the definition of Strouhal number, it can be concluded that non-uniform flow is capable of exciting more than one vibration mode of the structure. Since stay-cable bridges are normally built in boundary layer wind conditions, where wind speed increases with the height, it is possible that stayed cables would exhibit multi-mode vibrations. This phenomenon has been detected by field measurement. For example, Matsumoto et al. [78] analyzed the acceleration data from the field measurement and found 7th and 8th modes dominate wind-induced vibration on dry cables, whereas Zuo and Jones [80] have observed that the wind-induced vibration has notable components of 6th and 7th vibration modes, which can be attributed to the boundary layer wind profile where the wind speed varies along the height.

In order to study the behavior of vortex-induced vibration on cables, Chen et al. [82] adopted a $k-\omega$ turbulent model based on the Reynolds-averaged Navier–Stokes (RANS) method to simulate the response of cables under different wind profiles. The results showed that the cable displayed two different types of vibration: single-mode vibration when it is immersed in uniform flow and multi-mode vibration when it is subject to boundary layer flow. In addition to numerical simulations, Chen et al. [83] carried out some VIV tests of cables in the wind tunnel and the results indicated

that the cable could vibrate either in a single-mode or multi-mode method, depending on the conditions of the incoming flow. Additionally, they have discovered that the amplitude of single-mode VIV is larger than that of multi-mode VIV and the amplitude in cross-flow direction is larger than in-line direction for both single-mode and multi-mode VIVs. Gao et al. [84] also reproduced the multi-mode VIVs of cables from wind tunnel tests, in which the cable was exposed to uniform flow and by gradually increasing the wind speed, the first, second, and third mode of the vibration can be obtained. Since VIV of cables is a nonlinear phenomenon, it can be studied analytically by carrying out a nonlinear analysis. Zeinoddini et al. [85] studied the possibility of chaos of the VIV response of cylinders. The zero-one tests, Hilbert transforms, and Poincaré maps were used for the analysis, and the chaotic region is determined. Plaschko et al. [86] modeled the flow-induced vibration of cylinders as a fourth-order autonomous system, and they found that the mass ratio is the governing parameter can lead to a chaotic vibration. Huang et al. [87] proposed nonlinear partial differential equations (PDEs) to model the vibration of suspended cable-stayed beam. The solution for the PDEs was obtained using Galerkin method. Through Hopf bifurcation analysis, they found that the deformation of stay cables has remarkable effect on the aeroelastic instability.

Since the amplitude of vortex-induced vibration is dependent on the damping ratio of the structure, as derived from Eq. (4), viscous damper devices can be utilized to control the VIV on cables. Due to the intrinsic low damping ratio of stayed cables, which is inadequate to suppress vortex-induced vibrations, an external damper is usually required to be installed on stayed cables. Persoon and Noorlander [88] studied the dampers placed on the stay cables of the Erasmus Bridge, which is located in Rotterdam, Netherlands. They found that the dampers, originally designed to suppress vibrations by vortex shedding, were sufficient to absorb the vibration caused by vortex shedding. However, the damping ratio of such dampers is insufficient to control the resonance by the rain-wind-induced vibration. Main and Jones [89] derived an optimal damping ratio of the dampers for stayed cables, and then, they analyzed the performance of optimized dampers installed on Fred Hartman Bridge in Houston. The results showed that the dampers are very effective in suppressing all types of high-amplitude oscillations, including the vibration induced by the vortex shedding.

The aerodynamic load control, which can be divided into passive control method and active control method, is an alternative way to control the vortex-induced vibration on cables. The mechanism of this method lies in the interruption of vortex generation around the cable and hence minimize the wind load acting on cables. Passive control of vortex-induced vibration can be achieved by manipulating the aerodynamics of cables. Zdravkovich [90] classified the means of suppressing vortex shedding into three categories, namely surface protrusions, shrouds, and near-wake stabilizers. An assessment of those approaches was carried out in order to compare their effectiveness of reducing vortex shedding on cables. Nebres and Batill [91] and Igarashi [92] conducted an experimental test to study the Strouhal number of a cylinder with a single tripping wire attached in parallel to the cylinder's axis. In contrast, Hover et al. [93] investigated a cylinder with two tripping wires attached in parallel to the axis and symmetric to the stagnation point. The results of these experiments showed that the Strouhal number of such cylinders is a function of angular position and size of the wire, as well as the Reynolds number. Therefore, the vortex-induced vibration on a cylinder can be suppressed by deliberately changing the configuration of the cylinder's surface. Active vibration control method can be attained by managing the flow around a cylinder, which can be accomplished by using either flow blowing method or flow suction method. Fransson et al. [94] documented variations of vortex shedding by changing both flow blowing and suction rates on a smooth, porous cylinder. It is found that the Strouhal number decreases when the air blows out of the surface, while suction of air into the surface has the opposite effect. In addition, the vortex formation length is affected by whether the air blowing or suction is applied on the surface of a cylinder. Patil and Ng [95] studied the flow control of a cylinder with periodic porosity on its surface. It has been revealed that the suction of the flow on the surface of a cylinder can significantly suppress the formation of spanwise vortices and thereby reduce the oscillating force. Li et al. [96] used numerical simulations to investigate the control of vortex shedding through air blowing or suction on the surface of a cylinder. The results indicate that a robust control can be fulfilled if the time window is larger than the vortex shedding period. In addition, the absolute suppression of vortex shedding is still feasible even if the control time is only half of the period of vortex shedding. Chen

et al. [97] performed a wind tunnel test to explore the effectiveness of the air suction method in the mitigation of vortex-induced vibration on cylinders. The measurement of vibration response, along with pressure coefficients and aerodynamic load, showed the effectiveness of the air suction method in suppression of VIV. Additionally, an optimal flow rate for VIV control has been discovered.

The mitigation of VIV for cylinders can be achieved with the modification of system parameters, such as mass, damping, and stiffness. Gattulli and Ghanem [98] implemented an active control method to mitigate VIV of structures by attaching a tuned mass damper to the structure. By moving the mass along a particular path, the vibration of the structure can be controlled. Non-linear energy sink (NES), which is secondary system consisting of nonlinear damping or stiffness, can be used to suppress VIV of cylinders. The application of NES on the suppression of VIV for cylinders has been investigated in [99–103]. Dai et al. [104] proposed a time-delay feedback control system to control the VIV of an elastically mounted circular cylinder. They concluded that by carefully tuning the parameters of the time-delay system, the amplitude of VIV can be significantly reduced. Figure 15 shows few scenarios to control VIV on cylinders. In addition, Table 7 lists the methodologies to control VIV on cylinders.

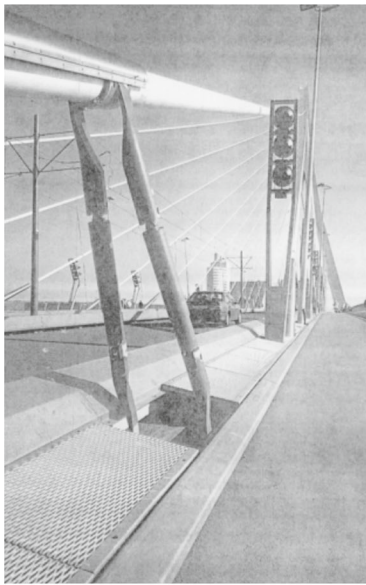
Energy harvesting is a process by which the kinetic energy, such as vibration, can be converted into a form of energy to power, sensors, actuators, and other electronic devices. Owing to its ability to convert vibration into energy and hence reduce the amplitude of vibration, it can be deemed as a way for vibration mitigation. The most widely used configuration for harvesting energy from VIV is a cylinder that is attached to the end of a piezoelectric cantilever beam. Such configuration has been extensively studied, as can be found in [105–108]. However, studies regarding the control of VIV for cylinders using energy harvesting are still limited.

5.2 Rain-wind-induced vibration (RWIV)

The cables on cable-stayed bridges could exhibit vibrations that are characterized by low frequency and large amplitude on rainy and windy days. This type of vibration, which is defined as rain-wind-induced vibrations (RWIVs), poses a significant threat to cables because the large amplitude may lead to a fatigue failure to the

cables' supports. As a result, RWIVs have attracted a lot of attention in the research community since it was firstly observed by Hikami and Shiraishi [11] during a construction of a cable-stayed bridge. By conducting a wind tunnel test, Hikami and Shiraishi [11] concluded that water rivulets formed in rainy days on the upper windward surface of a cable are able to change the cable's aerodynamic properties and hence accountable for RWIVs. Since then, RWIVs have been observed on numerous stayed-cable bridges around the world. A research community organized by the Japan Institute of Construction Engineering conducted field measurements on several cable-stayed bridges and then summarized the characteristics of the rain-wind-induced vibrations, such as low turbulence intensity, large-amplitude vibration, and a limited range of wind speeds at which the RWIVs could occur [109].

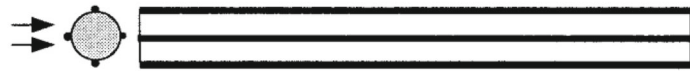
Main and Jones [110] installed a system on the Fred Hartman Bridge and recorded 4000 five-minute records for the amplitude of acceleration and meteorological conditions. The collected data on the Fred Hartman Bridge showed that three distinct types of vibration can be identified, namely no-rain vibration, moderate-rain vibration, and heavy-rain vibration. Further analysis revealed that the occurrence of low-amplitude vibration was corresponding to the absence of rainfall, while medium-amplitude vibration can be observed during a moderate rainfall. In addition, the high-amplitude vibration was also recorded in a heavy rain accompanied with relatively low wind speed. Numerous vibration modes had contributed to these vibrations, especially during the heavy rain. Phelan et al. [111] conducted field observations on Veterans' Memorial Bridge over a period of 2 years. They found that the rain-wind-induced vibration happened when rain was combined with wind speed in a velocity-restricted region, specifically, between 6.3 and 14 m/s (14 and 31 mph). Moreover, the stayed cables exhibit the characteristics of RWIVs when the wind comes from a certain direction, depending on the locations of cables. The critical yaw angle at which the large-amplitude vibration could occur is found to fall into the region between 30° and 50°. Ni et al. [112] carried out a 45-day field measurement of rain-wind-induced vibrations by installing accelerometers, anemometers, and a rain gauge on the Dongting Lake Bridge. The results showed that the combination of wind and rain was able to incur a vibration with a maximum acceleration of 10 g and displacement of 0.7 m. In addition,



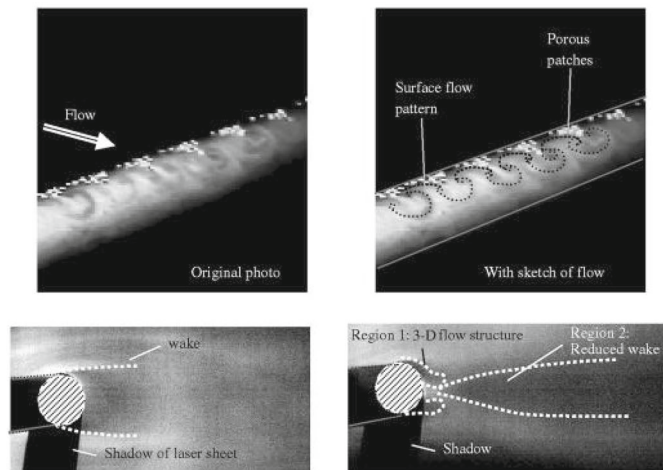
(a)



(b.1)



(b.2)



(c)

Fig. 15 Different methods to control VIV. (a) Dampers installed on Erasmus Bridge [88]. (b.1) Cylinder with 4 helical perturbation [91]. (b.2) Cylinder with 4 straight perturbation [91]. (c) Periodic porosity on cylinder and its effect on flow [95]

the large-amplitude RWIVs were normally associated with mean wind speeds ranging from 6 to 14 m/s at the deck level and rainfall varying from low to moderate. It has been observed that the vibration was dominated by the third mode of the cable and the critical yaw angle for the cables ranges from 10° to 50° . Zuo and Jones [80] presented the results from field measurements on the Fred Hartman Bridge. The comparison between

vortex-induced vibration and rain-wind-induced vibration suggested the similarities between these two types of vibrations other than that RWIVs occurred at higher wind speeds with larger amplitude.

Acampora and Georgakis [113] performed a full-scale monitoring of RWIVs on the Øresund Bridge cables. It has been revealed that RWIVs whose amplitude is greater than $0.2D$ are usually recorded at

Table 7 Methodologies to control VIV

References	Research type	Vibration control method	Conclusions
Persoon and Noorlander [88]	Field measurement	Dampers	Effective to suppress VIV Unable to control RWIV
Main and Jones [89]	Field measurement	Dampers	Effective in mitigating all types of vibration, including VIV
Nebres and Batill [91]	Experimental test	Tripping wires	Tripping wire will change Strouhal number of cylinders
Igarashi [92]			Vibration control can be achieved by selecting the size and location of tripping wires
Hover et al. [93]			
Fransson et al. [94]	Experimental test	Air blowing and air suction	Air blowing decreases Strouhal number Air suction increases Strouhal number
Patil and Ng [95]	Experimental test	Air suction	Air suction reduces oscillating force
Li et al. [96]	Numerical simulation	Air blowing and air suction	Control of VIV can be fulfilled if Time window is larger than vortex shedding period Control time is half of period of vortex shedding
Chen et al. [97]	Experimental test	Air suction	Effective in controlling VIV
Gattulli and Ghanem [98]	Numerical simulation	Tuned mass damper	Structural vibration is controlled Morison's equation for flow-induced forces has been validated
Dai et al. [104]	Numerical simulation	Time-delay feedback control	A good choice of parameters for the controller can effectively mitigate VIV of cylinders

wind speeds between 4–18 m/s with a rainfall of 0–20 mm/h. Additionally, the critical yaw angle for cables was observed to be predominantly between 35° and 55° and between –25° and –50°. In November 1996, it was reported that the cables of the Erasmus Bridge started to vibrate in a windy and rainy condition, which was subsequently identified as rain-wind-induced vibrations. The measurements showed that the cables mainly vibrate in their second mode with an amplitude of 0.5–0.7 m (2–3 times of the cable's diameter) [88]. Gu et al. [114] observed rain-wind-induced vibrations on two cable-stayed bridges that were built in Shanghai and Nanjing. It was found that the cables exhibited large amplitude vibrations under moderate rainfall conditions with the mean wind speed ranging from 10 to 17 m/s. The vibration of cables on the bridge in Shanghai was violent to the point that steel tubes, which were designed to protect the cables, were damaged.

The field measurements of RWIVs on cable-stayed bridges are summarized in Table 8. It can be concluded that rain-wind-induced vibrations are most likely to occur under low to moderate conditions with a wind speed between 4 and 20 m/s. In addition, the characteristics of cables that are prone to rain-wind-induced vibrations involve low damping ratio as well as low natural frequency. Some field measurements have mentioned the critical yaw angle of cables, which indicate that the occurrence of RWIVs is dependent on the wind directions. The inherent nature of low damping ratio and low natural frequency of cables results in a large amplitude of rain-wind-induced vibrations, which threatens the safety of the cable-stayed bridge. Therefore, numerous studies have been conducted to investigate the mechanism of RWIVs, and they will be outlined in the following section.

In spite of the extensive studies that have been carried out for rain-wind-induced vibration on cables, the

Table 8 Field measurement of RWIVs on cable-stayed bridges

Bridge name	Location	Cable properties			Wind speed (m/s)	Rain	RWIV amplitude (mm)
		Length (m)	Diameter (mm)	Frequency (Hz)			
Brottonne Bridge [109]	Upper Normandy France						300
Köhlbrand Bridge [109]	Hamburg, Germany						500
Farø Bridges [109]	Denmark	N/A	150–200	0.6–3	6–18	N/A	1000
Meiko West Bridge [109]	Nagoya, Japan						130
Aratsu Bridge [109]	Fukuoka, Japan						300
Tempozan Bridge [109]	Osaka, Japan						975
Meiko-Nishi [109]	Nagoya, Japan	65–100	140	1–3	14	Moderate to high	550
Fred Hartman Bridge [80]	Houston, USA	87–182	140/160	1.24/0.64	4–20	Low to high	N/A
Veterans' Memorial Bridge [111]	Port Arthur, USA	50.8–96.9	114	1.2–2.5	6.3–14	Low to moderate	Acceleration up to 5 g
Dongting Lake Bridge [112]	Yueyang, China	121.9	119	3.2 (3rd mode)	6–14	Low to moderate	70
Øresund Bridge [113]	Malmö, Sweden	192–262	250	0.47–3.19	4–18	Low to moderate	150
Erasmus Bridge [88]	Rotterdam, Netherlands	< 300	200	< 3	< 30	Low to moderate	500–700
Yangpu Bridge [114]	Shanghai, China	330	120	0.9–2.6	12–17	Moderate	1000
2nd Nanjing [114]	Nanjing, China	300	140	2	10–15	Low	1000

consensus of its underlying mechanism has not been reached. Among all the research, a wind tunnel test is considered the most effective way for its capability to simulate the conditions under which the RWIVs could occur. After they were first observed during the construction of the Meikonishi Bridge, the RWIVs were reproduced in a wind tunnel test by Hikami and Shiraishi [11]. They found that the formation of water rivulets on the upper windward surface would modify the cross section of the cable and hence made the cable aerodynamically unstable. A possible explanation for the mechanism of RWIVs could be the Den Hartog instability or the instability caused by coupled aerodynamic forces. Matsumoto et al. [115] proposed two factors that excite RWIVs on cables: axial flow in the near wake and the formation of upper water rivulets. In addition, they proposed that the rain-wind-induced vibration on cables can be treated as a vortex-induced vibration at high reduced velocity. The amplitude of the vibration is dependent on the yaw angle of the cables as well as the turbulence intensity of the wind.

More importantly, the location of the rivulets plays an important role in the RWIVs on cables, and measurements from wind tunnel tests showed that the rain-wind-induced vibration will be enhanced if the rivulets are formed at a specific angle on the cables. Flamand [116] verified the significance of the water rivulet and pointed out that it is the movement of the rivulet caused by the dirt coating that triggers the vibration of cables. Bosdogianni and Olivari [117] presented an idea that the existence of rivulets at a certain position causes the instability and therefore leads to an amplification of vibration in the form of galloping. Furthermore, they drew a conclusion that the movement of rivulets introduced by increasing wind velocity has little effect on the instability of cables. In order to investigate the influence of rivulets on rain-wind-induced vibrations, Gu et al. [118] conducted a wind tunnel test on a cable with artificial rivulets. The results from the test indicated that the relative location of an upper rivulet corresponding to the cable surface as well as the wind direction has a notable effect on the cable vibration, whereas the effects of a lower rivulet and the dimension of the upper rivulet can be ignored. Furthermore, the rain-wind-induced vibration can be considered as a type of galloping and it satisfies the Den Hartog's galloping theory, which echoed the conclusion made by Hikami and Shiraishi [11]. Xu et al. [119] obtained aerodynamic coefficients of an inclined cable with an

artificial rivulet attached to it. The measurements indicated that the negative slope of the lift coefficient might be the main reason for RWIVs on cables. Similarly, Du et al. [120] measured the pressure distribution on an inclined cable with an artificial rivulet. They proposed that the variation of aerodynamic force induced by the movement of rivulets is the excitation mechanism of RWIV. Given that most studies related to rain-wind-induced vibration on cables only take vertical vibration into account, Zhan et al. [121] presented a new experimental setup through which RWIV in the vertical and horizontal directions can be simulated simultaneously. In addition, the yaw angle of the cable can be easily adjusted in the newly designed vibration system, which significantly facilitates the wind tunnel test.

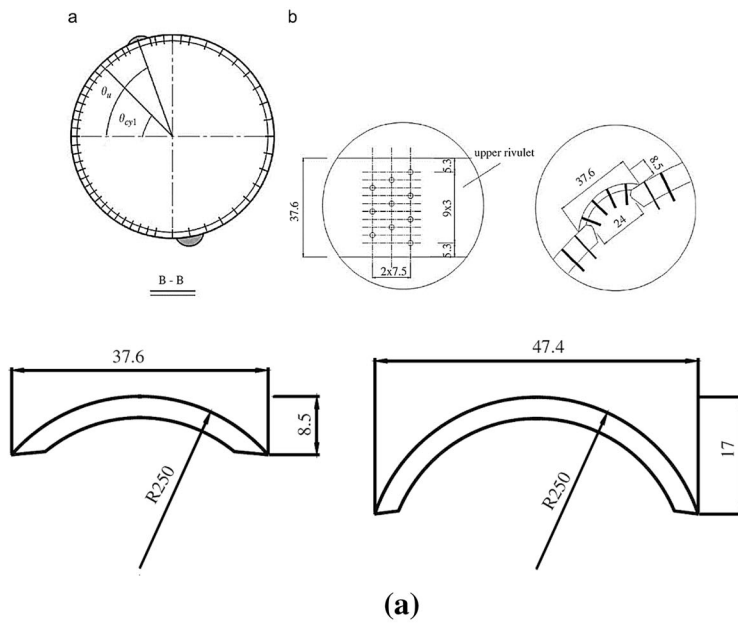
Based on the literature aforementioned, it can be concluded that the upper rivulet plays an important role in RWIVs on cables. As a result, various studies focused on the upper rivulet have been conducted. Cosentino et al. [122, 123] studied the movement and dimension of the rivulet when the cable was experiencing rain-wind-induced vibration. It was suggested that the flow regime modification, which was caused by the presence of the upper rivulet, is able to generate a downward aerodynamic load that would incur the RWIVs on cables. Wang et al. [124] examined the dependence of water rivulet formation on factors, such as wind speed, yaw angle of cable, and spraying water rate. In addition, the effects of water rivulets on the near wake of cables have been explored. It was proposed that the occurrence of RWIVs can be attributed to the coincidence of flow perturbation frequency and structural natural frequency. Chen et al. [125] reproduced RWIV of a cable in a wind tunnel test and measured the thickness, position, and shape of rivulets at a fixed section of the cable with an ultrasonic transmission thickness measurement system. However, they failed to provide sufficient information of the upper rivulet along the entire cable. The inherent nature of small size as well as the sensitivity to wind of the upper rivulet makes measurement techniques difficult to be employed. Li et al. [126] put forward a digital image processing technique to obtain the movement of water rivulets on cables. The movement of a water rivulet can be identified by processing the images recorded by a video system. The results have demonstrated that such a non-contact and non-intrusive technique is able to measure the rivulet efficiently with a high resolution. Jing et al. [127] quantitatively analyzed RWIVs

on cables using real water rivulets. The movement and the geometry of the upper rivulet were recorded by videogrammetry. The results showed that the attachment of a boundary layer to the cable induced by the vibration of rivulets can generate an aerodynamic force that would do positive work and hence render the cable to vibrate. Cheng et al. [128] developed a computer vision system, which consists of a high-resolution CCD camera and an image recognition technique. The rivulet width, film endpoints, and rivulet distribution along the cable were obtained through this system. Moreover, the oscillation frequency of the rivulet was calculated based on the time evolutions of a series of snapshot images. In order to improve the accuracy of simulation for rain-wind conditions, a high-precision raining simulator, which is capable of controlling rainfall intensity and raindrop size, was developed to replicate RWIVs on cables. Furthermore, coupling effects of wind velocity and rain intensity have been considered in the test carried out by Ge et al. [129]. In Fig. 16, some experimental designs and setups are presented.

In addition to the wind tunnel test, the mechanism of RWIVs on cables has been studied with various analytical approaches. Yamaguchi [131] analytically investigated the mechanism of RWIVs using the aerodynamic properties identified from a figure-eight-shaped section model. Two possible mechanisms, Den Hartog mechanism and two degree-of-freedom (DOF) instability, were examined. The results showed that the aerodynamic damping turns negative when the oscillating frequency of the upper rivulet becomes close to the natural frequency of the cable. The movement of the upper rivulet was coupled with the oscillation of the cable; therefore, the RWIVs on cables can be considered as a two-degree-of-freedom galloping instability. Xu and Wang [132] developed a single-degree-of-freedom (SDOF) numerical model to describe steady-state response of RWIVs on cables. The model, which assumed that the upper rivulet has the same oscillating frequency as the cable and that the amplitude ratio between the upper rivulet and the cable remains constant at a given wind speed, was capable of capturing some main characteristics of RWIV, such as velocity-restricted and amplitude-restricted vibration. Nevertheless, the axial flow and turbulence were not considered in this model due to the lack of information to quantify their effects. A similar SDOF model was proposed by Wilde and Witkowski [133]. Although the model was based on simplified assumptions by neglecting the

force between the water and cable surfaces as well as the three-dimensional air flowing around the cable, it can be employed to predict the maximum amplitude of rain-wind-induced vibration on cables.

Cao et al. [134] constructed a stochastic model in which the motion of water rivulets was described with a random process. The aerodynamic properties, such as lift and drag coefficients, corresponding to the location of water rivulets were obtained from the wind tunnel test. The simulated results based on this model indicated that the mechanism for large-amplitude rain-wind-induced vibrations on stay cables can be attributed to stochastic excitations induced by oscillating water rivulets. Cosentino et al. [122] presented a 3DOF model, which is made up of cable vibration in two directions and the motion of an upper rivulet. The velocity of the rivulet was expressed by empirical formula, from which the aerodynamic force was determined. Since the stability of a 3DOF model was demonstrated, it was also employed by Seidel and Dinkler [135]. The equations of motion were formulated by considering the motion of the upper rivulet as a movable disturbance. The influence of rivulets and its interaction with the cable are included in the equations. The numerical results showed that the proposed model is able to determine the lower limit and approximate upper limit of the velocity range over which the RWIVs on various inclined cables occur. Zhou and Xu [136] established a theoretical model that takes the consideration of wind speed distribution along the cable and the mode shape of cable vibration. The parametric study of the numerical simulations revealed that the decrease in tension on the cable would increase the maximum amplitude of RWIV. In addition, the amplitude of cable vibration would increase if the power exponent of wind speed decreased. Gu and Huang [130, 137] proposed a two-degree-of-freedom model that describes the motion of cable and rivulet, respectively. The governing equations were formulated and numerically solved using the aerodynamic properties identified from wind tunnel tests. Moreover, an instability criterion of rain-wind-induced vibrations on stayed cables were established and verified through the experiment. Wu et al. [138] developed a model that considers unsteady aerodynamics and hysteretic nonlinearity induced by the fluid memory, for which the quasi-steady theory fails to account. The parameters of unsteadiness and nonlinearity in this model were derived from the mapping of pressure and aerodynamic load obtained from wind tunnel tests. The



(b.1)



(b.2)

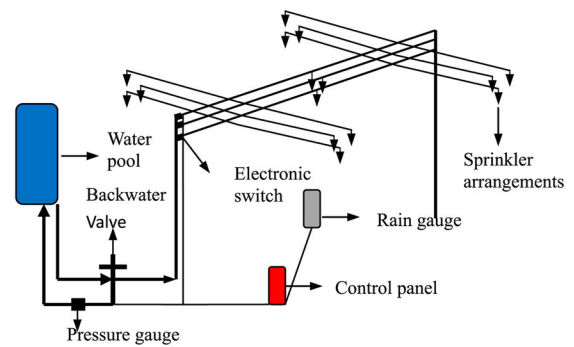


Fig. 16 Experimental studies on RWIV. (a) The artificial water rivulet used by Gu [130] to obtain aerodynamic properties. (b.1) Simple spraying tape system to simulate rainfall [129]. (b.2) High-precision raining simulator (HPRS) system to simulate

rainfall [129]. (c.1) Motion of upper rivulet captured by Li et al. [126]. (c.2) Motion of upper rivulet captured by Jing et al. [127]

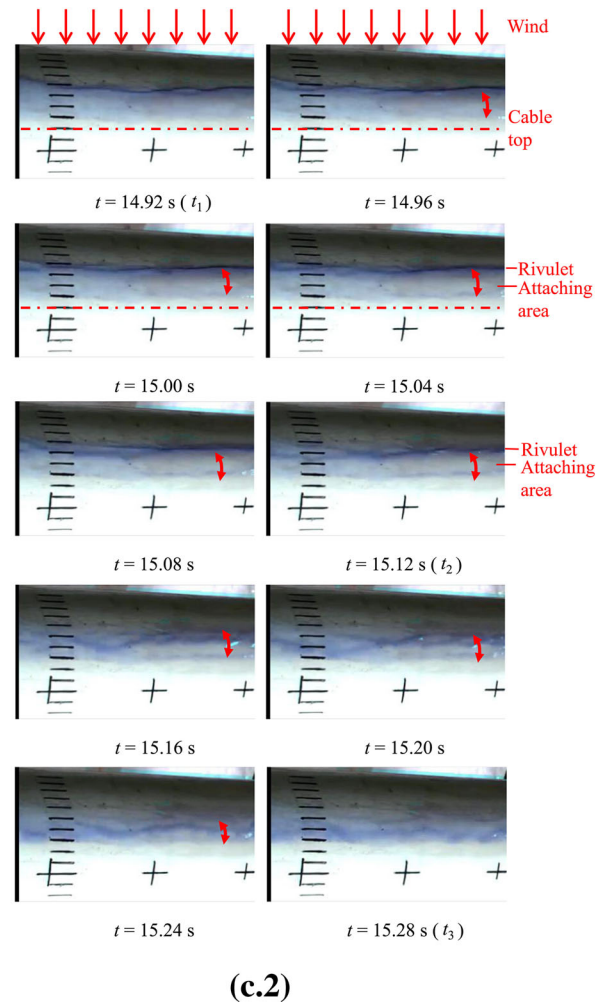
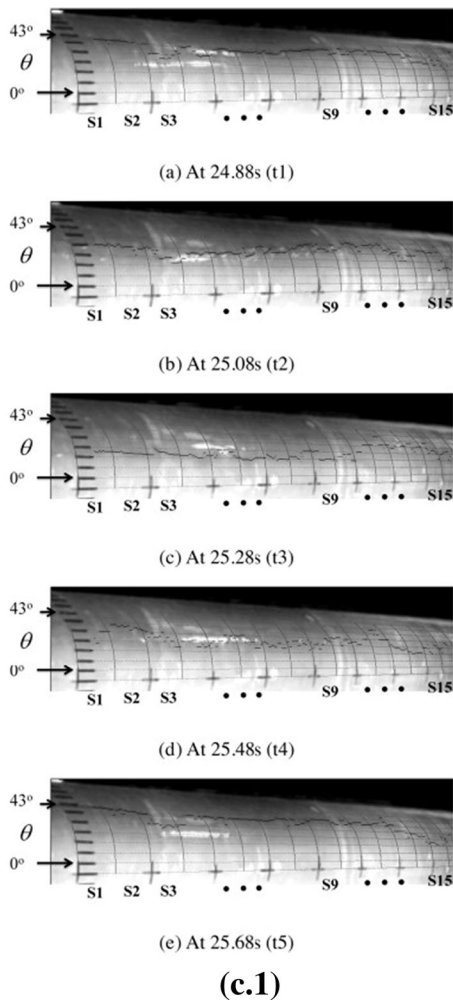


Fig. 16 continued

simulated results based on the proposed model exhibit a difference from the one obtained based on quasi-steady theory.

Lemaitre et al. [139] investigated the evolution of water film around a cable by developing a model involving gravity, surface tension, wind, and cable oscillation based on the lubrication theory. It can be observed from simulation results that the water film is accountable for the cable's instability. In addition, the location where the water rivulet appears is dependent on the wind speed. Xu et al. [140] used Lemaitre's model to study the influence of cable movement on the formulation of water rivulets. The evolution of water film was determined by varying a number of factors, such as gravitational force, wind pressure, friction, and sur-

face tension. Bi et al. [141] employed a computational fluid dynamics (CFD) technique to explore the evolution of water film on a vibrational cable. The gas-liquid two-phase theory and the volume-of-fluid (VOF) method were integrated to simulate the formulation of water film. The numerical simulations demonstrated that the upper rivulet, formed at a certain wind speed, generated an oscillating lift that has approximately the same frequency as the cable and leads to a large-amplitude vibration. Li et al. [142] established a model that represents the cable oscillation with two-degrees-of-freedom (in-plane and out-of-plane) and the motion of the rivulet as another degree of freedom. The interaction between the water rivulet and cable was first investigated, and the results suggested that RWIV can be

Table 9 Experimental studies of RWIV

Wind tunnel test								
References	m (kg/m)	n (Hz)	D (mm)	L (m)	α°	β°	U (m/s)	Water rivulet
Hikami and Shiraishi [11]	–	–	140	2.6	45	45	6–8	Real
Flamand [116]	16	0.1	160	7	25	0–90	6–13	Real
Bosdogianni and Olivari [117]	1	10.5	40	0.37	45	0–45	0–16	Real
Gu et al. [118]	3.5–10.4	1.06–2.09	120	2.5	30–45	0–45	3–16	Artificial
Du et al. [120]	–	–	350	3.5	30	0–45	5 and 10	Artificial
Zhan et al. [121]	11.9	1.21	140	2.13	30	35	9–14	Real
Cosentino et al. [122,123]	–	1.08	160	5.6	30–45	0–80	7–12	Real
Wang et al. [124]	–	–	45 and 19	0.6	45	0–45	8–15	Real
Chen et al. [125]	8.575	0.952	100	2	30	20–25	6–10	Real
Li et al. [126]	24.44	1.27	160	2.7	32	35	10–14	Real
Jing et al. [127]	24.44	1.27	160	2.7	32	35	12.1	Real
Cheng et al. [128]	–	–	98.36	8.31	23.39	45	7.92–15.85	Real
Ge et al. [129]	8.572	1.2	139	2.5	10–40	0–50	2–12	Real

considered as a type of galloping. Furthermore, Li et al. [143] carried out a wind tunnel test of RWIV on cables and validated that classical galloping can be triggered. Eight aerodynamic derivatives were determined from the test, and they concluded that unsteady, self-excited aerodynamic forces can model the RWIV more accurately than those from a quasi-steady model. Jing et al. [144] established a two-dimensional cable model based on the assumption that the instability of a stayed cable is introduced by interaction between boundary layer state, upper rivulet, and cable vibration. The effectiveness of such method was validated by the comparison between the numerical simulation and the experimental tests. A parametric study has been carried out in order to examine the influence of some factors, such as wind direction, wind speed, mechanical damping, and upper rivulet, on the amplitude of RWIV. The summaries of the past experimental studies and numerical modeling related to RWIV are shown in Tables 9 and 10, respectively.

Rain-wind-induced vibration is a great concern for engineers, as the large amplitude which RWIV tends to cause on the stayed cable could lead to a fatigue failure. Therefore, numerous methods have been proposed to mitigate the vibration on cables, and they can typically be categorized into aerodynamic and mechanical countermeasures. Since the upper rivulet formed on the cable's surface is critical in the occurrence of RWIV, aerodynamic countermeasures aim to modify a cable's

surface to disrupt the formation of an upper rivulet. Flamand [116] tested the effectiveness of spiraled wires and concluded that they are able to disorganize the movement of the upper rivulet and hence attenuate the vibration. Gu and Du [114] experimentally studied the effect of spiral wires in the mitigation of RWIVs on stayed cables. They have found that the diameter, twine direction, and pitch of the wires have significant influence on the mitigation efficiency. It was suggested that the optimized parameters for spiraled wires are 1 mm of diameter and 300 mm of parallel distance. Furthermore, they observed that the amplitude of RWIV decreases with the increase in mechanical damping. Miyata et al. [145] introduced discrete surface roughness as a way to suppress the cable vibration. Through the tests, it was ascertained that concave and convex patterns on the cable surface are effective against RWIV. Kleissl and Georgakis [146] performed a wind tunnel test to measure aerodynamic properties and employed a flow visualization technique to obtain the flow pattern around the cable with helical wire. Li et al. [147] carried out both experiments and numerical simulation to investigate the aerodynamic characteristics of stayed cables with helical wires. The results showed that helical wires have notable effects on cables, particularly on the aerodynamic forces and their correlation coefficients along the cable axis. Besides, the visual flow pattern around helical-wire cables was obtained from the numerical simulation results. Bi et al. [148] presented a numerical

Table 10 Numerical modeling studies of RWIV

Numerical simulation			
References	DOF	Model description	Conclusion
Yamaguchi [131]	2	Cable oscillates in vertical direction; upper rivulet moves in circumferential direction Quasi-steady theory is used to evaluate the unsteady aerodynamic forces	RWIV is a type of 2DOF galloping
Xu and Wang [132]	1	Upper rivulet has the same oscillating frequency with cable Amplitude ratio between upper rivulet and cable remains the same	The model is able to simulate velocity-restricted and amplitude-restricted characteristic of RWIV
Wilde and Witkowski [133]	1	Similar to Xu and Wang's model Initial position of rivulet depends on wins speed	The model can predict maximum amplitude of RWIV
Cao et al. [134]	2	Motion of water rivulet is described with a random process Aerodynamic force is formulated using quasi-steady theory	The mechanism of RWIV is attributed to the random vibration of water rivulet
Seidel and Dinkler [135]	3	The motion of cable is modeled in horizontal and vertical direction The rivulet is considered as a movable disturbance Aerodynamic force is formulated using quasi-steady theory	The model can determine the lower limit and approximate upper limit of the velocity range where RWIV occurs
Zhou and Xu [136]	1	The motion of upper rivulet is harmonic and follows the mode shape of cable Wind speed distribution along the cable and vibration mode of cable are considered Aerodynamic force is formulated using quasi-steady theory	Decrease cable's tension or power exponent of wind will increase the amplitude of RWIV
Gu and Huang [130, 137]	2	Cable vibrates in vertical direction; upper rivulet oscillates in circumferential direction on cable surface Aerodynamic force is formulated using quasi-steady theory Lyapunov stability criterion is employed to determine the stability criterion	The numerical simulated results agree well with experimental measurement
Wu et al. [138]	2	Cable vibrates in vertical direction; upper rivulet oscillates in circumferential direction on cable surface Unsteadiness and nonlinearity, which quasi-steady theory fails to account for, are considered Parameters are identified from mapping the pressure and load measurement of cable	The simulated results based on proposed model exhibit difference from the one obtained based on quasi-steady theory
Lemaitre et al. [139]	2	The evolution of water film on a cylinder is derived Effect of gravity, surface tension, wind, and motion of the support are considered	The model can recover the upper and lower rivulets that are responsible for RWIV

Table 10 continued

Numerical simulation			
References	DOF	Model Description	Conclusion
Bi et al. [141]	–	CFD is used to study the evolution of water film on cable Gas-liquid two-phase theory and the volume-of-fluid (VOF) method are adopted	The model can be used to calculate evolution of the water film, aerodynamic lift, and the vibration of cable
Li et al. [143]	3	The motion of cable is modeled with 2DOF (in-plane and out-of-plane) The rivulet is considered as another DOF The interaction between rivulet and cable is taken into account	RWIV can be considered as a type of galloping
Jing et al. [144]	2	Cable vibrates in vertical direction; upper rivulet oscillates in circumferential direction on cable surface Aerodynamic forces acting on the cable are determined by the boundary layer state	A comparison of numerical and experimental results shows that the model captures main characteristics of RWIV

model that is able to simulate the motion of a cable with arbitrary geometry and the evolution of water rivulets. The cable vibration and current state of water rivulets can be acquired by numerically solving the coupled equations. The proposed model was used to study a cable with ribs, and the results showed that the effectiveness of countermeasures is dependent on the number and location of ribs. The numerical and experimental tests carried out on cables with altered surfaces or cross sections will help to gain insight into a cable's aerodynamic characteristics and therefore reduce the rain-wind-induced vibration on stayed cables.

In addition to aerodynamic countermeasures, the rain-wind-induced vibrations on stayed cables can be suppressed with mechanical countermeasures through the modification of structural damping or stiffness. Damper is one of the most widely adopted mechanical countermeasures to mitigate RWIVs on stayed cables. Nakamura et al. [149] determined the damping coefficient of a high-damping rubber that is needed to control the rain vibration of cables. Tabatabai et al. [150] quantitatively studied the effect of viscous dampers on cable vibration and provided guidelines of designing a viscous damper to control rain-wind-induced vibration. Chen et al. [151] first installed MR dampers on the Dongting Lake Bridge to mitigate rain-wind-induced vibration. The advantage of MR dampers is that they

are capable of generating a high-damping force with a small amplitude and velocity. A 3-year yield measurement has been conducted in order to monitor the efficiency of MR dampers. The results proved that installation of MR dampers on cable-stayed bridges is an effective and durable way to suppress rain-wind-induced vibration. Li et al. [152] numerically investigated the effectiveness of dampers on RWIVs. The relationship between modal damping and the damping ratio of dampers has been revealed. It was found that 0.5% of the damping ratio is enough to reduce the RWIVs on No.2 Nanjing Yangtze River Bridge. Zhou and Xu [136] calculated the optimum damping ratio for dampers to fulfill the best suppression of RWIV of cables. Zhan et al. [121] performed an experimental test to check the effectiveness of dampers and spiral wires in the reduction of RWIVs. They have discovered that RWIV of cables nearly disappears if the damping ratio is greater than 0.43% or the cable is twined with spiral wires. Krarup et al. [153] proposed a pole allocation type active modal controller to control rain-wind-induced vibration on cables. The simulation results showed that the proposed method, which is able to add damping to several vibration modes, behaves better than an optimally tuned linear viscous damper. In Table 11, methodologies to control RWIV of cables are summarized.

Table 11 Methodologies to control RWIV of cables

	References	RWIV control method	Conclusions
Aerodynamic countermeasures	Flamand [116]	Wires	Spiraled wires are effective in RWIV mitigation
	Gu and Du [114]	Wires	The optimized parameters for spiraled wires to control RWIV are 1 mm of diameter and 300 mm of parallel distance
	Kleissl and Georgakis [146]	Wires	Aerodynamic properties and flow pattern of cable with helical wires are obtained, which can be used for RWIV control
	Li et al. [147]	Wires	Aerodynamic properties and flow pattern of cable with helical wires are obtained both numerically and experimentally, which can be used for RWIV control
	Bi et al. [148]	Wires	RWIV control can be achieved by changing the number and location of ribs on cable surface
Mechanical countermeasures	Miyate et al. [145]	Surface roughness	The concave and convex patterns on cable surface are effective against RWIV
	Nakamura et al. [149]	High-damping rubber	The damping coefficient of a high-damping rubber is determined to control RWIV
	Tabatabai et al. [150]	Viscous damper	Guidelines of designing viscous dampers to reduce RWIV are provided
	Chen et al. [151]	MR damper	MR damper is able to control RWIV of cables on Dongting Lake Bridge
	Li et al. [152]	Damper	Damper with 0.5% damping ratio is enough to suppress RWIV
	Zhou and Xu [136]	Damper	Optimized damping ratio of dampers is calculated to reduce RWIV
	Zhan et al. [121]	Damper and wires	Damper ratio greater than 0.43% is enough for cables with spiral wires to mitigate RWIV
	Krarpur et al. [153]	Damper	Active modal controller is proposed to control RWIV

5.3 Dry galloping (DG)

Dry-cable galloping has been frequently reported for cable bridges [154] and normally happens when there is a yaw and/or inclination angle between the cable axis and relative velocity. The past studies showed that dry-cable galloping is generally classified into two types of galloping. The first type, which is called unsteady galloping, happens when the axial flow is generated behind the yaw and/or inclined cable that interrupts the communication between vortices produced by the Karman vortex shedding. Unsteady galloping with a non-stationary amplitude can be studied using dynamic tests. The second classification of dry-cable galloping is called divergent-type, classical, or conventional galloping. This type has divergent motion and is explored

with static measurements of aerodynamic loads. Afterward, the aerodynamic damping of a cable is calculated with quasi-steady equations, and dry galloping appears on cases in which aerodynamic damping becomes negative. Divergent-type galloping has been mostly seen in the critical Reynolds number range or beyond due to variation of aerodynamic coefficients with respect to the angle of attack and Reynolds number. Although dry galloping has been investigated in the past with experimental methods and numerical approaches, the onset conditions of dry-cable galloping have not been fully explored for inclined/yawed cables.

Determining the required mechanical damping to suppress the dry galloping has been the most challenging part for designers of structural cables. The past studies proposed some empirical equations extracted from

Table 12 Constants to predict the reduced velocity [26]

β^{*o}	a	b	c
45°	7.03	0.6	46.07
40°	4.42	0.78	72.32
35°	5.95	0.79	86.33
30°	2.17	0.79	78.21
25°	3.32	0.78	70.71
20°	4.41	0.78	78.51
15°	1.23	0.8	81.94

wind tunnel dynamic tests to predict the critical velocity of the dry-cable galloping. The following equation is usually used to express these empirical equations.

$$RV_{cr} = a \times Sc^b \tag{5}$$

where $RV(= U_{cr}/nD)$ is the reduced velocity, Sc is the Scruton number, a and b are the constant numbers. Honda et al. [155] defined $a = 54$ and $b = 2/3$, and Irwin [156] determined $a = 35$ and $b = 1/2$. Other instability criteria have been introduced by the FHWA (Federal Highway Administration of U.S.) [157] and Saito [158], which proposed instability boundaries. Since this equation does not specify the effect of yaw angles, another research was conducted by Jafari and Sarkar [26] to determine the critical velocity for each yaw angle. They performed the wind tunnel experiments with a free vibration system to extract the critical reduced velocity based on aeroelastic parameters (flutter derivatives) of a yawed cable. The results of critical reduced velocity that were described as an empirical equation ($RV_{cr} = a \times Sc^b + c$) are summarized in Table 12.

Jafari and Sarkar [26] introduced a design procedure to determine the minimum required damping to suppress the dry galloping for different equivalent yaw angles. Their results can be used for yawed and/or inclined cables by finding the equivalent yaw angle. Furthermore, they extracted the aerodynamic buffeting admittance functions for yaw angles from 0° to 45° and provided empirical equations to calculate the drag coefficient and Strouhal number of a yawed cable. Figure 17 shows different criteria proposed to determine the critical wind speed of dry-cable galloping at a given Scruton number; unstable and stable regions are shown in this figure.

Since dry galloping can cause significant damages with high repair cost due to divergent motion, this phe-

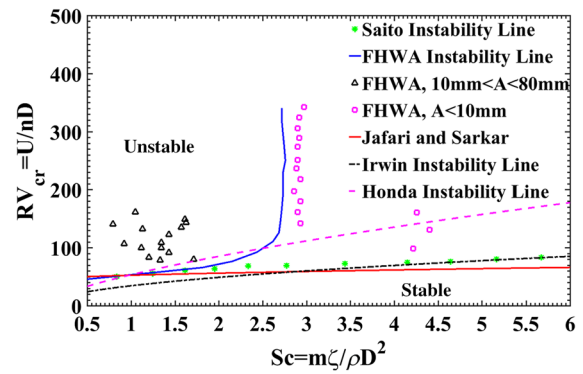


Fig. 17 Proposed criteria for unstable and stable regions of dry-cable galloping

nomenon has been widely studied to explore the vibration sources and propose the mitigation solutions using wind tunnel experiments or numerical approaches. The aerodynamic and aeroelastic flow characteristics of cables have usually been studied using a rigid/section model representing a section of a cable. Cheng et al. [159, 160] performed wind tunnel experiments in static and dynamic conditions to study the effects of Reynolds number, surface roughness, and wind speed on yawed/inclined dry-cable galloping. They observed the most divergent motions at a Scruton number of 0.88 and wind speed of 32 m/s. They also examined the applicability of Den Hartog’s criterion to predict the dry galloping and found it useful to determine the instability condition of dry-cable galloping. Moreover, they concluded that divergent motions in high speed might be because of the interaction between the axial flow and Karman vortex shedding. Katsuchi and Yamada [161] studied the effect of an indented surface on dry-cable galloping by performing wind tunnel experiments. They measured the reduced amplitude of a cable at different Scruton numbers and reduced velocities. As a result, they observed the divergent motion for both indented and smooth surfaces. Duy et al. [162] performed a series of wind tunnel tests for a yawed cable at different equivalent yaw angles. They studied the effect of spiral wire on a cable with a smooth surface and captured the divergent motions for yawed angles ranging from 30° to 60° at a reduced velocity of 110–130. Benidir et al. [163] studied the effect of surface roughness and circularity defect on dry-cable galloping by performing wind tunnel experiments to measure aerodynamic forces in static conditions. The obtained results showed that there is an obvious correlation between

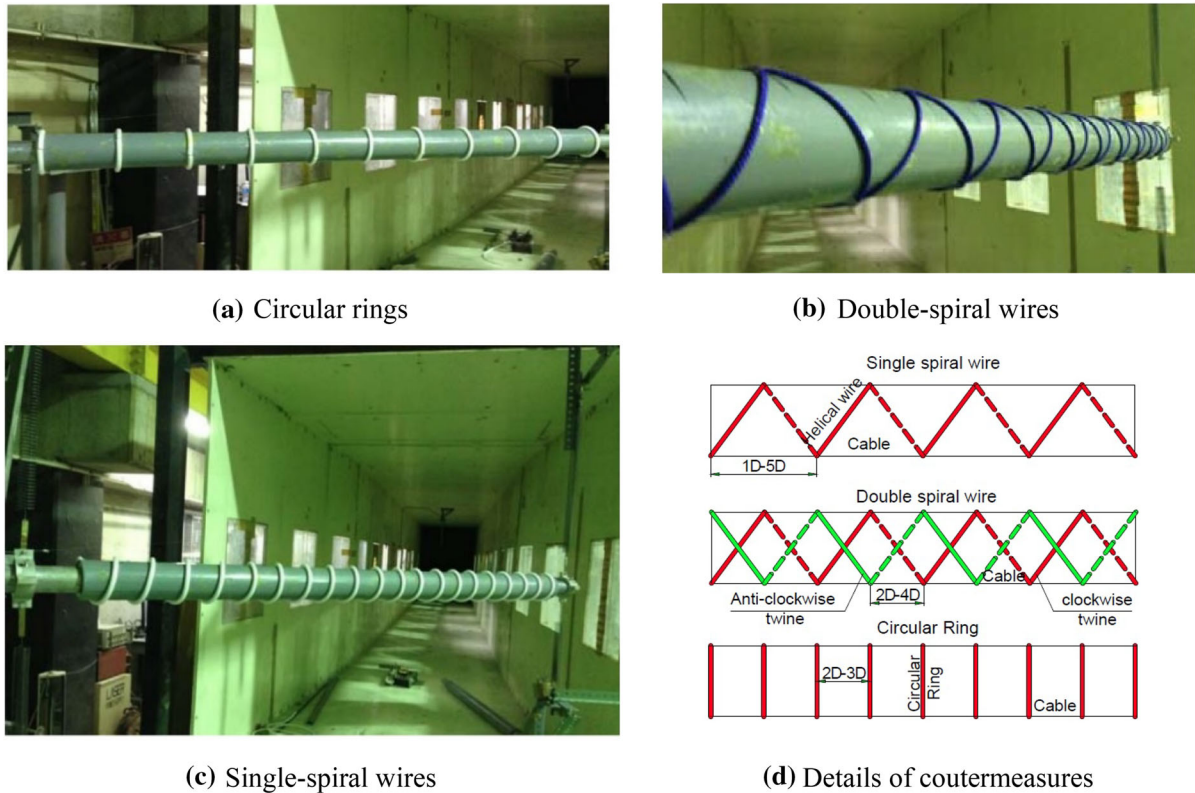


Fig. 18 Wind tunnel setup of different tested mitigation solutions [164]

the circularity defect and single bubble pressure pattern along the axis of the cable. Duy et al. [164] performed experimental tests in a wind tunnel to study the effect of helical strakes with diameters of 3 mm, 5 mm, 10 mm, and 15 mm on dry-cable galloping with and without helical strakes, as shown in Fig. 18. They found the critical equivalent yaw angle from 30° to 60° (see Fig. 19) by conducting experiments for equivalent yaw angles (β^*) from 20° to 70° . They concluded that single spiral wire, double spiral wire, and circular rings are more effective to suppress the dry-cable galloping if they are attached at specific spaces with an appropriate diameter. Another study [165] showed that dry cables with an attached helical fillet might experience large-amplitude responses at some angles for low mechanical damping. Therefore, further research is needed to completely explore the appropriate specification for helical strakes to mitigate dry-cable galloping.

Zuo and Jones [166] performed wind tunnel experiments for a circular cylinder, representing a section model of a cable, to study the effect of yaw and inclination angle on the excitation mechanism of dry-cable

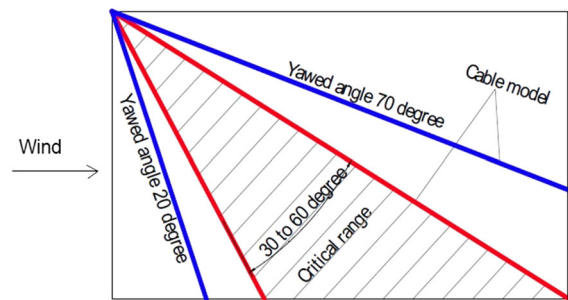


Fig. 19 Critical yaw angle range for single smooth cable [164]

galloping. They compared the experimental results with field measurements and concluded that a divergent response at high reduced velocity occurs for dry-cable because of high-speed vortex shedding, which is different from classical Karman vortex. They found a transitional mechanism between classical Karman vortex shedding and high-speed vortex shedding that occurs at high reduced velocity. Flamand and Boujard [167] captured the pressure distribution over a cable at different yawed angles and concluded that increasing

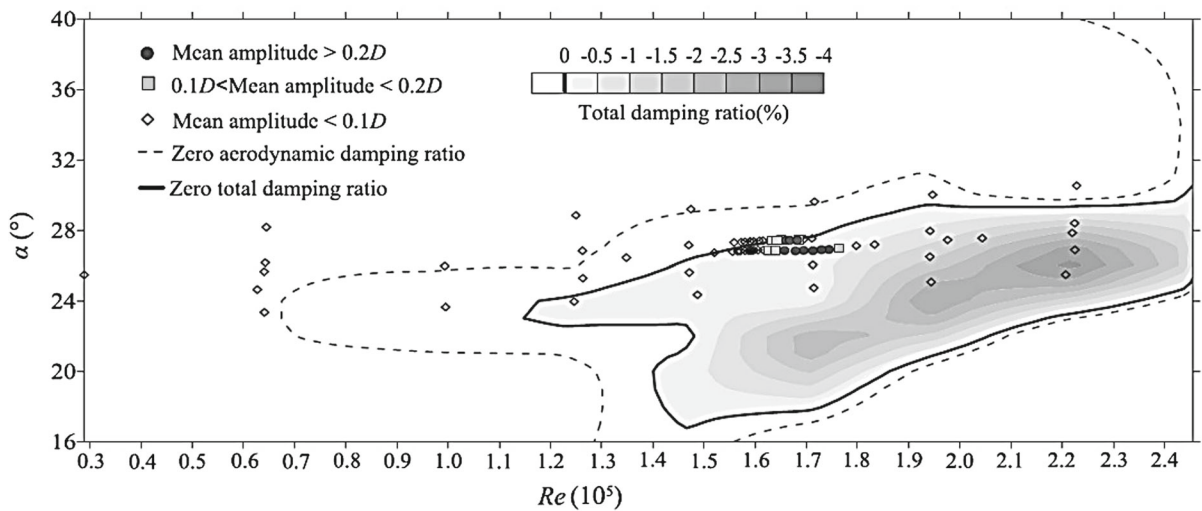


Fig. 20 Comparison of galloping instability for experimental data and predicted value [176]

the surface roughness is a solution for mitigating the vibration. Furthermore, they studied the effect of helical wire as a vibration mitigation device and indicated that using helical wires on cables is not only useful for suppression of rain-wind-induced vibration, but it is also effective for dry-cable galloping. Christiansen et al. [168] performed static and dynamic wind tunnel tests for an inclined cable with helical strakes to determine the characteristics of dry-cable galloping. The results showed that large-amplitude vibration can happen for a dry cable with inclination angle of 60° , and they concluded that the effect of surface irregularity on dry galloping is dominant. Kimura et al. [169] conducted a series of wind tunnel tests in smooth and turbulent flow at different yaw angles of 30° , 40° , and 45° . They observed divergent responses ($A/D = 2$) for some cases and concluded that the response becomes less intense by increasing the turbulence intensity. Matsumoto et al. [1] described the underlying mechanisms of dry-cable galloping due to wind-induced vibration through a series of experimental tests applying the splitter plates with various perforation (or porosity) ratios placed behind the cable in its wake to control the Kármán vortices. These results showed that the intensity of a Kármán vortex decreases, and divergent galloping arises when the perforation ratio decreases. The past studies also showed that the effect of axial flow is significant for the excitation of a cable because a non-yawed and inclined cable showed a divergent response when exposed to the generated artificial axial flow [1].

Moreover, they observed that the intensity and velocity of axial flow depend on the yaw angle significantly influencing the dry galloping.

Matsumoto and Shirashi [170] performed wind tunnel experiments for yawed and/or inclined cables to measure the dynamic response of a cable with and without rain. They conducted the dynamic experiments for only yawed cables without rain at yaw angles of 0° , 22.5° , 25° , 45° , and they concluded the response to be random rolling for yaw angles less than 25° , while the vibration amplitudes become more stable for yaw angles larger than 25° . In addition, the dynamic results indicated that the cable with yaw angle of 45° has the larger dynamic response at a given reduced velocity compared to other yaw angles. Zhou et al. [171] studied the behavior of vortex shedding from a yawed cable by conducting a point measurement with an eight-hot wire vorticity probe. They performed the experiments for yaw angles of 0 – 45° and concluded that the strength of the Kármán vortex shed decreases, while the three dimensionality of the flow over the yawed cylinder increases for yaw angles from 15° to 45° . McTavish et al. [172] conducted wind tunnel experiments for an inclined cable to extract the aerodynamic coefficients, such as drag, lift, and pressure coefficients. The results showed that dry galloping with large-amplitude vibration happens even for large damping or large Scruton number. They concluded that variations of aerodynamic coefficients in the critical range of Reynolds number can cause a large-amplitude motion;

even damping larger than that suggested by Post Tensioning Institution (PTI) is not enough to suppress the vibration.

Nikitas et al. [173] performed wind tunnel experiments to study the dry-cable galloping at the critical Reynolds number. According to the results, the aerodynamics of an inclined cable were different from a non-inclined cable, and the inclined cable generated nonzero lift components in the critical range of Reynolds numbers, concluded to be one source of dry-cable galloping. Nikitas and Macdonald [174] studied the aerodynamic characteristics of a cable by performing wind tunnel experiments. They observed the unsteady behavior in the critical Reynolds number range and concluded that the inclination angle was the most important parameter affecting this phenomenon. In another study, they used the aerodynamic properties of different cross sections to calculate the aerodynamic damping based on proposed quasi-steady criterion [175]. Ma et al. [176] studied the galloping of an elliptical cylinder at the range of critical Reynolds numbers since the cross section of a yawed and/or inclined cable is similar to an ellipse. They performed static and dynamic wind tunnel tests to study the aerodynamic and aeroelastic properties of an elliptical cylinder at different angles of attack. They observed the steady and unsteady galloping for a special range of angles of attack and Reynolds numbers. Afterward, they applied the quasi-steady theory to predict the galloping instability. The comparison matched in most cases with predicted values. Figure 20 shows the amplitude of vibration in a graphical plot for an elliptical cylinder at different angles of attack and Reynolds numbers, while total damping ratio changes.

Jubran et al. [177] studied the effect of interference and turbulence intensity on flow-induced vibration of single and tandem circular cylinders with rough and smooth surfaces. They performed wind tunnel experiments for smooth and turbulent flow with turbulence intensity up to 4.2% to measure the response of a cylinder at different reduced velocities. The results indicated that the amplitude of vibration increased for turbulence intensity of 0.2–3.5% by increasing the turbulent intensity, while the amplitude of response reduced by increasing turbulent intensity beyond 3.5%. Moreover, they showed that the vibration amplitude of a cylinder with a rough surface was higher than a smooth cylinder. In spite of the past studies that used rigid models to investigate the dry-cable galloping, Bartoli et al. [178]

built an aeroelastic cable including 48 sections to find the response and aeroelastic forces acting on a cable due to wind. They carried out their experiments for smooth and turbulent flow to capture the response in the along-wind direction. They compared their results with a numerical simulation and found a good match between them. Furthermore, they applied an incremental procedure along with an iterative procedure using a modified Newton–Raphson algorithm to predict the response in time domain.

Matteoni and Georgakis [179] investigated the effect of roughness and cross section distortion on dry-cable galloping due to wind-induced vibration. They concluded that the aerodynamics of a cable highly depend on the circularity of a cross section, and a little deviation may cause the generation of nonzero drag and lift coefficients leading to dry galloping in a special range of Reynolds numbers and wind angles of attack. They showed that aerodynamic damping calculated by quasi-steady method becomes negative for some angles of attack, which is the main source of dry galloping. In another theoretical and experimental study [180], it was showed that the galloping instability of cables significantly depends on angle of attack, and cables with a little non-circularity can considerably change the aerodynamic coefficients. They applied Eq. (6), which is derived based on quasi-steady theory and was used to calculate the aerodynamic damping. The definition of angles used in Eq. (6) is shown in Fig. 21 [181].

$$\zeta_{\text{aero}} = \frac{\mu \text{Re}}{4m\omega_n} \cos \alpha \left[\cos \alpha \left(C_D \left(2 \sin \Phi + \frac{\tan^2 \alpha}{\sin \Phi} \right) + \frac{\partial C_D}{\partial \text{Re}} \text{Re} \sin \Phi - \frac{\partial C_D}{\partial \alpha} \frac{\tan \alpha}{\sin \Phi} \right) - \sin \alpha \left(C_L \left(2 \sin \Phi - \frac{1}{\sin \Phi} \right) + \frac{\partial C_L}{\partial \text{Re}} \text{Re} \sin \Phi - \frac{\partial C_L}{\partial \alpha} \frac{\tan \alpha}{\sin \Phi} \right) \right] \quad (6)$$

where ζ_{aero} is the aerodynamic damping, μ denotes the dynamic viscosity, m represents the mass per unit length, ω_n is the circular natural frequency, and Re is the Reynolds number, α represents the angle of attack which is defined as $\alpha = \arctan(\tan \beta / \sin \theta)$, θ is the inclination angle, β is the yaw angle, and Φ denotes the cable-wind angle. The results of aerodynamic damping are plotted for different Reynolds numbers in Fig. 22. As shown in this figure, the aerodynamic damping becomes negative in the critical range of Reynolds number at specific angles of attack.

Fig. 21 Schematic view of inclined cable [179]

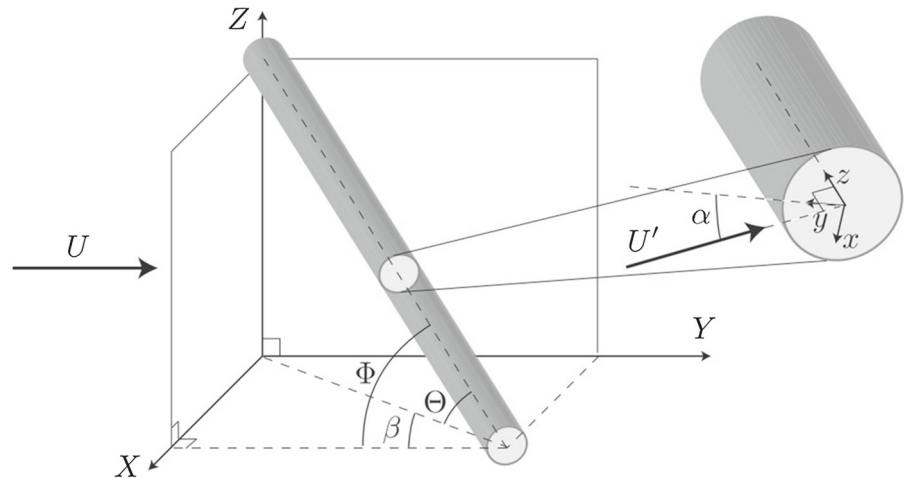
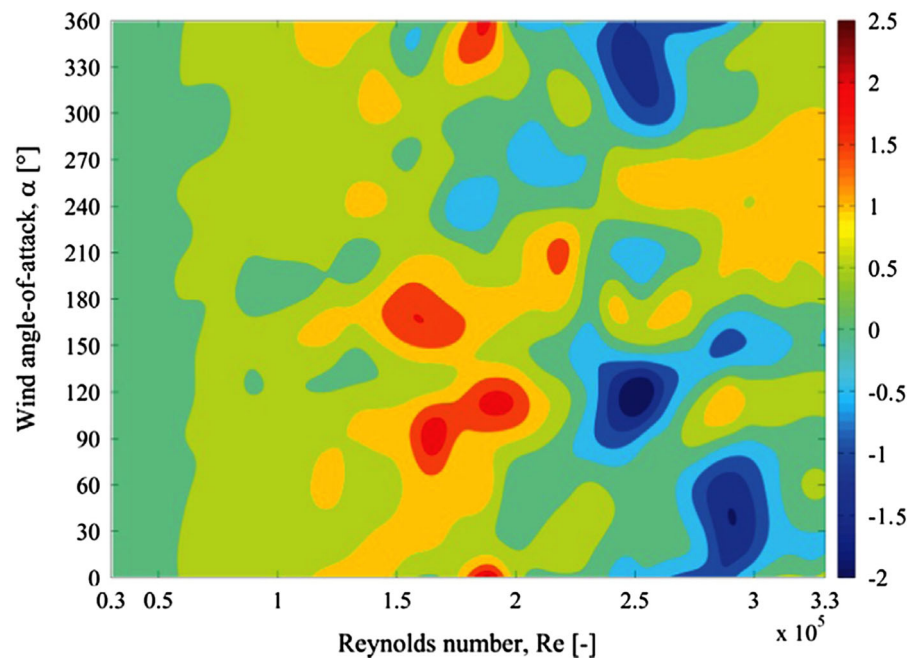


Fig. 22 Aerodynamic damping plot versus Reynolds number and wind angle of attack [180]



Kleissl and Georgakis [182] studied the effect of shapes including waviness, faceting, shrouding, and circularity (see Fig. 23) on cable vibration in dry conditions. They conducted the static wind tunnel tests in smooth and turbulent flow to calculate the aerodynamic damping. The results showed that dry galloping happens for plain, wavy, and faceted cylinders either from “drag crisis” or “Den Hartog galloping.” They found that the shrouded cylinder is the most stable case, generating positive aerodynamic damping. Moreover, the results indicated that cables have more positive aerodynamic damping in turbulent flow compared to smooth

flow due to a more constant lift force. Kleissl and Georgakis [183] studied the influences of helical fillets and pattern-indented surfaces on the aerodynamics of a yawed cable. They used the oil visualization tests to demonstrate the difference between the aerodynamics of a yawed cable with helical fillets and those with pattern-indented surfaces. The results with a pattern-indented surface showed the lowest drag coefficient, and the cable with helical fillets revealed a constant drag coefficient over the supercritical Reynolds number.



Fig. 23 Tested models, **a** circular cylinder, **b** shrouded cylinder, **c** wavy cylinder, **d** faceted cylinder [182]

Demartino and Ricciardelli [184] used numerical and experimental methods to determine the required mechanical damping using quasi-steady theory while studying the impact of cable irregularities, such as surface roughness, section distortion, and axis curvature. They found the aerodynamic coefficients of yawed and inclined cables at different angles. They used the experimental results to extract the aerodynamic damping at different Reynolds numbers, applying one-degree-of-freedom and two-degree-of-freedom (DOF) stability models. According to the results, cable irregularity had a significant effect on aerodynamic stability especially in the range of critical Reynolds numbers. Furthermore, they concluded that using a one-degree-of-freedom model is sufficient because it accurately predicts the required aerodynamic damping to prevent dry-cable galloping. Benidir et al. [185] studied the effect of circularity defects on dry-cable galloping by performing wind tunnel tests in the subcritical and critical range of Reynolds numbers. They applied artificial defects (up to 4.4% of the diameter) over the original cross section to investigate their effects on the aerodynamic coefficients leading to negative aerodynamic damping. They concluded that non-circularity of cables can significantly cause galloping instability. Additionally, they indicated that attaching helical strakes is helpful to mitigate dry-cable galloping.

Despite the extensive experimental research on dry-cable galloping, there are only a few studies using numerical simulations to study this phenomenon by simulating a section model. Yeo and Jones [186] conducted numerical simulations to investigate the impact of yawed angles on dry-cable galloping. They carried out their modeling for a yawed cable from 0° to 60° using a detached eddy simulation (DES) model for simulation and concluded that the strength of Karman vortices diminishes with increasing yaw angles. This phenomenon is significant because characteristics of flow in a three-dimensional model around a cylinder cannot be fully developed when Karman vortex shedding is strong and well correlated along the axis of a cylinder. They also numerically captured the characteristics of flow over a circular cylinder to determine the effect of yaw and inclination angles. The numerical results explained the mechanism of interaction between axial flow and vortex shedding causing unsteady low-frequency forces [187]. Wu et al. [188] used computational fluid dynamics (CFD) methods with the high accuracy model of a delayed detached eddy simulation (DDES) to simulate fluid flow over a yawed cable and verified the results by comparison with experimental data. Hoftzyer and Ragomirescu [189] carried out a three-dimensional numerical simulation using a computational fluid dynamics technique to study the effect of axial flow behind the yawed cable on inducing the dry-cable vibration. They used the turbulence model of a large eddy simulation (LES) for simulation of flow over yawed and inclined cables from moderate to high Reynolds numbers (110k–670k). Hayashi and Kawamura [190] conducted research on yawed circular cylinders using the direct numerical simulation (DNS) to study the effect of aspect ratio of a circular cylinder on flow characteristics. They demonstrated the applicability of the independence principle for the Reynolds number of 15,000 and validated their results by comparison with experimental data.

Analytical approach is another method that scholars have used to study this instability by deriving the mathematical equations to calculate the aerodynamic damping. Macdonald and Larose [181] applied quasi-steady theory to derive a theoretical formula describing dry-cable galloping. They derived an equation to calculate the aerodynamic damping and utilized the equation to determine the stability and instability of a yawed/inclined cable under dry conditions. In other studies [177, 178], they applied the quasi-steady the-

ory to demonstrate the galloping instability of a two-degree-of-freedom vibration system by calculating the aerodynamic damping. Raeesi et al. [193] theoretically derived formulae using a quasi-steady approach to show the effect of unstable/turbulent flow on dry galloping of an inclined cable. They applied their method to evaluate the aerodynamic stability of cables used in a cable-stayed bridge for unsteady wind, and their results satisfactorily predicted the aerodynamic instability. Furthermore, they proposed two- and three-degree-of-freedom aeroelastic models to estimate the response of a stayed cable and verified their results by comparing with field data [194, 195]. Luongo and Zulli [196] developed a nonlinear model to describe the non-planar dynamics of an inclined cable exposed to stationary wind. The simulations were conducted for different amplitudes of support motion, wind velocities, and excitation frequencies. The results showed that the galloping is perturbed when the support motion is small, and a considerable out-of-plan motion can be seen when a large support motion occurs. Carassale et al. [197] proposed a theoretical quasi-steady model to predict the galloping instability with high accuracy compared to the experimental results. They found that the galloping instability normally happens for a special range of Reynolds numbers, inclination angles, and yaw angles. Moreover, the proposed model was verified only for smooth flow, and the capability of the model was not assured for turbulent flow. Macdonald [198] proposed a theoretical model to predict the galloping instability by calculating the aerodynamic damping. He developed the proposed model to estimate the aerodynamic damping of an inclined cable for in-plane and out-of-plane vibrations. He found that this model can predict the galloping instability with reasonable accuracy. Piccardo et al. [199] reviewed the galloping of cables and described the existing theoretical quasi-steady models to explain the critical and post-critical conditions of galloping instability. Piccardo et al. [200] proposed a theoretical dynamic model considering sag due to dead weight of the cable and pre-stress, while it is applicable to model the dynamic response of dry-cable galloping for in-plane and out-of-plane vibrations. Some of the past studies on dry-cable galloping are summarized in Table 13.

5.4 Ice galloping (IG)

Galloping of power transmission lines that can also happen for cables with ice accretion occurs at low frequency (0.1–3 Hz), and high amplitude (5–100 times of the diameter of conductor, up to 10 m) [201]. Consequently, this large-amplitude vibration that induces the vibration of towers by $\sim 70\text{--}80\%$ [202] can cause severe hardware damages including flashover, wire burning, tripping, tower collapse, and accident. Some effective parameters on ice galloping are wind speed, ice shape, and wind angle of attack. After ice accretion on the conductor surface at wind speed of 0–2 m/s, the ice galloping can be seen at wind speed of 4–20 m/s when the ice thickness is within the range of 3–20 mm [201]. This type of galloping that can happen for cables especially power transmission lines arises when there is ice accretion on the surface of cable or conductor, and the ice usually accumulates on the windward side of cable. Atmospheric icing event in terms of time can be classified in three phases, namely accumulation, persistence, and shedding (dropping off) [203]. Although the icing event is a very complicated phenomenon that can change the physical properties, the ice accretion can be divided into three main processes: precipitation icing, in-cloud icing, and hoar frost [203]. Precipitation icing can be seen in different forms such as freezing rain (glaze) with density from 700 to 900 kg/m³ and temperature of -10° – 0° C, and wet snow with density of 400–600 kg/m³ and temperature of 0° to 3° C, and dry snow. In-cloud icing is a process that happens in the cloud or fog with rapid freezing of very cool water droplets. They can be as hard rime with density from 600 to 800 kg/m³ and temperature of -10° – -1° C, or soft rime with density from 200 to 600 kg/m³ and temperature of -20° – -1° C. Hoar frost is a process of ice accretion with density less than 300 kg/m³ that forms by direct condensation of water vapor to ice at the temperatures below freezing. Ice accretion might have different shapes, and the crescent and triangle shapes are the most common shapes. The ice thickness and two common shapes of ice accretion are shown in Fig. 24.

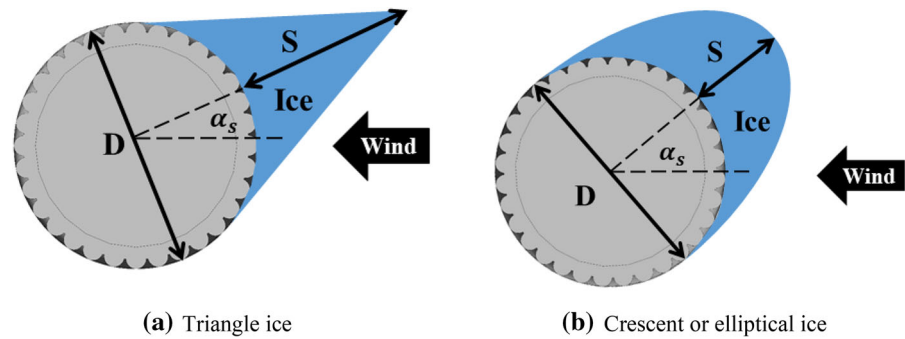
Two methods of anti-icing and de-icing are generally used to remove the ice from the surface of conductor. De-icing term is used for those methods that are applied after ice formation, but anti-icing term is used for those methods that are activated before ice accretion. De-icing methods mainly include thermal (ice melting), mechanical (ice breaking), and passive

Table 13 Numerical and experimental studies of dry-cable galloping

References	Re	Sc	U (m/s)	n (Hz)	ζ (%)	m (kg/m)	α°	β°	D (mm)	L (m)	I_a (%)	Sys. type	Test
Matsumoto et al. [170]	< 150k	NA	NA	NA	NA	NA	0, 30, 42.5	0, 22.5, 25, 45	160, 50	1.6, 1.5	Sm	Dyn	WT
Bartoli et al. [178]	25k–75k	NA	10–30	1.22–3.48	NA	0.937	0	0	40	1.92	< 1	Aeroelastic	WT
Duy et al. [162]	< 70k	0.586	< 14	1.15	0.127	3.322	25, 35, 45, 60, 70	55, 20–70	75	1.8	NA	Dyn	WT
Cheng et al. [159, 160]	100k–350k	1.76	15–65	1.4	0.03–0.6	60.8	20–60	0–45	160	6.7	0.13	St and Dyn	WT
Flamand and Boujard [167]	130k–350k	–	NA	–	–	–	0	0–70	200	4.7	0.75	St	WT
Katsuchi and Yamada [161]	65k–191k	1.42–2.91	< 25	1.78–2.77	NA	NA	0	0–30	86	1.8	NA	St and Dyn	WT
Zuo and Jones [166]	130k–670k	NA	2.06–11	3.52–3.8	0.35	2.14	0, 16	56.6, 90	91	1.45	0.1	Dyn	WT
Kleissl and Georgakis [183]	20k–300k	–	< 32	–	–	–	40, 55	NA	160	1.53	0.41–0.64	St	WT
Kimura et al. [169]	< 500k	0.76–0.92	< 60	0.784–1.012	0.044–0.541	12.66, ~26.00	30, 40, 45	0	114	1.18	Sm and 4.6, 10.4	Dyn	WT
Matteoni and Georgakis [179]	18k–320k	–	2–31	–	–	–	40, 55	NA	160	1.528	1.1, 0.5	St	WT
Matteoni and Georgakis [180]	< 320k	0.56	0–30	1.1	0.1	18.07	25, 55	30, 60	160	2.55	0.53	Dyn	WT
Larose et al. [165]	43k–391k	$Sc_x = 2.1–3.3$ $Sc_y = 1.5–1.7$	4–36	$n_x = 1.38$ $n_y = 1.40$	$\zeta_x = 0.10–0.15$ $\zeta_x = 0.07–0.08$	60.6	45, 60	0	162	6.7	NA	St and Dyn	WT
Benidir et al. [163]	96k–330k	–	NA	–	–	–	0	0	140, 200, 355	250, 2	–	St	WT
Benidir et al. [185]	103k–404k	–	0–28	–	–	–	90	0	250	2	< 1.1	St	WT
Christiansen et al. [168]	130k–370k	1.5–1.7	4–36	1.38–1.40	0.07, 0.08	66.7	45, 60	0	161.7	6.7	0.5	St and Dyn	WT
Demarino and Ricciardelli [184]	105k–320k	–	10–30	–	–	–	30	0–180	160	1.42	< 0.8	St	WT
Hoflyzer and Elena Dragomirescu [189]	110k–670k	–	8.6–57	–	–	–	0–60	45	89	2.67	NA	St	CFD
Yeo and Jones [186]	140k	–	NA	–	–	–	45	30	D	10, 20, 30	DNA	St	CFD

WT wind tunnel, St static, Dyn dynamic, Sm smooth, Th turbulent, CFD computational fluid dynamics, NA not available

Fig. 24 Schematic view of ice accretion on conductor with different shapes



(natural force) methods [204]. Some anti-icing techniques consist of freezing point depressant liquid, ferroelectric coating, ferromagnetic materials, electrical tracer, and Joule effect [203].

The wind-induced galloping of power transmission lines has been studied since early 1930 by using the one-degree-of-freedom (1DOF) dynamic system [27, 205, 206]. Afterward, the new approaches applying two-degree-of-freedom (2DOF) system in vertical and torsional directions [28, 207, 208] were proposed to model the galloping of structural cables and conductors that was also observed in the field measurement [209]. In fact, the results indicated that the torsional/twist motion initiates the galloping instability [210, 211]; thus, three-degree-of-freedom systems [212, 213] along with linear and nonlinear models were developed to consider vertical, lateral, and torsional effects on modeling this complex instability [214]. This phenomenon has been widely investigated using numerical or experimental techniques [215, 216] to determine the important factors being effective on ice accretion [217] on tower [202, 218] or wires and galloping [203, 219, 220] of cable or power transmission lines. In 1981, Nigol and Buchan [221] performed wind tunnel tests to evaluate the effect of ice accretion on the aerodynamic coefficients and used Den Hartog's criterion to estimate the aerodynamic damping. They concluded that the galloping instability of iced conductor cannot be predicted accurately with static measurements and dynamic system is required to better estimate the damping characteristics. Kim and Sohn [222] used a combination of numerical simulations and wind tunnel tests to determine the wind-induced response of iced conductor for two shapes of ellipse and triangle. They extracted the damping by the multi-body dynamic analysis using free vibration system and Rayleigh damping theory, and the aerodynamic coefficients were calcu-

lated by the ANSYS Fluent software. Finally, they concluded that the drag coefficient increases for larger ice thickness, while the lift coefficient is zero for angles of attack of 0° and 180° . Moreover, the vibration amplitude for triangle-shape ice was higher than ellipse shape.

Zdero and Turan [223] measured the Strouhal number and vortex shedding frequency of iced conductor at different angles of attack and ice thicknesses. They observed the dual-vortex shedding frequency peaks for a special case with the zero angle of attack and wind speed greater than 22 m/s. They also found that the Strouhal number at zero angle of attack has almost the highest value compared to other angles of attack. To extract the aerodynamic coefficients of single ice conductor, Xinmin et al. [224] performed the wind tunnel experiments for D-shape and elliptical-shape ice accretion. The results demonstrated that the aerodynamic coefficients widely change with angle of attack, and the absolute value of aerodynamic forces increases for conductors with thicker ice. Dyke and Laneville [225] used a D-shape artificial ice to simulate the ice accretion on power transmission lines and conducted the field measurement to capture the dynamic response of single iced conductor at different wind directions. They concluded that the yaw angle has a strong influence on the ice-conductor galloping. Chabart and Lilien [226] performed a series of wind tunnel experiments in stationary and dynamic conditions to measure the aerodynamic and aeroelastic forces acting on single iced conductor. The experiments were conducted for angles of attack ranging from -180° to $+180^\circ$ to measure the aerodynamic coefficients and observed that the lift coefficient is almost independent on wind speed ranging from 10 to 20 m/s. As a new approach, Meng et al. [227] studied the ice accumulation on power transmission lines through physical testing and hanging lumped

loads. They also developed a numerical code to simulate the response of iced conductor based on obtained results and verified the accuracy of results with method that was used for prediction of ice-conductor galloping. Chadha and Jaster [228] studied the effect of ice accretion using wind tunnel tests and presented a mathematical model for prediction of the galloping response of iced conductor with different ice shapes. They concluded that an iced conductor, which is stable based on Den Hartog's criterion, may still vibrate due to the effect of coupling motions. Additionally, the vibration amplitude estimated by the models that considers inertia coupling is larger than those calculated by Den Hartog's criterion. Gurung et al. [229] conducted a field measurement study on the Tsuruga Test Line, where is located near Tsuruga Bay, to characterize the galloping response and gust response of iced conductor. They measured the dynamic response, frequency, and aerodynamic damping and observed two-loop mode in case of dead-end span for typical galloping.

Matsumiya et al. [230] studied the effect of ice accretion on power transmission lines using wind tunnel tests for four-bundled conductors. They performed experiments in static and dynamic conditions to measure the aerodynamic/aeroelastic force and dynamic response. They presented two different formulations, while the first formulation studies all conductors as one group and the second one considers them individually. They found that it is better to study the galloping of iced conductor individually to have a better estimation. In another research to investigate the ice galloping of four-bundled conductors [231], a series of wind tunnel was performed to extract the aerodynamic forces of power transmission lines using the real conductors at different ice thicknesses, initial ice accretion angles, bundle spaces, and wind angles of attack. The results showed the change in initial ice accretion angle significantly influences the aerodynamic coefficients. For the iced eight-bundled conductors, Zhou et al. [232] conducted a research using wind tunnel experiments to investigate the effect of ice accretion on dynamic response, frequency, and vibration mode of bundle conductors. Moreover, they studied the effect of interphase spacer on the characteristics of iced-conductor galloping. Zhou et al. [233] performed the wind tunnel experiments for iced eight-bundled conductors and used the finite element code in ABAQUS software to simulate the wind-induced vibration of iced conductors. They reported the dynamic response and vibration mode for

different angles of attack and span lengths. They found that the galloping mode becomes more complicated in higher wind speed and consequently more loops may appear, while span length has no effect on galloping mode and more span length enlarges the amplitude of vibration. In another study on four-bundle conductors [234], the experimental data by wind tunnel tests and numerical results from simulation with ABAQUS were used to investigate the influence of wind speed, angle of attack, ice thickness, ice shape, and span length on ice-conductor galloping. They carried out the experiments for two shapes of crescent and sector with different thicknesses. The results indicated that the vibration amplitude increases with increment of wind speed, ice thickness, and span length. Additionally, they observed larger dynamic response of bundle conductors with sector-shape ice compared with crescent shape.

Ma et al. [235] conducted the experimental tests to explore the effect of Reynolds number on dry- and ice-cable galloping using circular cylinders with and without semi-elliptical cross sections. The results of semi-elliptical cross section showed that ice accretion on the surface of cables has some considerable effects on the aerodynamic forces acting on this structure. Li et al. [236] studied the effect of six different shapes on ice-cable galloping with performing the experiments in wind tunnel to extract the aerodynamic coefficients in stationary condition. Afterward, they used the obtained results to calculate the critical wind speed for real structural cables based on quasi-steady theory and linear and nonlinear models. They reported the critical wind speed of the cable-stayed bridge named Yangpu Bridge within the range of 18.3–27.5 m/s, while these velocities are less than design wind speed at that location. Demartino et al. [237] simulated the ice accretion on the bridge cables for fix inclination angle of 30° and yaw angles ranging from 0° to 180° using climatic wind tunnel at temperature ranging from -10° to +20° C. They measured the aerodynamic coefficients of drag, lift, and moment at different wind speeds, yaw angles, and temperatures. The results indicated that the mean aerodynamic coefficients are independent on wind speed and observed a strong effect of type and dimension of either rims or glaze ice on the flow characteristics around inclined cable. Figures 25 and 26 show the development of ice on the surface of cable that depends on the time and temperature.

Analytical models, e.g., quasi-steady theory, and numerical simulations, e.g., computational fluid dynam-

Fig. 25 Development of ice accretion with time [237]

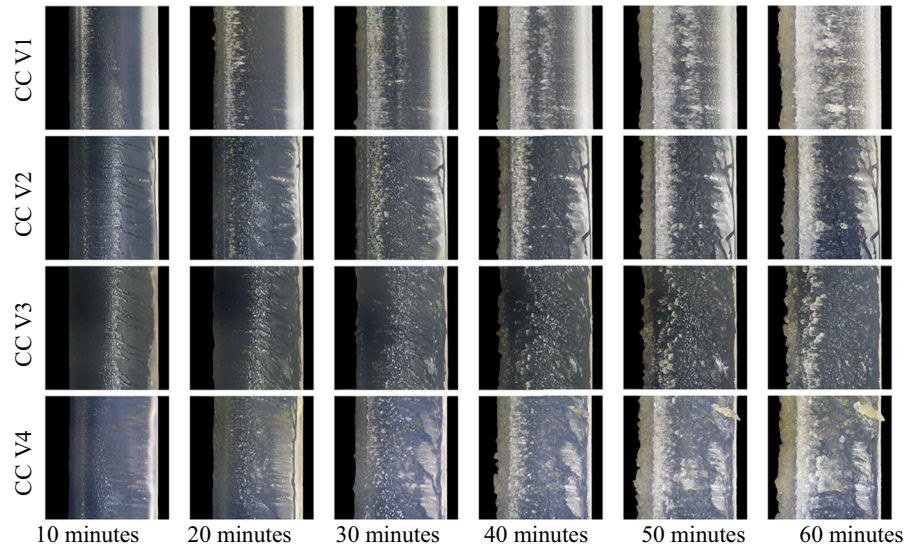
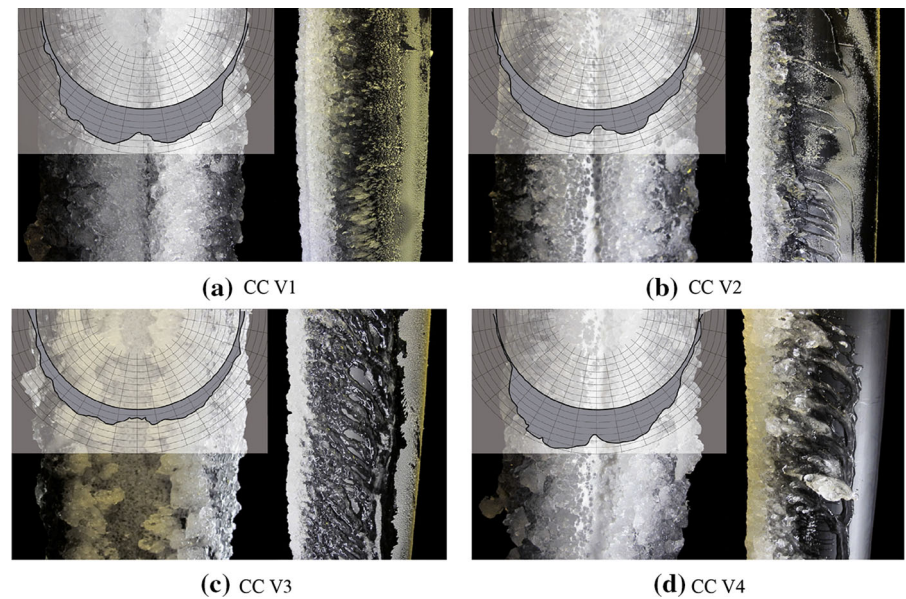


Fig. 26 Front and lateral view and contour tracing of cable after ice accretion for different cases [237]



ics (CFD) techniques and finite element models (FEM), have been used to model the ice galloping and predict the instability region or critical wind speed that cable or conductor is prone to the galloping. Zhang et al. [238] studied the influence of conductor shape on icing collision efficiency using a series of numerical simulations to determine the effect of conductor's strand number on the collision efficiency. They carried out the simulations for conductors with strand number ranging from 6 to 18 and wind speed from 5 to 30 m/s. The numerical results of two-dimensional simulations showed that the collision efficiency at the same envi-

ronmental conditions slightly changes for conductors with different strand numbers, while wind speed and median volume diameter (MDV) of the droplet distribution influence the collision efficiency of conductors with different strand numbers. McComber and Paradis [239] proposed a new approach to predict the galloping instability of power transmission lines with a thin ice accretion while including the influence of torsional vibration on the lift force by the existing quasi-steady model. They showed that the proposed model can accurately predict the galloping of conductors with thin ice which helps to determine the solutions for prevention

of iced galloping. Foti et al. [240] proposed a model to predict the galloping instability of smooth cables with ice accretion using finite element method and validated the proposed procedure with a case from the literature. Gjelstrup and Georgakis [241] and Gjelstrup et al. [242] developed a three-degree-of-freedom (3DOF) model to determine the galloping instability of smooth cables with ice accretion that was applicable for other prismatic bluff bodies. For the proposed model, it is required to measure the drag, lift, and drag forces at different Reynolds numbers and angles of attack. Finally, the results of this model provide the required external damping to prevent the ice-cable galloping.

Richardson [243] conducted the field measurement to determine the critical wind speed of ice galloping of a conductor with diameter of 29.5 mm. He observed the galloping and flashover for wind speed of 8.9 m/s and greater. Furthermore, the results indicated that using drag enhancement and conductor twisting device prevents the flashover, while the detuning pendulum was not useful to suppress the vibration. Kim and Byun [244] proposed a new discretization method to simulate the galloping of conductor with ice accretion. Additionally, they studied the effect of some reduction methods to suppress the ice galloping and found them practical solutions. He and Macdonald [245] proposed a two-dimensional 3DOF model based on quasi-steady theory to predict the galloping instability of an iced power transmission line. They validated the results of proposed model by comparison with the past data from the literature. Moreover, the results indicated that a little change in cross section due to ice accretion influences the aerodynamic and stability of cable. In another study, a linearized method was proposed by Mcdaniel [246] to analyze the galloping of power transmission lines with ice accretion and this method was found to be a practical model for prediction of ice galloping. Foti and Martinelli [247] applied the formulation of beam and cable element theory to study the dynamic response of power transmission line with ice accretion. The simulation results showed that the critical wind speed of iced galloping is 5 m/s. Moreover, the comparison between the results of cable and beam element theory indicated similar results while both predicting the galloping response accurately.

Desai et al. [248] studied the ice galloping of conductors using finite element method (FEM) and verified the results with experimental data. They found that it is necessary to model the multi-span conductors for esti-

mation of vibration. In another research, a new model was introduced by Zhang et al. [249] that included the coupling motions of vertical, horizontal, and torsional directions for prediction of iced galloping. Yan et al. [250] developed an analytical model based on curved beam theory for single iced conductor considering the coupled translational and torsional motions. The results indicated that the angle of attack changes at high wind speed which results in instability of conductor. Another significant result is that the critical wind speed increases as ice thickness enlarges over the surface of conductor. They also observed the one- and two-loop galloping at different angles of attack. Yan et al. [251] developed a model based on curved beam element method to simulate the dynamic response of multi-span bundle quad-conductors with ice accretion. They also used the cable element theory to compare its results with curved element theory. They concluded that the curved beam model that includes more degrees of freedom and coupled transitional and torsional motions have a better prediction of iced-conductor galloping. They found that using hinges are more helpful to suppress the galloping of ice galloping compared with rigid connections. The capability of curved beam theory in prediction of ice galloping was also studied by Yan et al. [252] using a nonlinear model with involving the components of three transitional and one twist directions. In another 2DOF model that was developed by Ye et al. [253], the galloping instability of iced conductor was captured by numerical analysis, and a mixed-mode phenomenon was observed for galloping of the eccentric conductor with accumulated ice. Wang and Lou [254] applied finite element method and cable element theory to simulate the ice accretion on power transmission line. They modeled the insulator strings, remote span, and turbulence flow by the time-domain simulation. The support condition and wind speed were found the most significant factors impacting on the vibration amplitude of conductors.

Wang and Lilien [255] proposed a 3DOF mathematical model to predict the dynamic response of ice galloping that can be used for single and bundle conductors. This model can simulate the one-, two-, and three-loop galloping with the second-order coupling between all three vertical, lateral, and torsional directions. They studied the effect of some anti-galloping devices on mitigation of iced-conductor galloping. Furthermore, they concluded that those devices which mix the detuning and torsional damping effects are the most

effective solutions to reduce the large-amplitude vibration of ice galloping. Kollár et al. [256] used the ADINA software to numerically simulate the dynamic response of iced conductor with interphase spacer. The numerical results were verified with experimental data from the literature. They observed the significant effect of spacer in suppression of ice galloping to reduce the flashover. Furthermore, they studied the effects of different ice shedding processes on the dynamic response and stress generation due to iced-conductor galloping. The capability of this software in modeling the dynamic response of ice conductor has been also evaluated by other studies [257, 258]. Some of the past experimental studies on ice galloping of cables or conductors are summarized in Table 14.

5.5 Wake galloping (WG)

Wake-induced galloping of twin circular cylinders has been widely studied in the past by performing wind or water tunnel tests to study the aerodynamic or hydrodynamic forces, dynamic responses, and flow characteristics. Over the past decades, several review papers have been published by Zdravkovich [259, 260], Sumner [261], Bearman [262], and Zhou et al. [263] on this interesting topic due to its wide applications. However, the wake-induced cable vibration has not been fully studied because the distance between parallel cables is usually greater than critical range that stabilizes them to wake galloping. In this section, the flow characteristics over twin cables and circular cylinders are reviewed to understand the effects of different parameters such as incident angle and vertical and horizontal space ratios on the dynamic response of downstream model. In general, twin cables or circular cylinders may have three major arrangements of tandem, staggered, and side by side, and some effective parameters such as incident angle (θ), vertical ($T^* = T/D$), horizontal ($L^* = L/D$), and inclined ($P^* = P/D$) space ratios are defined as shown in Fig. 27. Tandem arrangement is the most common case that happens for twin cables.

The flow behavior around twin cylinders is classified into three interference regions which depends on vertical and horizontal space ratios as shown in Fig. 28. Wake interference occurs when one cylinder is partially or completely in the wake of another one, and proximity interference happens when two cylinders are close to each other, but neither of them is in the wake area. In

another classification, Zdravkovich [260] divided the flow regime over twin cylinders into three types: (1) single bluff-body behavior happening for space ratios ranging from $1.0 < L^* < 1.2$ – 1.8 where the downstream cylinder is close to upstream one and they act as a combined single cylinder; (2) shear layer attachment behavior that usually occurs for space ratios ranging from 1.2 – $1.8 < L^* < 3.4$ – 3.8 where the shear layer of upstream cylinder reattaches the downstream one; and (3) vortex shedding generation from cylinders that can be seen for space ratios of 3.4 – $3.8 < L^*$, where each cylinder produces the vortex shedding separately [264].

Wake-induced cable galloping has been reported for smooth cables and power transmission lines that usually happens for moderate space ratios [2]. For smooth tandem cable, the only criterion to describe the onset of the wake galloping instability has been proposed by FHWA [157] that is triggered when the wind speed exceeds $U_{\text{crit}} = c f_n D \sqrt{Sc}$, where c is a constant dependent on inter-cable spacing and orientation, f_n is a natural frequency, D is the cable diameter, and Sc is the Scruton number. The constant number of c is 25 and 80 for horizontal space ratios (L^*) of 2–6 and $L^* \geq 10$, respectively [157]. Although this type of galloping, which can occur for smooth cables and power transmission lines, has been reported less than other vibration sources, it has been studied by using wind tunnel tests and numerical approach to determine the critical velocity and flow characteristic of twin cable describing the wake-induced cable galloping.

Yoshimura et al. [266] conducted a research performing wind tunnel tests to develop a new mitigation device to suppress the wake galloping of two parallel cables. They did the experiments for staggered configuration at different incident angles and concluded that the critical incident angle is 5° . Tokoro et al. [2] studied the aerodynamics of tandem cables by performing a series of wind tunnel tests for different space ratios ranging from 4.3 to 8.7 to study the wake galloping of parallel aeroelastic model. They concluded that the cables are stable for space ratios greater than 6.5 and showed that the vibration of leeward (downstream) cable depends on both reduced velocity and Reynolds number. Figure 29 shows the vibration trajectory of leeward cable at different Reynolds numbers and reduced velocities. This figure demonstrates that the trajectory direction depends on Reynolds number and reduced velocity.

Table 14 Summary of the past experimental studies on ice galloping of cables or conductors

References	Re	Sc	U (m/s)	n (Hz)	ζ (%)	m (kg/m)	AOA (α_e°)	α°	β°	D (mm)	L (m)	I_u (%)	ST	TF	IS	IT (S) (mm)	No
Zadero and Turan [223]	2k-70k	-	0.2-30	-	-	-	0, 45, 90, 135, 150, 160, 170, 180	0 0 0	0 0	30.5	0.52	0.3-0.9	St	WT	Cr	3.05, 9.15, 12.2	S
Li et al. [236]	99k	-	12	-	-	-	0-180	90 0	0	120	0.6	NA	St	WT	Cr	10, 50, 80	S
Demarino et al. [237]	NA	-	8-29	-	-	-	-180	30 0-180	0	160	1.42	< 0.8	St	WT	NA	NA	S
Chabart and Lilien [226]	NA	NA	8-20	$n_x = 0.995$ $n_y = 0.845$ $n_\theta = 0.865$	$\zeta_x = \zeta_y = 0.08$ $\zeta_\theta = 0.3$	3.74	-180 to 0	0 0	0	32.5	0.8	1	St and Dyn	WT	Ec	21.45	S
Van Dyke and Laneville [225]	NA	NA	0-16	NA	NA	1.522	0	0	-180 to 180	27.8	450	NA	Dyn	FM	D	$D = 75$	S
Ma et al. [235]	34k-175k	-	NA	-	-	-	0-180	0 0	0	100	2	0.5	St	WT	Cr	50, 25	S
Matsumiya et al. [230]	NA	NA	6.7, 10.2	$n_x = 0.379$ $n_y = 0.450$ $n_\theta = 0.416$	NA	6.692	0-30	0 0	0	28.5	1	< 0.5	St and Dyn	WT	Tr	14.25	4-B
Hu et al. [234]	NA	-	10-18	-	-	-	0-180	90 0	0	27.6	0.7	NA	St	WT	Cr Sc	12, 20, 28 18	4-B
Xin-min et al. [231]	NA	-	10, 20, 30	-	-	-	0-180	90 0	0	26.82	1.4	NA	St	WT	D, Cr	6, 12, 15, 23, 33	4-B

AOA angle of attack (ice), ST system type, TF test facility, IS ice shape, IT ice thickness, No number of models, S single, 4-B four-bundle, WT wind tunnel, FM field measurement, Dyn dynamic test, St static test, NA not available, Tr triangle shape, Sc sector shape, D D shape, Ec crescent shape, D D shape, Ec eccentric shape

Fig. 27 Arrangement of twin cables or circular cylinders

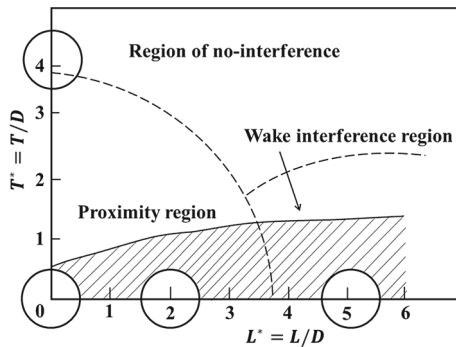
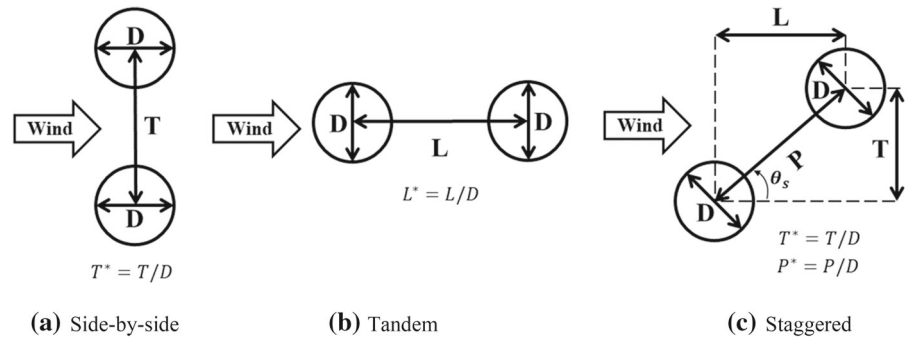


Fig. 28 Classification of interference region for twin cylinders, replotted from [265]

Mattiello et al. [267] measured the aerodynamic damping using passive-dynamic wind tunnel tests on twin inclined cables. They compared the results with full-scale data and analytical results from quasi-steady theory and found a good match between them. Acampora et al. [268] performed the full-scale monitoring and wind tunnel test on the arrangement of twin cables for the Øresund Bridge to extract the aerodynamic damping and stiffness using the eigenvalue realization algorithm (ERA). The results showed that the effect of Reynolds number is more than reduced velocity on the damping terms. As a results, a reduction can be seen for the total damping in the range of critical Reynolds number. Although the total damping was positive, they believed that the reduction in critical range of Reynolds number has some influence on large-amplitude motion of wake galloping. Li et al. [269] studied the wake galloping of parallel stay cables performing wind tunnel tests on the aeroelastic models. They investigated the effects of different parameters such as yaw angle, space ratio, incident angle, and connection type (flexible and rigid). The experimental results of this research are shown in Table 15. They carried out the experiments

for yaw angles ranging from 0° to 30° and three incident angles of 0° , 3° , and 5° . The results showed that wake galloping is dependent on incident angle, while the critical yaw angle is from 10° to 20° .

Kim et al. [270] performed the wind tunnel test to study the characteristics of twin cables using free vibration system and particle image velocimetry (PIV). They showed that the wake galloping disappeared for space ratios greater than 7. Furthermore, the results showed that the interaction of downstream cylinder and vortex shedding of upstream model generates the aerodynamic lift force when the space ratio is small. According to the results, the wake galloping occurred at space ratios ranging from 3 to 6. Gawronski [271] simulated the wake-induced vibration of bundle power transmission lines and smooth cables and indicated that wake galloping occurs at higher wind speed by increasing the space ratio. The comparison between twin smooth cables and conductors demonstrates that the galloping instability occurs in higher wind speed for smooth cables compared to power transmission lines. The simulations showed that the amplitude of vertical vibration is larger for cable with longer span length, while the horizontal and torsional vibrations are more for cables with shorter span length. He et al. [264] studied the wake-induced galloping of tandem cables performing wind tunnel experiments. They observed a large-amplitude vibration for downstream cable and showed the tendency of increase in vibration frequency with increasing the wind speed. They installed the elastic cross ties to suppress the wake-induced vibration and concluded that it can mitigate the vibration amplitude by 74%. The large-amplitude vibration happened for downstream cable at reduced velocity of 55 and Reynolds number of 4.5×10^4 . Furthermore, they measured the in-plane and out-of-plane displacement by using the accelerometer. Cigada et al. [272] studied the wake galloping of power

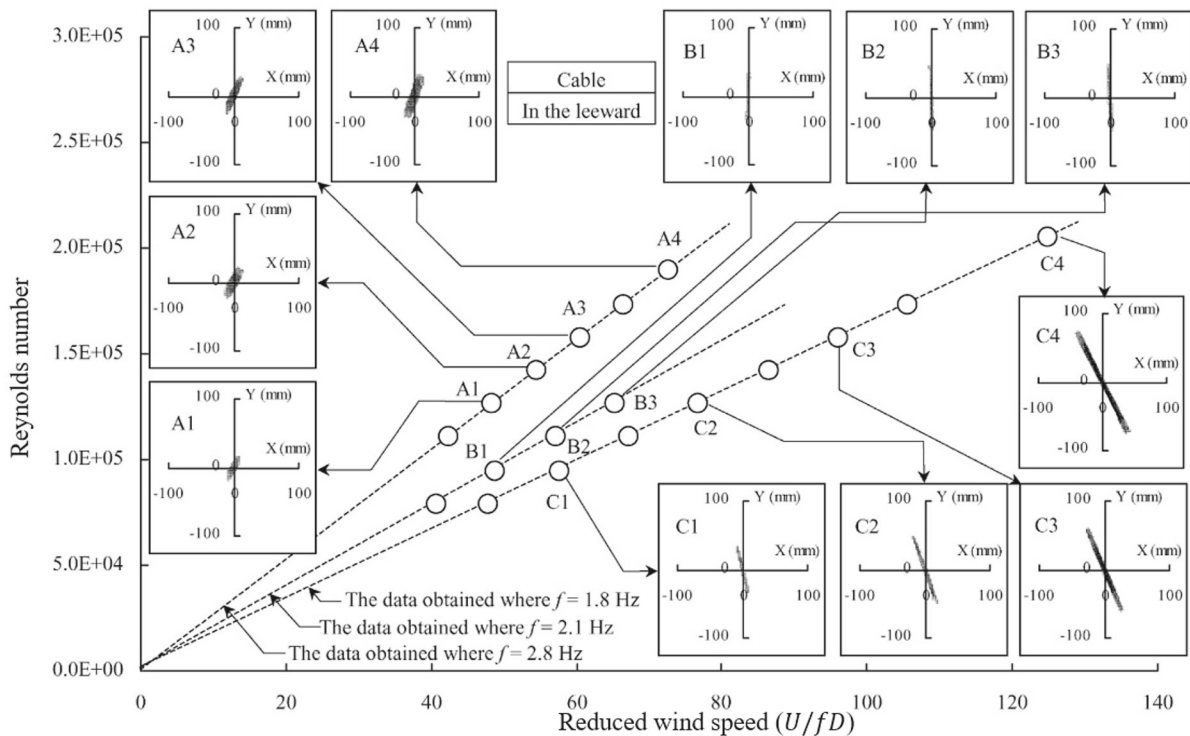


Fig. 29 Vibration trajectory of different reduced velocities and Reynolds number ($L^* = 4.3$, $\theta = 15^\circ$, $Sc = 3.18$) [2]

transmission lines with a two-degree-of-freedom system performing wind tunnel tests. Additionally, they used an analytical approach to define a linearized model to predict the galloping instability. Table 16 summarizes the past experimental researches on wake galloping of cables.

Some of the past important papers on flow-induced vibration of twin cylinder are reviewed here because of similarity between wake galloping of tandem cables and flow-induced vibration of twin circular cylinders. Liu et al. [273] performed the wind tunnel tests to extract the aerodynamic coefficients of twin circular cylinders with equal and unequal diameters. They conducted the experiments for in-line (tandem) cylinders as groups of two, three, and four models at different space ratios in both smooth and turbulent flow. The results indicated that the turbulence intensity has significant effects on aerodynamic coefficients of cylinders. Furthermore, they observed the wake galloping for horizontal space ratios of 3–5 which is consistent with the past studies. Assi [274] studied the wake-induced vibration of twin circular cylinders with two-degree-of-freedom vibration system for

in-line and staggered arrangements performing water channel tests. He conducted the experiments for horizontal space ratios of 4, while the vertical space ratios were changed from 0 to 3. The results indicated that the dynamic response of downstream cylinder becomes smaller by increasing the vertical space ratio from zero. Assi et al. [275] conducted another research on vibration of tandem cylinders with horizontal space ratio of 4 using water channel to study the wake-induced vibration of twin circular cylinders. They showed that the vortex- and wake-induced vibration of downstream cylinder can be suppressed by using a free to rotate parallel plates. Figure 30 shows the different configurations that were tested to study the effect of free to rotate parallel plates. They also studied the effect of single splitter and helical strakes on mitigation of wake-induced vibration of downstream cylinder, but they found them almost ineffective for this type of flow-induced motion. The dynamic response of downstream cylinder is plotted in Fig. 31 with and without mitigation system while showing the good capability of suggested

Table 15 Influence of cable connection on the critical wind speeds of cable wake galloping [269]

No.	Connection	Spacing	Connection position	$U_{cr}(\frac{m}{s})$ in wind tunnel	$U_{cr}(\frac{m}{s})$ in full-scale bridge		
1	Flexible	8D	No connection	13.7	44.0		
2			$L/2$	11.2	36.0		
3			$L/4, 3L/4$	14.4	46.3		
4		12D	No connection		13.1	42.1	
5				$L/2$	10.1	32.4	
6				$L/4, 3L/4$	11.3	36.3	
7		16D	No connection		13.8	44.3	
8				$L/2$	12.8	41.1	
9				$L/4, 3L/4$	No galloping	–	
10		20D	No connection		15.	48.2	
11				$L/2$	No galloping	–	
12				$L/4, 3L/4$	No galloping	–	
13	Rigid			8D	No connection	13.7	44.0
14					$L/2$	16.7	53.6
15					$L/4, 3L/4$	No galloping	–
16		12D	No connection		13.1	42.1	
17				$L/2$	14.2	45.6	
18				$L/4, 3L/4$	No galloping	–	
19	16D	No connection		13.8	44.3		
20			$L/2$	No galloping	–		
21			$L/4, 3L/4$	No galloping	–		
22			20D	No connection		15.	48.2
23					$L/2$	No galloping	–
24					$L/4, 3L/4$	No galloping	–

mitigation system in the suppression of the wake-induced vibration.

Arie et al. [276] conducted a series of static wind tunnel tests to measure the aerodynamic coefficients of tandem cylinders such as pressure, lift, and drag coefficients. The results showed that the root mean square (rms) of downstream cylinder is much larger than upstream one for horizontal space ratios less than 7. They concluded that the behavior of downstream cylinder is independent of upstream one for horizontal space ratios greater than 10. Jenkins et al. [277] used 2-D particle image velocimetry (PIV) technique and hot wire to study the unsteady characteristics of tandem cylinders for two horizontal space ratios of 1.435 and 3.7. Their results indicated that wakes for space ratio of 3.7 are more organized than space ratio of 1.435. Sun et al. [278] performed a series of wind tunnel tests to study the characteristics of flow over twin cylinders for tandem, side-by-side, and staggered arrangements

in high Reynolds number. The results of flow measurement showed that the effect of interference in supercritical Reynolds number range is less than subcritical range. Moreover, they observed a big difference between subcritical and supercritical regime associated with the flow characteristics of downstream cylinder. Kim et al. [279,280] captured the wake-induced vibration of tandem cylinders using wind tunnel experiments for horizontal space ratios of 0.1–3.2. They identified five different regimes for this range of space ratios where the aerodynamic forces and vibration characteristics are dependent on space ratio. The results indicated that the dependency of dynamic response of upstream and downstream cylinders is less for space ratios larger than 2.7. Lin et al. [281] studied the flow over tandem circular cylinders employing high-image-density particle image velocimetry (PIV). They conducted their experiments for space ratios ranging from 1.15 to 5.1. As a result, although the past studies showed

Table 16 Summary of the past experimental studies on the wake galloping of cable

References	Re	Sc	U (m/s)	n (Hz)	ζ (%)	m (kg/L)	θ_s°	α°	β°	Space ratio	D (mm)	L (m)	I_r (%)	Type	Test
Tokoro et al. [2]	30k–200k	3.18, 15.9	<28	1.8–3.7	0.095–0.64	53	0, 5, 10, 15, 20	90	0	$L^* = 4, 3.5, 6.5, 8, 7.0$	115	10	Sm	Dyn	WT
Acampora et al. [268]	30k–230k	–	131	–	–	–	0–30	0	0	$L^* = 5.88$	114	1.49	.64	St	WT
Li et al. [269]	21k–32k	7.1	<23	1.27–3.607	0.197, 0.212	4.54	0, 3, 5	NA	NA	$L^* = 8, 12, 16, 20$	32	2.85	Sm	St	WT
Cigada et al. [272]	NA	NA	6, 14	$n_x = 3.13$ $n_y = 3.5$	$n_x = 0.2$ $n_y = 0.4$	0.78	NA	NA	NA	$L^* = 2.5, T^* = 1.2$	60	0.9	Sm	Dyn.	WT
Kim et al. [270]	NA	NA	<23	2.411	0.12	6.74	0	0	0	$L^* = 3, 4, 5, 6, 7, 8$	100	0.9	<1	Dyn.	WT
He et al. [264]	16k–160k	6.3	5–26	4.5	0.1	1.75	–10	16	5	$L^* = 5.7–9.0, T^* = 8.4$	47.5	2.81	<0.5	St	WT

Sm smooth, St static test, Dyn dynamic test

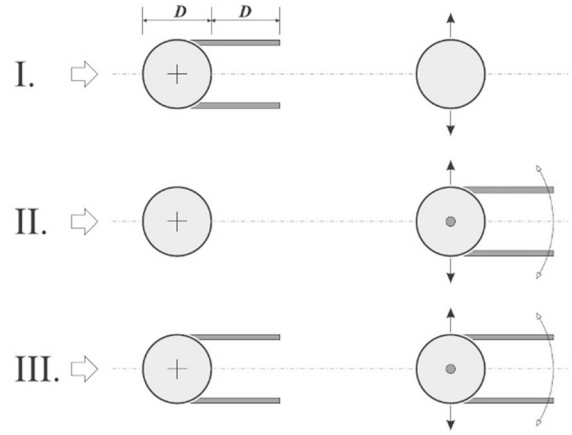
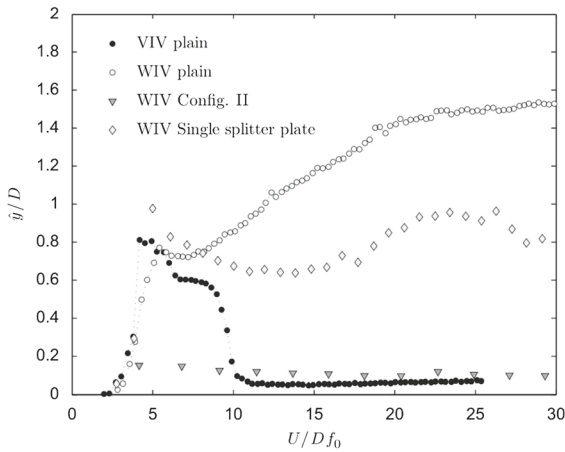


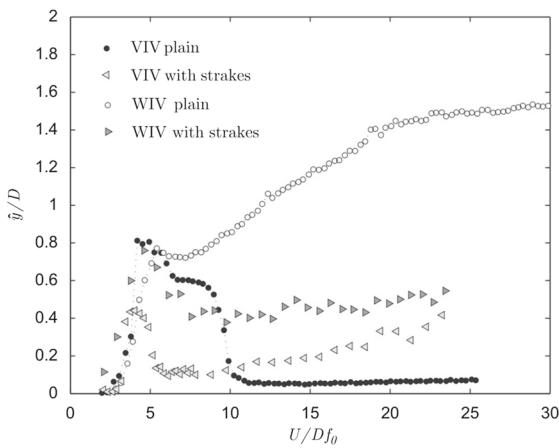
Fig. 30 Arrangement of upstream (fixed) and downstream cylinders fitted with f-t-r parallel plates at $L^* = 4$ [275]

that Kelvin–Helmholtz vortices are visible in space ratio of 4, they could not observe this type of vortex shedding and found it due to the technique used for measurement. Alam and Meyer [282] studied the flow-induced vibration of twin circular cylinders using wind tunnel tests for staggered arrangement. They classified the flow field over twin cylinders into seven regimes depending on space ratio and arrangement. These regimes are included: no interaction regime; boundary layer and cylinder interaction regime; shear-layer/wake and cylinder interaction regime; shear-layer and shear-layer interaction regime; vortex and cylinder interaction regime; vortex and shear-layer interaction regime; and vortex and vortex interaction regime.

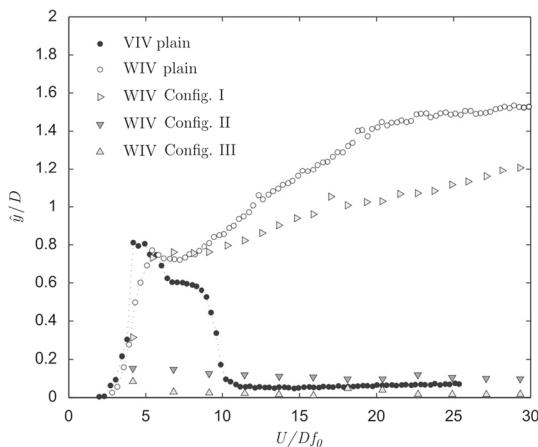
Numerical simulations are another way to study the features of this vibration source. Palau-Salvador et al. [283] conducted numerical simulation using large eddy simulation (LES) turbulence model to investigate the flow behavior around tandem circular cylinders. The space ratio of two was selected for simulations, and they showed the capability of this turbulence model in modeling tandem cylinders by comparing with the PIV results. Braun and Awruch [284] developed a numerical code using the LES turbulence model to capture the wake galloping of bundle power transmission lines and captured the wake galloping of twin cylinders by simulation of interaction between the fluid and solid domain. Wu et al. [285] simulated the wake-induced galloping of bundle conductors using the commercial software of Fluent and ABAQUS to study the effect of aerodynamic and electromagnetic loads on twin cables. The results showed that the conductors with longer span



(a) Cylinders with f-t-r splitter plate and parallel plates.



(b) Cylinders with strakes.



(c) Cylinders with parallel plates.

Fig. 31 Comparison of wake- and vortex-induced response of downstream cylinder [275]

length are more vulnerable to wake galloping and concluded that the electromagnet forces have significant effects on wake galloping, which need to be considered in design procedure. Brzozowski and Hawks [286] studied the wake galloping of bundle power transmission lines using a linearized model and found the stable and unstable regions at different wind speeds by applying the linearized motion equations. In another study [287], the results of the linearized motion equations showed that the horizontal galloping of bundle power transmission lines is dominant, while vertical galloping is more significant in higher wind speed, and torsional galloping might occur only at very high wind speed. Bokaian [288] proposed a quasi-steady model to predict the galloping instability of a cylinder in the wake of another cylinder and showed that the wake galloping happens for downstream cylinder when the drag force becomes negative for downstream cylinder. He also found that the galloping happens in higher velocity as the mass or damping ratio increases.

Nguyen et al. [289] conducted the numerical simulation using hybrid detached eddy simulation (DES) turbulence model to study the flow over tandem circular cylinders. They measured the force components, pressure field, and dynamic response of tandem cylinders at subcritical range of Reynolds number and space ratio of 4–5. The results showed that the Reynolds number has a strong effect on wake galloping, and the numerical simulations accurately predicted the increase in response frequency with increasing the wind speed. Armin et al. [33] studied the wake-induced galloping of tandem circular cylinders with space ratio of 3.5D–20D at the Reynolds number ranging from 8.7×10^3 – 5.2×10^4 . They used water tunnel to measure the dynamic response of downstream cylinder at different space ratios to determine the interaction of vortex shedding generated by upstream and downstream cylinders. The results demonstrated that the behavior of downstream cylinder for horizontal space ratio greater than 10 ($L^* > 10$) is similar to a single cylinder, and the amplitude of dynamic response reduces with increasing the space ratio. Table 17 summarizes the past experimental studies on twin circular cylinders to measure different aerodynamic coefficients.

Table 17 Experimental studies at the subcritical and supercritical Re range of twin cylinders [263]

References	Re	Geometry	AR	Blockage ratio (%)	I_u (%)	Test	Measurements
Abdulhadi [290]	$1.2 \times 10^4 - 7.3 \times 10^4$	$L^* = 3-25,$ $T^* = -3.5-3.5$	18	5	0.21	WT	C_P, C_D, C_L
Akosile and Summer [291]	5×10^4	$P^* = 1.125-1.25, \alpha = 0^\circ-90^\circ$	18	4	0.6	WT	St, C_{PB}, C_D, C_L
Alam and Sakamoto [292]	5.5×10^4	$P^* = 1.1-6, \alpha = 10^\circ-75^\circ$	6	8	0.5	WT	St
Alam et al. [293]	5.5×10^4	$P^* = 1.1-6, \alpha = 10^\circ-75^\circ$	6	8	0.5	WT	$C_P, \dot{C}_P, C_D, \dot{C}_D, C_L, \dot{C}_L$
Alam et al. [294]	6.5×10^4	$L^* = 1.1-9$	8.2	8.1	0.19	WT	$St, C_P, \dot{C}_P, C_D, \dot{C}_D, C_L, \dot{C}_L$
Alam et al. [295]	5.5×10^4	$T^* = 1.1-5$	6	8	0.5	WT	$St, C_P, \dot{C}_P, C_D, \dot{C}_D, C_L, \dot{C}_L$
Alam et al. [296]	5.5×10^4	$T^* = 1.1-6$	6	4	0.5	WT	$St, C_P, C_D, \dot{C}_D, C_L, \dot{C}_L, FS$
Alam and Zhou [297]	4.7×10^4	$T^* = 1.1-1.2$	6	8	0.5	WT	C_P, C_L
Alam and Zhou [298]	$5.5 \times 10^4 - 6.5 \times 10^4$	$L^* = 1.1-9$	6	8	0.5	WT	phase, \dot{C}_L
Alam and Meyer [299]	5.5×10^4	$P^* = 1.1-6, \alpha = 0^\circ-90^\circ$	6	8	0.5	WT	$St, C_P, C_D, \dot{C}_D, C_L, \dot{C}_L$
Alam and Meyer [282]	5.5×10^4	$P^* = 1.1-6, \alpha = 0^\circ-90^\circ$	6	8	0.5	WT	C_L, \dot{C}_L, FS
Alam [300]	$1 \times 10^4 - 6.5 \times 10^4$	$L^* = 1.1-4.5$	6	8	0.5	WT	St, \dot{C}_D, \dot{C}_L
Arie et al. [276]	1.57×10^5	$L^* = 2-10$	11	9	0.3	WT	$St, C_P, \dot{C}_P, \dot{C}_D, \dot{C}_L$
Bearman and Wadcock [301]	2.5×10^4	$T^* = 1-6$	31	4	0.2	WT	$St, C_P, C_{PB}, C_D, C_L$
Biermann and Hernstein [302]	$6.1 \times 10^4 - 1.5 \times 10^5$	$L^* = 1-9, T^* = 1-5.3$	48-120	1.2-3, 2-6	-	WT	C_D
Brun et al. [303]	1.4×10^4	$T^* = 1.583$	10	14	-	WaT	St, velocity profile
Cooper [304]	$1 \times 10^4 - 1.25 \times 10^5$	$P^* = 1.35-50, T^* = 0-7.5$	24	8	-	WT	C_P, C_D, C_L
Gu and Sun [305]	$2.2 \times 10^5 - 3.33 \times 10^5$	$P^* = 1.1-3.5, \alpha = 0^\circ-90^\circ$	6.4	8	0.2	WT	-
Gu et al. [306]	6.5×10^5	$P^* = 1.05-4, \alpha = 0^\circ-90^\circ$	15	11.4	0.12-10	WT	C_P, C_D, C_L
Hiwada et al. [307]	$1.5 \times 10^4 - 8 \times 10^4$	$L^* = 1-6$	8, 20	7, 13	0.2	WT	St, C_D, \dot{C}_D
Hori [308]	1.2×10^4	$T^* = 1.2-3$	120	1	0.03	WT	$St, C_P, C_{PB},$ velocity profile
Igarashi [309]	5.2×10^4	$L^* = 1-5$	4	6	0.6	WT	St, C_P, \dot{C}_P, C_D
Igarashi [310]	$1.15 \times 10^4 - 10.3 \times 10^4$	$L^* = 1-1.5$	3	13	0.6	WT	St, C_P, \dot{C}_P, C_D

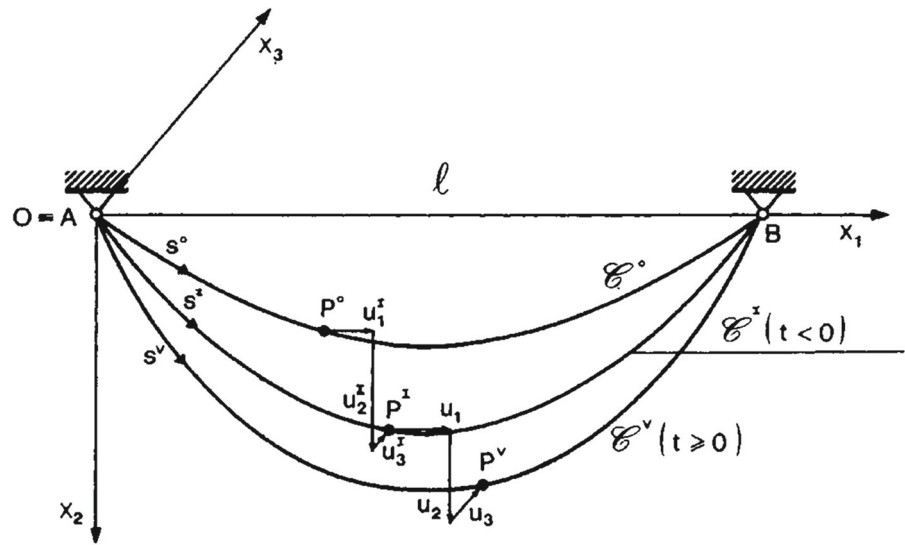
Table 17 continued

References	Re	Geometry	AR	Blockage ratio (%)	I_u (%)	Test	Measurements
Ishigai et al. [311, 312]	1.5×10^4	$L^* = 1-5, T^* = 0.5-3$	11	9	-	WT	St, C_p
Jendrzejczyk and Chen [313]	$1.5 \times 10^4 - 1.5 \times 10^5$	$L^* = 1.4-10, T^* = 1.35, 2.7$	12	9	1-11	WaT	St, \dot{C}_D, \dot{C}_L
Kamemoto [314]	3×10^4	$T^* = 1-3$	5	13	-	WT	St
Kiya et al. [315]	1.58×10^4	$P^* = 1-5, \alpha = 0^\circ-90^\circ$	10.5	4.77	0.8	WT	St
Kiya et al. [316]	$2 \times 10^4 - 3.7 \times 10^4$	$L^* = 2.5-4$	11	10	0.1-10	WT	-
Kobayashi [317]	$2.53 \times 10^4 - 5.9 \times 10^4$	$L^* = 1-3, T^* = 1-3$	-	-	-	WT	St, C_D, C_L, F_S
Kostic and Oka [318]	$1.3 \times 10^4 - 4 \times 10^4$	$L^* = 1.6-9$	5	20	2.8	WT	C_p, C_D
Kwon et al. [319]	1.7×10^4	$L^* = 1-5$	11	2	2.5	WaT	VF
Lee and Basu [320]	$2.4 \times 10^4 - 5.1 \times 10^4$	$L^* = 2, 3.2$	20	6.3	0.35	WT	St, C_p
Lee and Panagakos [321]	$2.4 \times 10^4 - 5.1 \times 10^4$	$L^* = 2, 3.2$	20	5	0.35	WT	St, C_p, \dot{C}_p
Lin et al. [281]	1×10^4	$L^* = 1.15-5.1$	5.3	10	-	WaT	VF
Ljungkrona and Sunden [322]	4×10^4	$L^* = 1.25-4$	16	6	0.1	WT	St, C_p, \dot{C}_p
Ljungkrona et al. [323]	2×10^4	$L^* = 1.25-5$	16	6	0.1-3.2	WT	St, C_p, \dot{C}_p, C_D
Maekawa [324]	$1.7 \times 10^4 - 2.3 \times 10^4$	$P^* = 5.85-15.8, \alpha = 0^\circ-30^\circ$	-	-	-	WT	C_D, C_L
Moriya and Sakamoto [325]	6.53×10^4	$L^* = 2-6, T^* = 0-1.5$	10	20	0.4	WT	St, $C_p, \dot{C}_p, C_D, \dot{C}_D, C_L, \dot{C}_L$
Ng et al. [326]	5.4×10^4	$T^* = 1.4-2$	-	-	0.4	WT	C_D, C_L
Nishimura et al. [327]	1×10^4	$L^* = 1.2-7.2$	5	9	0.6	WaT	-
Novak [328]	1.05×10^4	$T^* = 2.5$	8	4.2	2.2	WT	St
Okajima [329]	4×10^4	$L^* = 2.1-7.3$	7	8	0.1	WT	St, C_D
Ozono et al. [330]	3×10^4	$L^* = 1-4, T^* = 0-2$	14.6	8.8	2	WT	St, C_{PB}
Price [331]	$1.7 \times 10^4 - 8 \times 10^4$	$L^* = 6-18, T^* = 0-2.42$	37, 42	5-12	1-11	WT	C_p, C_D, C_L
Price and Paidoussis [332]	$1.7 \times 10^4 - 8.6 \times 10^4$	$L^* = 1.5-5, T^* = 0.75-2$	24	6	0.5	WT	C_D, C_L
Spivack [333]	9.3×10^4	$T^* = 2-7$	39	5	0.02	WT	St, velocity profile

Table 17 continued

References	Re	Geometry	AR	Blockage ratio (%)	I_u (%)	Test	Measurements
Summer and Richards [334]	3.2×10^4	$P^* = 2-2.5, \alpha = 0^\circ-90^\circ$	24	5.6	0.6	WT	St, C_D, C_L
Summer [335]	5×10^4	$P^* = 1.125-1.25, \alpha = 0^\circ-90^\circ$	18	4	0.6	WT	St, C_{PB}, C_D, C_L
Summer et al. [336]	3.2×10^4	$P^* = 1.125-4, \alpha = 0^\circ-90^\circ$	18, 24	3.5, 5.6	0.6	WT	St, C_D, C_L
Summer and Schenstead [337]	$3.2 \times 10^4 - 7.4 \times 10^4$	$P^* = 1.125-4, \alpha = 0^\circ-90^\circ$	18, 24	3.5, 5.6	0.6	WT	St, C_{PB}, C_D, C_L
Sun et al. [278]	3.25×10^4	$L^* = 2.2-4, T^* = 2.2$	15	5, 10	0.12-10	WT	C_P, \dot{C}_P
Suzuki et al. [338]	1×10^5	$P^* = 1.1-3.9, \alpha = 0^\circ-15^\circ$	6-18	12-14	-	WT	C_P, C_D
Ting et al. [339]	$4 \times 10^4 - 2 \times 10^5$	$L^* = 1.5-5, T^* = 0.1-1.05$	5.3-12.8	10.6-25	0.8	WT	C_D, \dot{C}_D
Tsutsui [190]	$3.8 \times 10^4 - 1.3 \times 10^5$	$L^* = 1.2-1.3$	1.5	10	0.4	WT	$FS, C_P, \dot{C}_P, C_D, C_L$
Wardlaw and Cooper [340]	$1.2 \times 10^4 - 1.4 \times 10^5$	$P^* = 1.2-3.5, \alpha = 0^\circ-75^\circ$	45	3	-	WT	C_D, C_L
Wong et al. [341]	2×10^4	$P^* = 1.2-6.0, \alpha = 0^\circ-90^\circ$	48	4.2	0.4	WT	St
Wu et al. [342]	$1.7 \times 10^4 - 4.7 \times 10^4$	$L^* = 3-7$	20	5	0.15	WT	St
Xu et al. [343]	1.4×10^4	$T^* = 1.2-1.6$	47	4.2	0.4	WT	St, velocity profile
Xu and Zhou [344]	$1 \times 10^4 - 4.2 \times 10^4$	$L^* = 1-15$	40, 16	2.5, 6.7	-	WT	St
Zdravkovich and Pridden [345]	6×10^4	$L^* = 2.5-7, T^* = 1.25-2$	33	2, 4	0.1	WT	C_P, C_{PB}, C_D
Zhang and Melbourn [346]	1.11×10^5	$L^* = 2-10$	8	5	0.4-11.5	WT	$C_P, \dot{C}_P, C_D, \dot{C}_D, \dot{C}_L$
Zhou et al. [347]	2×10^4	$P^* = 1.2-4.0, \alpha = 0^\circ-90^\circ$	48	4	0.4	WT	St
Okajima [329]	6.2×10^5	$T^* = 3.8$	6.67	7.5	0.1	WT	St, C_D
Sun et al. [278]	$3.25 \times 10^5, 6.5 \times 10^5$	$P^* = 2.2-4.0, \alpha = 0^\circ-90^\circ$	15, 15	0.95	0.12	WT	C_P, \dot{C}_P
Gu et al. [306]	6.5×10^5	$P^* = 1.05-4.0, \alpha = 0^\circ-90^\circ$	15	11.	0.12-10	WT	C_P, C_D, C_L
Gu [348]	4.5×10^5	$P^* = 1.2-3.5, \alpha = 0^\circ-90^\circ$	6.4	8	0.2	WT	$C_P, C_{PB}, \dot{C}_D, C_L$

Fig. 32 Configurations and displacement component in a cable coordinate system [358]



5.6 Nonlinear dynamics of cable vibration

5.6.1 Nonlinearities in cable vibration

Due to the versatile applications of structural cables, *i.e.*, power transmission lines and cable-stayed bridges, cable vibration has attracted considerable attention among research communities, and as a result, numerous models have been proposed in order to describe the cable vibration. Linear models were firstly developed for the sake of simplicity. Irvine and Caughey [349] presented a prominent linear theory to model the free vibration of a horizontally suspended cable with a small sag. The in-plane motion was decoupled from out-of-plane motion, and in addition, the in-plane motion can be further decomposed into symmetric or anti-symmetric vibration modes with respect to its mid-span. However, nonlinearities in cable vibration, which can be observed due to the wind loads or other excitations, have been widely studied in the past [350–354]. In this regard, the linear cable vibration theory was later extended by taking into account nonlinearities mainly arising from geometric nonlinearity or coupling between in-plane and out-of-plane motions.

When the amplitude of oscillations is in the same order of magnitude of sag, the cable vibration has to be represented with a nonlinear model. Hagedorn and Schäfer [355] firstly derived nonlinear in-plane cable vibration equations to account for geometric nonlinearities, which are represented by quadratic and cubic terms in the governing equations of the motion. In order

to study the coupling effects, a two-degree-of-freedom model was established with one being used to describe in-plane oscillations and the other for the out-of-plane oscillations [356,357]. Those nonlinear equations of motions for the cable were obtained through the Hamilton's principle, where the kinetic energy, the potential energy, and the virtual work associated with gravity, external, and damping forces were expressed in terms of the in-plane and out-of-plane motions. Figure 32 shows the coordinate system that is usually used to derive the motion equations of a horizontally suspended cable exposed to steady and stretched profiles.

Internal resonance plays an important role when it comes to the investigation of the coupling effect, as it is able to produce strong coupled responses in multi-degree-of-freedom systems. Therefore, numerous researches have been performed with the goal of revealing its effect on either free or forced nonlinear cable vibrations [359,360]. Lee and Perkins [361] analyzed the near-resonance response of suspended cable using a coupled two-degree-of-freedom system while assuming the ratio of 2:1 for the in-plane and out-of-plane natural frequencies. Saturation and jump phenomena were observed for suspended cable after using first-order analysis, while the second-order analysis resulted in the disruption in saturation [361]. The nonlinear excitation of suspended cables including the existing model and analysis has been comprehensively reviewed in three review articles by Rega [358,362] and Ibrahim [363]. The majority of the research has been focused on nonlinear vibration of horizontally sus-

pended cables; however, nonlinear inclined cable vibrations are still needed to be addressed. To this end, Srinil et al. [364–367] described the theoretical formulation and model validation of inclined cables exposed to nonlinear vibration. Rega et al. [368] conducted a series of linear free and nonlinear forced vibration experiments on the vibration of an inclined cable to study the cable dynamics. Moreover, they applied numerical approaches for better understanding the galloping instability of inclined cables and concluded that inclination angle, sag ratio, and dynamic insensibility play an important role in cable excitation. Karoumi [369] studied the nonlinear behavior of an inclined cable using finite element modeling, and the reliability of this approach was checked through modeling the Great Belt suspension bridge. In another research [370], a nonlinear state observer was developed to capture the nonlinearity of cable excitation using the Galerkin approach. The goal in this study was to minimize the number of measurements to describe the cable dynamics. Arena et al. [371] studied the nonlinear dynamic response of a flexible cable through the special Cosserat theory of rods while considering extension, bending, shear stress, and twist effects. They found the proposed model has approximately up to 30% error within boundary layers to predict the stress value. They also presented the results for several case studies on the taut and shallow cables. In another study, the nonlinearity behavior of overhead cables was evaluated by Barbieri et al. [372] through using the analytical model and finite element technique. The results were compared with experimental data collected by measuring the force under impulsive excitation or electromechanical shaker. Additionally, they found that an increase in the central sag or fluctuation in tension can change the natural frequency of cable.

It has to be noted that boundary conditions could be another source where the nonlinearity could be generated. Georgakis and Taylor [371, 372] studied the effect of sinusoidal cable support displacement on nonlinear vibrations of a cable. They found new regions of instability for cable response and observed cable stiffening for several cases. They also employed finite element analysis to capture the stress and displacement for different cases. Gattulli and Lepidi [373] proposed a model to investigate the nonlinear interactions between the stayed beam and cable using quadratic and cubic nonlinearities in cable and boundary conditions. They

also presented the influence of detuning from internal and external resonance.

5.6.2 Nonlinear wind-induced cable vibration

Nonlinear wind-induced vibration of cables can be caused either by aerodynamic nonlinearities from wind load or geometric nonlinearities from the structure. Yu et al. [212, 213] derived three-degree-of-freedom governing equations to describe the galloping behavior of a transmission line. Bifurcation theory and approximate perturbation technique were employed, and the aerodynamic coefficients, which are nonlinear functions of angle of attack, were represented with a cubic polynomial function. Explicit solutions and stability conditions for the internal resonant cases can be obtained with this approach. However, in their works, only aerodynamic nonlinearities were considered, and the geometric nonlinearities were ignored, although the latter has a significant impact on the dynamics of cable structures. Therefore, a comprehensive model that encompasses both types of nonlinearity is needed.

In order to address this issue, Luongo et al. [374] investigated the nonlinear multimodal galloping of a suspended cable through the development of an analytical model considering the geometrical nonlinearity and quasi-steady aerodynamic forces. They applied the finite difference method and Galerkin special discretization to solve the motion equation of suspended cable. They found that the classical galloping mode shows unstable behavior for simultaneous non-stabilization of the anti-symmetric planar mode. Moreover, Luongo and Piccardo [375] analyzed the coupled in-plane and out-of-plane motions of a suspended cable in 1:2 internal resonance conditions. Besides, they also investigated the nonlinear post-critical behavior around a simple Hopf bifurcation. In order to provide a complete scenario of the critical conditions as well as the information on the post-critical behavior of the cable, Luongo et al. [376] developed amplitude and phase equations using the multiple-scale perturbation method. Steady-state amplitude was obtained as a function of the wind speed; in addition, analysis corresponding to stability and attraction basins was carried out. For inclined cables, Luongo et al. [377] developed a simplified two-degree-of-freedom using the Galerkin method to study the effect twist angle on nonlinear galloping of an inclined cable. To capture the Hopf bifurcations and post-critical behaviors, they

used the multiple-scale approach under 2:1 internal resonance and without resonance. The numerical results showed that the twist angle has a significant impact on the modification of natural frequencies of the cable due to changing the predefined cable force, and the influence of twist angle can be significant for symmetric galloping modes.

In addition to galloping, rain-wind-induced nonlinear vibration of cables has also been extensively studied. Van der Burgh [378] proposed a new method using a simple oscillator to study the rain-wind-induced vibration of inclined cable. The results of developed nonlinear method based on the quasi-steady approach revealed three types of excitation mechanisms consisting of self-excitation, parametric excitation, and ordinary forcing. Seidel and Dinkler [135] proposed a nonlinear model to study the nonlinear dynamics of rain-wind-induced vibration and presented the results for a few bridges. The numerical results implied that the cable's natural frequency has no effect on the range of critical wind speed. Additionally, they concluded that nonlinear characteristics pertaining to frequency are a function of wind speed. Xu and Wang [132] developed an analytical model using nonlinear terms to study the rain-wind-induced vibration of a suspension cable. They evaluated the influence of mean wind speed and rivulet position and its movement on wind response of the cable. The results of proposed model were validated by wind tunnel data. Marsico et al. [379] conducted wind tunnel experiment to study the nonlinear cable vibrations while taking into account the influence of out-of-plane response. They also compared the obtained results from the analytical model with experimental data for the sake of verification, while the cable is excited by sine waves. Liu et al. [380] studied the nonlinear dynamics of rain-wind-induced vibration through establishing a three-degree-of-freedom model to calculate the in-plane and out-of-plane responses. The effects of mean wind speed, Coulomb damping force, damping ratio, span length, and initial tension on the nonlinear response of RWIV were studied in this research. They found that the mean wind speed has a significant impact on jump phenomena. Abdel-Rohman and Spencer [381] studied the wind effect on in-plane and out-of-plane responses of a suspended cable considering the nonlinear aspects. They proposed an analytical formulation to predict the critical wind speed of dry-cable galloping. They showed that the installation of a mechanical damper near the cable's end

can suppress the dry galloping. Chang et al. [382] studied the nonlinear fluid–structure interactions between cable and flow for the first two across-flow modes. They observe large-amplitude motion beyond a critical wind speed where both stretching and transverse motions show up. Xie [383] proposed a new algorithm to study the effect of excitation frequency, excitation amplitude, and cable's damping coefficient on the nonlinearity of cable vibration. They found that the nonlinear finite element methods have promising results for the prediction of nonlinear cable excitation. Xie et al. [384] studied the influence of nonlinear geometry and material on wind response and suspended cable. A new aspect of cable galloping, which is called nonlinear energy sink (NES), was studied by Guo et al. [385] through proposing a new method to model wind-induced load acting on a suspended cable. They also discussed the influence of mass ratio, damping, stiffness, and NES location on the mitigation of cable vibration. The galloping instability of a non-shallow cable was investigated by Lacarbonara et al. [386], and the critical wind speed for ice-accumulated cable galloping as well as post-critical cable response. It was found that critical speed quickly reduces, while sag ratio increases in the transition range from taut to slack cables. Pasa et al. [387] assessed the effectiveness of longitudinal control on suppression of cable vibration due to wind load. In this regard, they developed a model with the capability of capturing the nonlinearity of cable vibration up to third order for both in-plane and out-of-plane directions. They also discussed the cable response under harmonic and random excitations. Ruoqiang et al. [388] proposed a simplified method to evaluate the nonlinear wind response of cables by using continuous membrane theory. For the validation part, they compared the results with the nonlinear finite element method and found a good match. Luongo and Zulli [196] studied the wind response of an inclined cable used for cable-stayed bridges by developing an analytical model. They considered the effects of wind, rain, and motion induced by moving cars. Kang et al. [389] through analytical modeling and using Galerkin and multiple-scale perturbation methods found that inclination angle and unreasonable cable tension are two major factors that may cause the large-amplitude nonlinear vibration for inclined cables. Taylor and Robertson [390] conducted a numerical simulation to study the nonlinear dynamics of rain-wind-induced vibration by modeling the rivulet on the surface of an inclined cable. They discussed the effects

of rivulet position and thickness on the aerodynamics of cable causing undesirable vibration. Furthermore, they found that the rivulet thickness is self-limiting because of variation in aerodynamic load as a result of rivulet growth. Wu et al. [138,391] proposed a new model considering high-order polynomial terms for lift coefficients to simulate the hysteretic nonlinear behavior of rain-wind-induced vibration. They validate the numerical results with wind tunnel data and found a good match between them. Moreover, they observed a difference between the results taken from quasi-steady theory, unsteady, and nonlinear hysteretic model. Li et al. [392] performed numerical and experimental tests to study the rain-wind-induced vibration of an inclined cable. In this regard, they proposed a nonlinear model to predict the cable's dynamic response. They used experimental results as input for CFD modeling and captured the transient aerodynamic forces of a stay cable. This hybrid method revealed the promising results to simulate the nonlinear characteristics for the RWIV.

5.6.3 Mitigation approaches of nonlinear cable vibration

There are a number of researches on how to suppress the wind-induced vibration of suspended cable by attaching the crossties and mechanical dampers [393–396]. Similar to the mitigation of other types of vibration, damping is a very effective parameter to increase the critical wind speed at which wind-induced vibration of cables could occur. Therefore, dampers are deemed as an effective way to control the vibration. Abdel-Rohman and Spencer [381] introduced a vertical viscous damper, which is connected to a fixed platform like a bridge deck, to control the nonlinear galloping vibration of a cable. The efficiency and the locations of the viscous damper were also investigated, and the results showed that the damper is capable of increasing the wind speed where galloping initiates. Xu and Yu [397, 398] presented a general approach to study the nonlinear vibration of a sagged cable with viscous dampers. The second-order nonlinear partial differential equations were first reduced to first-order nonlinear ordinary differential equations with the state-space method and generalized modal superposition method. The solutions of those functions for the cable-damper system were obtained using the harmonic balance method. The locations of viscous dampers are usually restricted to the cable ends, which significantly hinders the appli-

cation of viscous dampers in the mitigation of cable vibration. Moreover, passive dampers can only work well at a fixed range of frequency. In order to increase the effectiveness, semi-active dampers, such as tuned mass dampers (TMD) and electro/magnetorheological (ER/MR) dampers, were introduced as they can either be placed at any locations along the cable or be adjusted to control the vibration of any frequency. Ni et al. [399] proposed a neuro-control method to control the vibration of a sagged cable using MR dampers. Two neural network control strategies were developed, and their effectiveness was verified numerically to control the wind-induced vibration of a cable that has geometric nonlinearities. Cai et al. [400,401] developed TMD-MR (tuned mass damper-magnetorheological) damper system that combines the location flexibility of TMD damper and the adjustability of MR damper. They carried out a theoretical analysis on both horizontal taut cable and inclined cable with a sag. The cable parameters, as well as the damper parameters that could influence the efficiency of the system, were analyzed in this study. However, their work was limited to control the in-plane vibration of cables. Casciati and Ubertini [395,402] used a variable out-of-plane inclination TMD that was attached to the mid-span of the cable in order to control the cable vibration under the turbulent wind. A control algorithm was employed, and the effectiveness of the damper was validated with numerical simulation.

In addition to dampers, the cable vibration can also be controlled by applying a longitudinal motion on the cable support. Chen [403] found that the longitudinal motion of cable support is equal to the damping effect. Fujino et al. [404] obtained the optimal algorithm of the longitudinal motion of the cable support based on energy analysis. Such an algorithm was later validated with an experiment. Moreover, Susumpow and Fujino [405] designed controllers to suppress the free vibration and random vibration of cables. Gattulli et al. employed longitudinal displacement of one support to control the transverse in-plane and out-of-plane vibrations of a cable with geometric nonlinearities. The in-plane steady-state solutions and their stability under an out-of-plane disturbance were investigated with the perturbation method, and their accuracy was validated by comparing the results with those obtained by direct integration of the governing equations.

Table 18 Comparison of different types of wind-induced cable and conductor vibration [2,406]

Vibration type	Smooth cable	Power transmission line
Vortex-induced vibration (VIV)	$f = 0.6\text{--}3.5$ Hz $A/D < 0.02$ $U_{VS} = 1\text{--}3.5$ m/s $St(\beta = 0) = 0.2$ No concern for small diameter cables	$f = 3\text{--}150$ Hz $U_{VS} = 1\text{--}7$ m/s, steady wind $A/D = 0.05\text{--}0.5$ $St(\beta = 0) = 0.2\text{--}0.23$ Bare or uniformly iced surface All types of conductors
Rain-wind-induced vibration (RWIV)	Moderate amplitude, $A/D = 2$ $f = 1\text{--}3$ Hz $U_{RWIV} = 4\text{--}18$ m/s Rain with yawed wind Critical angle of rivulet: $20^\circ\text{--}60^\circ$	Limited research on this topic
Dry galloping (DG)	Low frequency High amplitude (A) Moderate to high wind speed Critical yaw angle range (β): $30^\circ\text{--}60^\circ$ Critical inclination angle (θ): $45^\circ\text{--}60^\circ$ Critical cable-wind angle (Φ): $75^\circ\text{--}90^\circ$	Limited research on this topic
Ice galloping (IG)	Large amplitude (A) Low frequency Moderate to high wind Limited research on this topic	$f = 0.08\text{--}3$ Hz $A/D = 2.5\text{--}150$ $U_{IG} = 7\text{--}18$ m/s, steady wind All type of conductors Asymmetric ice deposit: crescent and triangle are common
Wake galloping (WG)	Moderate wind speed ($U_{WG} \geq U_{VS}$) Moderate amplitude Critical $T^* = 4\text{--}6.5$ Instability for downstream cable	$f = 0.15\text{--}10$ Hz $A/D = 0.25\text{--}40$ (rigid-body mode) $0.25\text{--}10$ (subspan mode) Low wind speed ($U_{WG} \geq U_{VS}$) Critical $T^* = 10\text{--}20$ Bare or uniform ice bundled conductors

6 Conclusions

During the past century, cables have played a significant role in development of infrastructures and have used for many applications such as cable-stayed/suspension bridges, power transmission lines, and suspension roofs. Since the construction and maintenance of these structures are very expensive, it is very crucial to stabilize them being safe to different vibration sources. Therefore, the aerodynamics of cables have been extensively investigated by conducting different numerical simulations and experimental tests. Although only a few important properties of circular cylinders/cables

are reviewed in this study, the main focus was on cable vibration due to various wind-induced loads. This paper first explains the mechanism of vibration sources and then briefly reviews the existing literature on the topic to reveal the influence of effective parameters on dynamic response of cables. According to the literature, vortex- and rain-induced cable vibrations, which have limited amplitude, can be easily suppressed or mitigated by adding a little positive damping to the system, and the occurrence chance of wake-induced cable galloping is almost low since they have large space ratio which prevents cable vibration. In contrast, the dynamic response of cables exposed to dry and ice gal-

loping is very large that requires to provide enough positive mechanical or aerodynamic damping to suppress the cable galloping. Although these two vibration sources produce the divergent-amplitude motions, they only occur in specific conditions such as areas with snowfall or at high-speed wind with special orientation. As a result, rain-wind-induced vibration can be the most common type that has relatively large-amplitude vibration compared to other sources. However, it is necessary to consider the effect of all these sources in design procedure to build safe structures invulnerable to wind loads. This paper helps to better understand these aeroelastic phenomena and their effects on the cables by providing the results and conclusion of the past literature while studying the wind-induced cable vibration by different methods and approaches. Moreover, this review can help other scholars to come up with new mitigation solutions to suppress the dynamic response of cables and prevent the future catastrophic damage of structural cables. Although all aeroelastic phenomena are explained before in details, a comparison between smooth cables and conductors has been made in Table 18 to clarify the differences and similarities between them.

According to the past studies that have been reviewed here, the following perspectives related to wind-induced cable vibration can be investigated in the future:

- Developing a comprehensive and simplified analytical model. The majority of the researches corresponding to wind-induced vibration of cables, i.e., RWIV, are developed based on wind tunnel data. Although the experimental test has the capability to reproduce the conditions under which the cable vibrates, there are some challenges for wind tunnel tests on inclined and long cables such as matching non-dimensional numbers Reynolds number for dynamic tests. The free and forced vibration tests have their own limitations and cannot reproduce the actual condition for structural cables due to having a long span. Therefore, analytical models would be very useful to give some insights into the mechanisms of cable vibration and provide some guidelines on the prediction of the critical wind speed and suppression of wind-induced cable vibration in atmospheric boundary layer wind profile.
- Studying the nonlinear cable vibration under wind load. The nonlinear vibration of cables with geometric nonlinearities has been extensively studied,

and several models have been proposed. However, investigations corresponding to the nonlinear cable vibration under wind load are very limited. The majority of this type of research is focused on galloping and rain-wind-induced vibration; other types of wind load, such as self-excited load and buffeting, are still needed to be explored. The existing methods to predict the aeroelastic wind loads are required to be modified in order to accurately predict the linear and nonlinear cable vibration.

- Conducting more full-scale measurements for cable excitation. The number of researches on wind-induced cable vibration especially dry and ice galloping that is based on field measurement is limited. In order to validate the existing models, it is required to conduct more full-scale measurements for structural cables especially bridge's cables. This helps the applicability and reliability of introduced algorithms to predict the critical wind speed, and the proposed suppression devices would be more practical in the actual conditions.
- Performing nonlinear wind tunnel measurements. Although there are many studies on wind-induced cable vibration using wind tunnel tests, there is a few experimental researches to capture the nonlinear dynamics of cable excitation. It is required to come up with new algorithms with the capability of performing free or forced vibration tests in order to identify the wind load parameters in nonlinear regions. This nonlinearity has been widely explored through the proposed theoretical models; however, it is required to concrete the analytical models through validation with nonlinear experimental data.

Funding No funding for this manuscript.

Compliance with ethical standards

Conflict of interest The authors declare that they have no conflict of interest.

7 Appendix

7.1 Wind loads measurement

In the following sections, three main force sources of wind loads are explained to calculate the time history of response for cable due to these loads.

7.1.1 Vortex shedding loads

A nonlinear empirical model can be used to formulate vortex shedding load in the form of Van der Pol oscillator as follows:

$$F_{se} = \frac{1}{2} \rho U^2 (2D) \left[Y_1(K) \left(1 - \varepsilon(K) \frac{y^2}{D^2} \right) \frac{\dot{y}}{U} + Y_2(K) \frac{y}{D} + \frac{1}{2} C_L(K) \sin(\omega t + \theta) \right] \quad (7)$$

where ρ is the air density, U is the mean wind speed, D is the cable diameter, $K = \omega D/U$ is the reduced frequency, Y_1 , ε , Y_2 and C_L , both of which are dependent on reduced frequency, K , are the parameters that can be extracted from wind tunnel tests, ω and θ are the frequency and phase angle of the oscillating force resulting from vortex shedding, respectively. Y_1 and ε are related to aerodynamic damping, whereas Y_2 is corresponding to aerodynamic stiffness. According to, in the lock-in region where $\omega \cong \omega_1$, being ω_1 the natural frequency of the structure, Y_2 and C_L can be neglected as their effects are relatively small compared to those reflecting the aerodynamic damping. As a result, Eq. (7) can be simplified as [409]

$$F_{se} = \frac{1}{2} \rho U^2 (2D) \left[Y_1(K) \left(1 - \varepsilon(K) \frac{y^2}{D^2} \right) \frac{\dot{y}}{U} \right] \quad (8)$$

The method of slowly varying parameters can be used to solve the nonlinear dynamic equation of the system, which gives the result as follows:

$$\frac{y(s)}{D} = A(s) \cos(K_1 s - \psi_0) \quad (9)$$

where $s = Ut/D$ is the reduced time, $K_1 = \omega_1 D/U$ is the reduced frequency of the system, ψ_0 is the phase angle at the initial time, $A(s)$ is the envelope of the response, whose equation can be expressed as

$$A(s) = \frac{\beta}{\sqrt{1 - \left(\frac{A_0^2 - \beta^2}{A_0^2} \right) e^{-(\alpha\beta^2/4)s}}} \quad (10)$$

where A_0 is the initial displacement of the system, α and β are defined as

$$\alpha = m_r Y_1 \varepsilon \quad (11)$$

$$\beta = \frac{2}{\sqrt{\varepsilon}} \sqrt{1 - \frac{2\xi K_1}{m_r Y_1}} \quad (12)$$

where $m_r = \rho D^2/m$ is the mass ratio and ξ is the damping ratio of the system. It can be derived from Eq. (10) that the steady-state amplitude

$$A(\infty) = \beta \quad (13)$$

The parameters of Y_1 and ε can be identified by conducting a decay-to-resonance test, through which an initial displacement that is larger than the steady-state amplitude is imposed on the system at the wind speed where the maximum displacement is achieved. A set of data, $[s, A(s)]$, can be measured in the transient period, and a new parameter $Z(s)$ can be defined as follows:

$$Z(s) = \ln \left\{ \frac{A_0^2 [A^2(s) - \beta^2]}{A^2(s) (A_0^2 - \beta^2)} \right\} = -\frac{\alpha\beta^2}{4} s \quad (14)$$

where β can be obtained by measuring the steady-state response and α can be acquired by curve-fitting the data set $[s, Z(s)]$. Y_1 and ε can be calculated using Eqs. (11) and (12) once α and β are known.

7.1.2 Buffeting loads

This type of wind load that originates due to wind turbulence can be calculated in time domain for both vertical and lateral DOFs, as given in Eqs. (15) and (16):

$$F_b^h(s) = 0.5 \rho U D \int_0^s [2C_L u(\sigma) \phi'_h(s - \sigma) + (C_D + C'_L) w(\sigma) \phi'_h(s - \sigma)] d\sigma \quad (15)$$

$$F_b^p(s) = 0.5 \rho U D \int_0^s [2C_D u(\sigma) \phi'_p(s - \sigma) - C_L w(\sigma) \phi'_p(s - \sigma)] d\sigma \quad (16)$$

where ρ = air density, U = mean wind speed, C_D = drag coefficient, D = cable diameter, $C'_L = \frac{dC_L}{d\alpha}$, $u(\sigma)$ and $w(\sigma)$ = zero mean wind turbulence components in along- and across-wind directions, respectively, $s = Ut/D$ = non-dimensional time, $\phi'_h(s)$ and $\phi'_p(s)$ are derivatives of buffeting indicial functions $\phi_h(s)$ and $\phi_p(s)$ with respect to 's', respectively, referred here as buffeting indicial derivative functions that can be extracted using the aerodynamic admittance functions $\chi_h^2(K)$ and $\chi_p^2(K)$. Aerodynamic admittance functions, $\chi_h^2(K)$ and $\chi_p^2(K)$, are functions of reduced frequency (K) that relate turbulence in upstream wind flow to the fluctuating wind load in the frequency domain. To extract the aerodynamic admittance functions of a cable in the frequency domain, Eqs. (17) and (18) can be used:

$$S_{F_b^h F_b^h}(K) = \left(\frac{1}{2}\rho U^2 D\right)^2 \left[(2C_L)^2 \frac{S_{uu}(K)}{U^2} + (C_D + C_L')^2 \frac{S_{ww}(K)}{U^2} \right] \chi_h^2(K) \tag{17}$$

$$S_{F_b^p F_b^p}(K) = \left(\frac{1}{2}\rho U^2 D\right)^2 \left[4C_D^2 \frac{S_{uu}(K)}{U^2} + C_L^2 \frac{S_{ww}(K)}{U^2} \right] \chi_p^2(K) \tag{18}$$

where $S_{F_b^h F_b^h}(K)$ and $S_{F_b^p F_b^p}(K)$ are power spectral densities of the buffeting load in across- and along-wind directions, respectively, $S_{uu}(K)$ and $S_{ww}(K)$ are power spectral densities of wind turbulence in along- and across-wind directions, respectively, and $\chi_h^2(K)$ and $\chi_p^2(K)$ are aerodynamic admittance functions in vertical and lateral directions. The buffeting indicial derivative function takes the form given in Eq. (19):

$$\phi'(s) = A_1 e^{-A_2 s} + A_3 e^{-A_4 s} \tag{19}$$

where $A_i, i = 1 \dots 4$, are constants that can be computed for each of the two DOF using Eq. (20) that is derived from the Fourier transform relationship between the aerodynamic admittance function, as identified from wind tunnel tests, and buffeting indicial derivative function.

$$\chi^2(K) = \left(\frac{A_1 \cdot K}{A_2^2 + K^2} + \frac{A_3 \cdot K}{A_4^2 + K^2} \right)^2 + \left(\frac{A_1 \cdot A_2}{A_2^2 + K^2} + \frac{A_3 \cdot A_4}{A_4^2 + K^2} \right)^2 \tag{20}$$

Finally, buffeting loads can be computed for both vertical and lateral DOFs by applying Eqs. (15) and (16) after identifying the buffeting indicial derivative functions.

7.1.3 Self-excited force

Self-excited loads are motion-induced loads that are proportional to displacements and velocities of the cable motion and mean speed of the incoming wind. Parameters describing these loads can be extracted using two methods: direct measurement of aerodynamic force using strain gauges, or indirect measurements using a free vibration system or force vibration system wind tunnel test. Flutter derivatives have been widely used to find the flutter wind speed of different structures, mainly long-span bridges, and many studies

Table 19 Flutter derivatives (FDs) associated with vertical and lateral motions of a cable

	Degree of freedom (DOF)	FDs
1	1DOF vertical (h)	H_1^*, H_4^*
2	1DOF lateral (p)	P_1^*, P_4^*
3	2DOF (h, p)	$H_1^*, H_4^*, H_5^*, H_6^*$ $P_1^*, P_4^*, P_5^*, P_6^*$

have been conducted to extract flutter derivatives using section models. Flutter derivatives associated with vertical and lateral motions are listed in Table 19.

The following equation describes the extraction of flutter derivatives for two-degree-of-freedom (2DOF) tests. The general equation of motion for a structure due to self-excited loads of vertical motion is defined as follows:

$$\ddot{y} + M^{-1}C\dot{y} + M^{-1}ky = M^{-1}F_{se} \tag{21}$$

where

$$y = \{h \ p\}^T$$

$$M = \begin{bmatrix} m_h & 0 \\ 0 & m_p \end{bmatrix}$$

$$M^{-1}C = \begin{bmatrix} 2\zeta_h\omega_h & 0 \\ 0 & 2\zeta_p\omega_p \end{bmatrix}, M^{-1}K = \begin{bmatrix} \omega_h^2 & 0 \\ 0 & \omega_p^2 \end{bmatrix}$$

and the aeroelastic force (F_{se}) is given in Eq. (22):

$$F_{se} = \begin{Bmatrix} L_{se} \\ D_{se} \end{Bmatrix} = \begin{bmatrix} 0.5\rho U^2 D & 0 \\ 0 & 0.5\rho U^2 D \end{bmatrix} \begin{bmatrix} \dot{h} \\ \dot{p} \\ h \\ p \end{bmatrix}$$

$$\begin{bmatrix} KH_1^*/U & KH_5^*/U & K^2H_4^*/D & K^2H_6^*/D \\ KP_5^*/U & KP_1^*/U & K^2P_6^*/D & K^2P_4^*/D \end{bmatrix} \begin{bmatrix} \dot{h} \\ \dot{p} \\ h \\ p \end{bmatrix} \tag{22}$$

where K is the reduced frequency ($K = \omega D/U$), ω is the angular frequency, D is a typical across-wind dimension of the cross section of the structure or cable diameter here, and U is the mean wind speed. By substituting Eq. (21) in Eq. (22) and gathering all terms to the left-hand side, the modified free-vibration equation including aeroelastic effects is

$$\ddot{y} + \underline{C}^{eff}\dot{y} + \underline{K}^{eff}y = 0 \tag{23}$$

where \underline{C}^{eff} and \underline{K}^{eff} are the aeroelastically modified effective damping and stiffness, respectively. In addition, if \underline{C}^{eff} and \underline{K}^{eff} are mechanical damping and stiff-

ness under zero-wind conditions, the flutter derivatives of H_i^* and P_i^* , $i = 1, 4, 5, 6$, can be derived as follows:

$$H_1^*(K) = -\frac{2m_h}{\rho D^2 \omega} (C_{11}^{\text{eff}} - C_{11}^{\text{mech}}) \tag{24}$$

$$H_4^*(K) = -\frac{2m_h}{\rho D^2 \omega^2} (K_{11}^{\text{eff}} - K_{11}^{\text{mech}}) \tag{25}$$

$$H_5^*(K) = -\frac{2m_h}{\rho D^2 \omega} (C_{12}^{\text{eff}} - C_{12}^{\text{mech}}) \tag{26}$$

$$H_6^*(K) = -\frac{2m_h}{\rho D^2 \omega^2} (K_{12}^{\text{eff}} - K_{12}^{\text{mech}}) \tag{27}$$

$$P_1^*(K) = -\frac{2m_p}{\rho D^2 \omega} (C_{22}^{\text{eff}} - C_{22}^{\text{mech}}) \tag{28}$$

$$P_4^*(K) = -\frac{2m_p}{\rho D^2 \omega^2} (K_{22}^{\text{eff}} - K_{22}^{\text{mech}}) \tag{29}$$

$$P_5^*(K) = -\frac{2m_p}{\rho D^2 \omega} (C_{21}^{\text{eff}} - C_{21}^{\text{mech}}) \tag{30}$$

$$P_6^*(K) = -\frac{2m_p}{\rho D^2 \omega^2} (K_{21}^{\text{eff}} - K_{21}^{\text{mech}}) \tag{31}$$

An iterative least-squares (ILS) method was used for the extraction of flutter derivatives. This system identification method was successfully used to extract all 18 flutter derivatives of a 3DOF section model of a bridge [407]. To apply this method, the displacement response of a section model that is released from a fixed state of rest with an initial displacement, measured in free vibration, is filtered digitally and used as an input to this method. A low-pass filter is usually employed to remove all noises from the recorded displacement time history with frequencies higher than the natural frequency of the section model. In the ILS method, a state-space model is used as given by Eq. (32):

$$\dot{X} = AX \tag{32}$$

where

$$X = \begin{bmatrix} y \\ \dot{y} \end{bmatrix}, A = \begin{bmatrix} 0 & 1 \\ -K^{\text{eff}} & -C^{\text{eff}} \end{bmatrix}$$

A is a 2×2 square matrix. After calculating the filtered displacement time history from the measured time history displacement and calculating the velocity, \dot{h} , \dot{p} , and acceleration, \ddot{h} , \ddot{p} time histories of the section model, A or C^{eff} and K^{eff} can be identified using the ILS method at a given wind speed, and by subtracting their zero-wind values C^{mech} and K^{mech} , respectively, H_i^* and P_i^* , $i = 1, 4, 5, 6$, can be extracted at a given wind speed using Eqs. (24)–(31). Full description of the ILS method can be obtained in [407]. For maintaining accuracy, all initial displacements and sampling time

of the time history records were kept the same for all wind speeds. Similarly, flutter derivatives for 1DOF lateral (p) and vertical motion (h) can be extracted by conducting free vibration tests.

References

1. Matsumoto, M., Yagi, T., Hatsuda, H., Shima, T., Tanaka, M., Naito, H.: Dry galloping characteristics and its mechanism of inclined/yawed cables. *J. Wind Eng. Ind. Aerodyn.* **98**, 317–327 (2010)
2. Tokoro, S., Komatsu, H., Nakasu, M., Mizuguchi, K., Kasuga, A.: Study on wake-galloping employing full aeroelastic twin cable model. *J. Wind Eng. Ind. Aerodyn.* **88**, 247–261 (2000)
3. Lilien, J.L., Snegovski, D.: Wake-induced vibration in power transmission line. Parametric study. In: *Flow Induced Vibration-FIV*, p. 5 (2004)
4. Virlogeux, M.: Cable vibrations in cable-stayed bridges. In: Larsen, A., Eisdahl, S. (eds.) *Bridge Aerodynamics*, pp. 213–233. Balkema, Rotterdam (1998)
5. Zuo, D., Jones, N., Main, J.: Vortex- and rain-wind-induced stay cable vibrations in a three-dimensional environment. In: *Proceedings of the 5th International Colloquium on Bluff Body Aerodynamics and Applications*, Ottawa, pp. 397–400 (2004)
6. Hjorth-Hansen, E., Strømmen, E.: Wind-excited vibration of the longest suspenders of a suspension bridge. In: *Proceedings of the 5th ISCD*, St. Margherita, pp. 541–543 (2003)
7. Fujino, Y., Kimura, K., Tanaka, H.: *Wind Resistant Design of Bridges in Japan: Developments and Practices*. Springer, New York (2012)
8. Ruscheweyh, H., Hirsch, G.: Vibration measurements at the cable stayed Kohlbrand Bridge in Hamburg. Technical report, Institute for Lightweight Structures, University of Aachen (RWTH) (1974) **(in German)**
9. Wianeck, J.: Cables wind excited vibrations of cable-stayed bridges. In: *Proceedings of the 5th International Conference of Wind Engineering*, pp. 1381–1393 (1979)
10. Hikami, Y.: Rain vibrations of cables in cable-stayed bridge. *Wind Eng. JAWE.* **27**, 17–28 (1986). **(in Japanese)**
11. Hikami, Y., Shiraishi, N.: Rain-wind induced vibrations of cables stayed bridges. *J. Wind Eng. Ind. Aerodyn.* **29**, 409–418 (1988)
12. Langsoe, H.E., Larsen, O.D.: Generating mechanisms for cable stay oscillations at the FARO bridges. In: *Proceedings of the International Conference on Cable-Stayed Bridges*, Bangkok (1987)
13. Miyasaka, Y., Ohshima, K., Nakabayashi, S.: Experimental study on Ajikawa Bridge cable vibration. Hanshin expressway public corporation engineering report (1987) **(in Japanese)**
14. Ohshima, K., Nanjo, M.: Aerodynamic stability of the cables of a cable-stayed bridge subjected to rain: a case study of the Aji river bridge. In: *Proceedings of the US-Japan Joint Seminar on Natural Resources* (1987)

15. Yoshimura, T., Savage, M., Tanaka, H.: Wind induced vibrations of bridge stay-cables. In: Proceedings of the 1st ISCD, Liege, pp. 437–444 (1995)
16. Lilien, J.L., Pinto da Costa, A.: Vibration amplitudes caused by parametric excitation of cable stayed structures. *J. Sound Vib.* **174**(1), 69–90 (1994)
17. Cremer, J., Counasse, C., de Ville de Goyet, V., Lothaire, A., Dumortier, A.: The stays, their dynamic behaviour, their equipments: bridges at Ben-Ahin, Wandre and upon Alzette. In: Proceedings of the 1st ISCD, Liege, pp. 489–496 (1995)
18. Gu, M.: Rain-wind induced vibration of cables on cable-stayed bridges and its control. *Shanghai J. Mech.* **25**, 281–288 (1998)
19. Geurts, C., Vrouwenvelder, T., Van Staaldin, P., Reusink, J.: Numerical modelling of rain-wind-induced vibration: Erasmus Bridge, Rotterdam. *Struct. Eng. Int.* **8**, 129–135 (1998)
20. Larsen, A., Lafrenière, A.: Application of a limit cycle oscillator model to bridge cable galloping. In: Proceedings of the 6th International Symposium on Cable Dynamics, pp. 19–22 (2005)
21. Irwin, P.A.: Field monitoring of cable supported bridges. In: Proceedings of the 6th ISCD, Charleston, South Carolina (2005)
22. Irwin, P.A., Nedim, A., Telang, N.: Wind induced stay cable vibrations—a case study. In: Proceeding of the 3rd International Symposium on Cable Aerodynamics, pp. 171–176 (1999)
23. Narita, N., Yokoyama, K.: A summarized account of damping capacity and measures against wind action in cable-stayed bridges in Japan. In: *Cable-Stayed Bridges: Recent Developments and Their Future*, pp. 257–278 (1991)
24. Toriumi, R., Furuya, N., Takeguchi, M., Miyazaki, M., Saito, Z.: A study on wind-induced vibration of parallel suspenders observed at the Akashi-Kaikyo bridge. In: Proceedings of the 3rd International Symposium on Cable Dynamics, Trondheim, pp. 177–182 (1999)
25. Matsumoto, M.: Effects of axial flow and Karman vortex interference on dry-state galloping of inclined stay-cables. In: Proceedings of the 6th International Symposium on Cable Dynamics, USA, pp. 19–22 (2005)
26. Jafari, M., Sarkar, P.P.: Parameter identification of wind-induced buffeting loads and onset criteria for dry-cable galloping of yawed/inclined cables. *Eng. Struct.* **180**, 685–699 (2019)
27. Ribeiro, J.D.: Fluctuating lift and its spanwise correlation on a circular cylinder in a smooth and in a turbulent flow: a critical review. *J. Wind Eng. Ind. Aerodyn.* **40**, 179–198 (1992)
28. Blevins, R.D.: *Flow-Induced Vibration*. Van Nostrand Reinhold Co, New York (1977)
29. Fujisawa, N., Tanahashi, S., Srinivas, K.: Evaluation of pressure field and fluid forces on a circular cylinder with and without rotational oscillation using velocity data from PIV measurement. *Meas. Sci. Technol.* **16**, 989–996 (2005)
30. Perrin, R., Cid, E., Cazin, S., Sevrain, A., Braza, M., Moradei, F., Harran, G.: Phase-averaged measurements of the turbulence properties in the near wake of a circular cylinder at high Reynolds number by 2C-PIV and 3C-PIV. *Exp. Fluids* **42**, 93–109 (2006)
31. Oruç, V., Akilli, H., Sahin, B.: PIV measurements on the passive control of flow past a circular cylinder. *Exp. Therm. Fluid Sci.* **70**, 283–291 (2016)
32. Yayla, S., Teksin, S.: Flow measurement around a cylindrical body by attaching flexible plate: a PIV approach. *Flow Meas. Instrum.* **62**, 56–65 (2018)
33. Gao, W., Nelias, D., Liu, Z., Lyu, Y.: Numerical investigation of flow around one finite circular cylinder with two free ends. *Ocean Eng.* **156**, 373–380 (2018)
34. Dehkordi, B.G., Moghaddam, H.S., Jafari, H.H.: Numerical simulation of flow over two circular cylinders in tandem arrangement. *J. Hydrodyn. Ser. B.* **23**, 114–126 (2011)
35. Pereira, F.S., Vaz, G., Eça, L., Girimaji, S.S.: Simulation of the flow around a circular cylinder at $Re = 3900$ with partially-averaged Navier–Stokes equations. *Int. J. Heat Fluid Flow* **69**, 234–246 (2018)
36. Jiang, H., Cheng, L., Draper, S., An, H.: Prediction of the secondary wake instability of a circular cylinder with direct numerical simulation. *Comput. Fluids* **149**, 172–180 (2017)
37. Zdravkovich, M.: *Flow Around Circular Cylinders Volume 1: Fundamentals*. Oxford University Press, Oxford (1997)
38. Demartino, C., Ricciardelli, F.: Aerodynamics of nominally circular cylinders: a review of experimental results for Civil Engineering applications. *Eng. Struct.* **137**, 76–114 (2017)
39. Zdravkovich, M.M.: Conceptual overview of laminar and turbulent flows past smooth and rough circular cylinders. *J. Wind Eng. Ind. Aerodyn.* **33**, 53–62 (1990)
40. Keefe, R.T.: Investigation of the fluctuating forces acting on a stationary circular cylinder in a subsonic stream and of the associated sound field. *J. Acoust. Soc. Am.* **34**, 1711–1714 (1962)
41. Leehey, P., Hanson, C.E.: Aeolian tones associated with resonant vibration. *J. Sound Vib.* **13**, 465–483 (1970)
42. Sonnevile, P.: Etude du champ de pressions fluctuantes a la surface d'un cylindre circulaire. *Comptes Rendus Acad. des Sci. Paris Ser. A* **277**, 383–385 (1973)
43. Mohr, K.-H.: Messungen instationären Druckes bei Queranströmung von Kreiszyklindern unter Berücksichtigung fluidelastischer Effekte. Ph.D. thesis, KFA Julich GmbH, Germany (1981)
44. Moeller, M.J., Leehey, P.: Unsteady forces on a cylinder in cross flow at subcritical Reynolds numbers. In: *ASME Symposium on Flow Induced Vibrations*, vol. 1, pp. 57–71 (1984)
45. Gartshore, I.S.: Some effects of upstream turbulence on the unsteady lift forces imposed on prismatic two dimensional bodies. *ASME J. Fluids Eng.* **106**, 418–424 (1984)
46. Szepešy, S., Bearman, P.W.: Aspect ratio and end plate effects on vortex shedding from a circular cylinder. *J. Fluid Mech.* **234**, 191–217 (1992)
47. West, G.S., Apelt, C.J.: Measurements of fluctuating pressures and forces on a circular cylinder in the Reynolds number range 10^4 to 2.5×10^5 . *J. Fluids Struct.* **7**, 227–244 (1993)
48. Sakamoto, H., Haniu, H.: Optimum suppression of fluid forces acting on a circular cylinder. *J. Fluids Eng.* **116**, 221 (1994)
49. Norberg, C.: Fluctuating lift on a circular cylinder review and new measurements. *J. Fluids Struct.* **17**, 57–96 (2003)

50. Batchelor, G.K.: *An Introduction to Fluid Mechanics*. Cambridge University Press, Cambridge (2000)
51. Norberg, C.: Pressure forces on a circular cylinder in cross flow. In: Eckelmann, H., Michael, J., Graham, R., Huerre, P., Monkewitz, P.A. (eds.) *Bluff-Body Wakes, Dynamics and Instabilities*, pp. 275–278. Springer, Berlin (1992)
52. Lienhard, J.H.: *Synopsis of Lift, Drag, and Vortex Frequency Data for Rigid Circular Cylinders*. Technical Extension Service, Washington State University, Pullman (1966)
53. Wieselsberger, C.: New data on the laws of fluid resistance. Report No. NACA TN 84; National Advisory Committee for Aeronautics (1922)
54. Hallam, M., Heaf, N., Wootton, L.R.: *Dynamics of marine structures: methods of calculating the dynamic response of fixed structures subject to wave and current action*. Technical report (1977)
55. Schewe, G.: On the force fluctuations acting on a circular cylinder in crossflow from subcritical up to transcritical Reynolds numbers. *J. Fluid Mech.* **133**, 265–285 (1983)
56. Williamson, C.H.K.: Oblique and parallel modes of vortex shedding in the wake of a circular cylinder at low Reynolds numbers. *J. Fluid Mech.* **206**, 579–627 (1989)
57. Roshko, A.: Experiments on the flow past a circular cylinder at very high Reynolds number. *J. Fluid Mech.* **10**, 345–356 (1961)
58. Achenbach, E., Heinecke, E.: On vortex shedding from smooth and rough cylinders in the range of Reynolds numbers 6×10^3 to 5×10^6 . *J. Fluid Mech.* **109**, 239–251 (1981)
59. Kwok, K.C.: Turbulence effect on flow around circular cylinder. *J. Eng. Mech.* **112**, 1181–1197 (1986)
60. Wong, H.Y.: A means of controlling bluff body flow separation. *J. Ind. Aerodyn.* **4**, 183–201 (1979)
61. Batham, J.P.: Pressure distributions on circular cylinders at critical Reynolds numbers. *J. Fluid Mech.* **57**, 209–228 (1973)
62. Sadeh, W.Z., Saharon, D.B.: Turbulence effect on crossflow around a circular cylinder at subcritical Reynolds numbers. NASA contractor report 3622 (1982)
63. Chiu, W.S., Lienhard, J.H.: On real fluid flow over yawed circular cylinders 1. *J. Basic Eng.* **89**, 851–857 (2018)
64. Feng, C.C.: The measurement of vortex induced effects in flow past stationary and oscillating circular and d-section cylinders. MASC. Thesis, Department of Mechanical Engineering, The University of British Columbia (1968)
65. Wootton, L.: The oscillations of large circular stacks in wind. *Proc. Inst. Civ. Eng.* **43**, 573–598 (1969)
66. Simiu, E., Scanlan, R.H.: *Wind Effects on Structures: Fundamentals and Applications to Design*. Wiley, New York (1996)
67. Surt, J., Surry, D.: The effect of inclination on the Strouhal number and other wake properties of circular cylinders at subcritical Reynolds numbers. Technical Report, Institute for Aerospace Studies, University of Toronto, (1967)
68. Van Atta, C.: Experiments in vortex shedding from yawed circular cylinders. *AIAA J.* **6**, 931–933 (1968)
69. Willden, R., Guerbi, M.: Vortex dynamics of stationary and oscillating cylinders in yawed flow. In: *IUTAM Symposium on Bluff Body Wakes and Vortex-Induced Vibrations (BBVIV-6)*, pp. 47–54. Capri, Italy (2010)
70. Ramberg, S.E.: The effects of yaw and finite length upon the vortex wakes of stationary and vibrating circular cylinders. *J. Fluid Mech.* **128**, 81–107 (1983)
71. Lucor, D., Karniadakis, G.E.: Effects of oblique inflow in vortex-induced vibrations. *Flow Turbul Combust* **71**, 375–389 (2003). <https://doi.org/10.1023/B:APPL.0000014929.90891.4d>
72. Zhao, M., Cheng, L., Zhou, T.: Direct numerical simulation of three-dimensional flow past a yawed circular cylinder of infinite length. *J. Fluids Struct.* **25**, 831–847 (2009)
73. Buresti, G.: The effect of surface roughness on the flow regime around circular cylinders. *J. Wind Eng. Ind. Aerodyn.* **8**, 105–114 (1981)
74. Diana, G., Belloli, M., Giappino, S., Muggiasca, S.: Vortex induced vibrations at high Reynolds numbers. In: *VI International Colloquium on Bluff Bodies Aerodynamics & Applications BBAA VI*. pp. 20–24 (2008)
75. Górski, P., Pospíšil, S., Kuznetsov, S., Tatara, M., Marušić, A.: Strouhal number of bridge cables with ice accretion at low flow turbulence. *Wind Struct. Int. J.* **22**, 253–272 (2016). <https://doi.org/10.12989/was.2016.22.2.253>
76. Trush, A., Pospíšil, S., Kuznetsov, S., Kozmar, H.: Wind-tunnel experiments on vortex-induced vibration of rough bridge cables. *J. Bridge Eng.* **22**, 06017001 (2017)
77. Evangelinos, C., Lucor, D., Karniadakis, G.E.: DNS-derived force distribution on flexible cylinders subject to vortex-induced vibration. *J. Fluids Struct.* **14**, 429–440 (2000)
78. Matsumoto, M., Shirato, H., Yagi, T., Goto, M., Sakai, S., Ohya, J.: Field observation of the full-scale wind-induced cable vibration. *J. Wind Eng. Ind. Aerodyn.* **91**, 13–26 (2003)
79. Matsumoto, M., Yagi, T., Shigemura, Y., Tsushima, D.: Vortex-induced cable vibration of cable-stayed bridges at high reduced wind velocity. *J. Wind Eng. Ind. Aerodyn.* **89**, 633–647 (2001)
80. Zuo, D., Jones, N.P., Main, J.A.: Field observation of vortex- and rain-wind-induced stay-cable vibrations in a three-dimensional environment. *J. Wind Eng. Ind. Aerodyn.* **96**, 1124–1133 (2008)
81. Zuo, D., Jones, N.P.: Interpretation of field observations of wind- and rain-wind-induced stay cable vibrations. *J. Wind Eng. Ind. Aerodyn.* **98**, 73–87 (2010)
82. Chen, W.-L., Li, H., Ou, J.-P., Li, F.-C.: Numerical simulation of vortex-induced vibrations of inclined cables under different wind profiles. *J. Bridge Eng.* **18**, 42–53 (2013). [https://doi.org/10.1061/\(ASCE\)BE.1943-5592.0000323](https://doi.org/10.1061/(ASCE)BE.1943-5592.0000323)
83. Chen, W.-L., Zhang, Q.-Q., Li, H., Hu, H.: An experimental investigation on vortex induced vibration of a flexible inclined cable under a shear flow. *J. Fluids Struct.* **54**, 297–311 (2015)
84. Gao, D., Chen, W.-L., Zhang, R.-T., Huang, Y.-W., Li, H.: Multi-modal vortex- and rain-wind- induced vibrations of an inclined flexible cable. *Mech. Syst. Signal Process.* **118**, 245–258 (2019)
85. Zeinoddini, M., Bakhtiari, A., Gharebaghi, S.A.: Towards an understanding of the marine fouling effects on VIV of circular cylinders: a probe into the chaotic features. *Non-linear Dyn.* **94**, 575–595 (2018)

86. Plaschko, P., Berger, E., Brod, K.: The transition of flow-induced cylinder vibrations to chaos. *Nonlinear Dyn.* **4**, 251–268 (1993)
87. Huang, K., Feng, Q., Qu, B.: Bending aeroelastic instability of the structure of suspended cable-stayed beam. *Nonlinear Dyn.* **87**, 2765–2778 (2017)
88. Persoon, A., Noorlander, K.: Full scale measurements on the Erasmus Bridge after rain/wind induced cable vibration. In: Proceedings of the 10th International Conference on Wind Engineering, pp. 1019–1026. Copenhagen, Denmark (1999)
89. Main, J., Jones, N.: Evaluation of viscous dampers for stay-cable vibration mitigation. *J. Bridge Eng.* **6**, 385–397 (2001)
90. Zdravkovich, M.M.: Review and classification of various aerodynamic and hydrodynamic means for suppressing vortex shedding. *J. Wind Eng. Ind. Aerodyn.* **7**, 145–189 (1981)
91. Nebres, J., Batill, S.: Flow about a circular cylinder with a single large-scale surface perturbation. *Exp. Fluids* **15**, 369–379 (1993)
92. Igarashi, T.: Effect of tripping wires on the flow around a circular cylinder normal to an airstream. *Bull. JSME* **29**, 2917–2924 (1986)
93. Hover, F., Tvedt, H., Triantafyllou, M.: Vortex-induced vibrations of a cylinder with tripping wires. *J. Fluid Mech.* **448**, 175–195 (2001)
94. Fransson, J.H.M., Konieczny, P., Alfredsson, P.H.: Flow around a porous cylinder subject to continuous suction or blowing. *J. Fluids Struct.* **19**, 1031–1048 (2004)
95. Patil, S.K.R., Ng, T.T.: Control of separation using spanwise periodic porosity. *AIAA J.* **48**, 174–187 (2010). <https://doi.org/10.2514/1.43321>
96. Li, Z., Navon, I.M., Hussaini, M.Y., Le Dimet, F.-X.: Optimal control of cylinder wakes via suction and blowing. *Comput. Fluids* **32**, 149–171 (2003)
97. Chen, W.-L., Xin, D.-B., Xu, F., Li, H., Ou, J.-P., Hu, H.: Suppression of vortex-induced vibration of a circular cylinder using suction-based flow control. *J. Fluids Struct.* **42**, 25–39 (2013)
98. Gattulli, V., Ghanem, R.: Adaptive control of flow-induced oscillations including vortex effects. *Int. J. Nonlinear Mech.* **34**, 853–868 (1999)
99. Blanchard, A., Bergman, L.A., Vakakis, A.F.: Vortex-induced vibration of a linearly sprung cylinder with an internal rotational nonlinear energy sink in turbulent flow. *Nonlinear Dyn.* **99**, 593–609 (2019)
100. Mehmood, A., Nayfeh, A.H., Hajj, M.R.: Effects of a nonlinear energy sink (NES) on vortex-induced vibrations of a circular cylinder. *Nonlinear Dyn.* **77**, 667–680 (2014)
101. Dongyang, C., Abbas, L.K., Guoping, W., Xiaoting, R., Marzocca, P.: Numerical study of flow-induced vibrations of cylinders under the action of nonlinear energy sinks (NESs). *Nonlinear Dyn.* **94**, 925–957 (2018)
102. Zhang, Y.-W., Zhang, Z., Chen, L.-Q., Yang, T.-Z., Fang, B., Zang, J.: Impulse-induced vibration suppression of an axially moving beam with parallel nonlinear energy sinks. *Nonlinear Dyn.* **82**, 61–71 (2015)
103. Dai, H.L., Abdelkefi, A., Wang, L.: Vortex-induced vibrations mitigation through a nonlinear energy sink. *Commun. Nonlinear Sci. Numer. Simul.* **42**, 22–36 (2017)
104. Dai, H.L., Abdelkefi, A., Wang, L., Liu, W.B.: Time-delay feedback controller for amplitude reduction in vortex-induced vibrations. *Nonlinear Dyn.* **80**, 59–70 (2015)
105. Dai, H.L., Abdelkefi, A., Wang, L.: Piezoelectric energy harvesting from concurrent vortex-induced vibrations and base excitations. *Nonlinear Dyn.* **77**, 967–981 (2014)
106. Liu, H., Gao, X.: Vibration energy harvesting under concurrent base and flow excitations with internal resonance. *Nonlinear Dyn.* **96**, 1067–1081 (2019)
107. Javed, U., Abdelkefi, A.: Characteristics and comparative analysis of piezoelectric-electromagnetic energy harvesters from vortex-induced oscillations. *Nonlinear Dyn.* **95**, 3309–3333 (2019)
108. Dai, H.L., Abdelmoula, H., Abdelkefi, A., Wang, L.: Towards control of cross-flow-induced vibrations based on energy harvesting. *Nonlinear Dyn.* **88**, 2329–2346 (2017)
109. Matsumoto, M., Shiraishi, N., Shirato, H.: Rain-wind induced vibration of cables of cable-stayed bridges. *J. Wind Eng. Ind. Aerodyn.* **43**, 2011–2022 (1992)
110. Main, J., Jones, N.P.: Full-scale measurements of stay cable vibration. *Wind Eng.* **2**, 963–970 (1999)
111. Phelan, R.S., Sarkar, P.P., Mehta, K.C.: Full-scale measurements to investigate rain-wind induced cable-stay vibration and its mitigation. *J. Bridge Eng.* **11**, 293–304 (2006). [https://doi.org/10.1061/\(ASCE\)1084-0702\(2006\)11:3\(293\)](https://doi.org/10.1061/(ASCE)1084-0702(2006)11:3(293))
112. Ni, Y.Q., Wang, X.Y., Chen, Z.Q., Ko, J.M.: Field observations of rain-wind-induced cable vibration in cable-stayed Dongting Lake Bridge. *J. Wind Eng. Ind. Aerodyn.* **95**, 303–328 (2007)
113. Acampora, A., Georgakis, C.: Recent monitoring of the Øresund Bridge: observations of rain-wind induced cable vibrations. In: 13th International Conference on Wind Engineering (2011)
114. Gu, M., Du, X.: Experimental investigation of rain-wind-induced vibration of cables in cable-stayed bridges and its mitigation. *J. Wind Eng. Ind. Aerodyn.* **93**, 79–95 (2005)
115. Matsumoto, M., Yagi, T., Goto, M., Sakai, S.: Rain-wind-induced vibration of inclined cables at limited high reduced wind velocity region. *J. Wind Eng. Ind. Aerodyn.* **91**, 1–12 (2003)
116. Flamand, O.: Rain-wind induced vibration of cables. *J. Wind Eng. Ind. Aerodyn.* **57**, 353–362 (1995)
117. Bosdogianni, A., Olivari, D.: Wind- and rain-induced oscillations of cables of stayed bridges. *J. Wind Eng. Ind. Aerodyn.* **64**, 171–185 (1996)
118. Gu, M., Liu, C., Xu, Y., Xiang, H.: Response characteristics of wind excited cables with artificial rivulet. *Appl. Math. Mech.* **23**, 1176–1187 (2002)
119. Xu, Y., Li, Y., Shum, K., Kwok, K., Kwok, K., Hitchcock, P.: Aerodynamic coefficients of inclined circular cylinders with artificial rivulet in smooth flow. *Adv. Struct. Eng.* **9**, 265–278 (2006)
120. Du, X., Gu, M., Chen, S.: Aerodynamic characteristics of an inclined and yawed circular cylinder with artificial rivulet. *J. Fluids Struct.* **43**, 64–82 (2013)
121. Zhan, S., Xu, Y.L., Zhou, H.J., Shum, K.M.: Experimental study of wind-rain-induced cable vibration using a new model setup scheme. *J. Wind Eng. Ind. Aerodyn.* **96**, 2438–2451 (2008). <https://doi.org/10.1016/J.JWEIA.2008.03.011>

122. Cosentino, N., Flamand, O., Ceccoli, C.: Rain-wind induced vibration of inclined stay cables-Part I: experimental investigation and physical explanation. *Wind Struct.* **6**, 471–484 (2003)
123. Cosentino, N., Flamand, O., Ceccoli, C.: Rain-wind induced vibration of inclined stay cables-Part II: mechanical modeling and parameter characterisation. *Wind Struct.* **6**, 485–498 (2003)
124. Wang, Z.J., Zhou, Y., Huang, J.F., Xu, Y.L.: Fluid dynamics around an inclined cylinder with running water rivulets. *J. Fluids Struct.* **21**, 49–64 (2005)
125. Chen, W.-L., Tang, S.-R., Li, H., Hu, H.: Influence of dynamic properties and position of rivulet on rain-wind-induced vibration of stay cables. *J. Bridge Eng.* **18**, 1021–1031 (2013). [https://doi.org/10.1061/\(ASCE\)BE.1943-5592.0000443](https://doi.org/10.1061/(ASCE)BE.1943-5592.0000443)
126. Li, Y., Jing, H., Xia, Y., Xu, Y., Xiang, H.: Measurement of rivulet movement on inclined cables during rain-wind induced vibration. *Sens. Actuators A Phys.* **230**, 17–24 (2015)
127. Jing, H., Xia, Y., Li, H., Xu, Y., Li, Y.: Excitation mechanism of rain-wind induced cable vibration in a wind tunnel. *J. Fluids Struct.* **68**, 32–47 (2017)
128. Cheng, P., Li, W.-J., Chen, W.-L., Gao, D.-L., Xu, Y., Li, H.: Computer vision-based recognition of rainwater rivulet morphology evolution during rain-wind-induced vibration of a 3D aeroelastic stay cable. *J. Wind Eng. Ind. Aerodyn.* **172**, 367–378 (2018)
129. Ge, Y., Chang, Y., Xu, L., Zhao, L.: Experimental investigation on spatial attitudes, dynamic characteristics and environmental conditions of rain-wind-induced vibration of stay cables with high-precision raining simulator. *J. Fluids Struct.* **76**, 60–83 (2018)
130. Gu, M.: On wind-rain induced vibration of cables of cable-stayed bridges based on quasi-steady assumption. *J. Wind Eng. Ind. Aerodyn.* **97**, 381–391 (2009)
131. Yamaguchi, H.: Analytical study on growth mechanism of rain vibration of cables. *J. Wind Eng. Ind. Aerodyn.* **33**, 73–80 (1990)
132. Xu, Y.L., Wang, L.Y.: Analytical study of wind-rain-induced cable vibration: SDOF model. *J. Wind Eng. Ind. Aerodyn.* **91**, 27–40 (2003)
133. Wilde, K., Witkowski, W.: Simple model of rain-wind-induced vibrations of stayed cables. *J. Wind Eng. Ind. Aerodyn.* **91**, 873–891 (2003)
134. Cao, D.Q., Tucker, R.W., Wang, C.: A stochastic approach to cable dynamics with moving rivulets. *J. Sound Vib.* **268**, 291–304 (2003)
135. Seidel, C., Dinkler, D.: Rain-wind induced vibrations—phenomenology, mechanical modelling and numerical analysis. *Comput. Struct.* **84**, 1584–1595 (2006)
136. Zhou, H., Xu, Y.: Wind-rain-induced vibration and control of stay cables in a cable-stayed bridge. *Struct. Control Heal. Monit.* **14**, 1013–1033 (2007)
137. Gu, M., Huang, L.: Theoretical and experimental studies on the aerodynamic instability of a two-dimensional circular cylinder with a moving attachment. *J. Fluids Struct.* **24**, 200–211 (2008)
138. Wu, T., Kareem, A., Li, S.: On the excitation mechanisms of rain-wind induced vibration of cables: Unsteady and hysteretic nonlinear features. *J. Wind Eng. Ind. Aerodyn.* **122**, 83–95 (2013)
139. Lemaitre, C., Hémon, P., de Langre, E.: Thin water film around a cable subject to wind. *J. Wind Eng. Ind. Aerodyn.* **95**, 1259–1271 (2007)
140. Xu, L., Zhao, L., Ge, Y.: Numerical analysis and real-time measurement of water-film on rain-wind induced vibration dable. *Acta Aerodyn. Sin.* **1**, 015 (2011)
141. Bi, J.H., Lu, P., Wang, J., Bao, C., Guan, J.: Numerical simulation and analysis of the effects of water-film morphological changes on the aerodynamic lift of stay cables. *J. Fluids Struct.* **48**, 376–392 (2014)
142. Li, S., Chen, Z., Wu, T., Kareem, A.: Rain-wind-induced in-plane and out-of-plane vibrations of stay cables. *J. Eng. Mech.* **139**, 1688–1698 (2013)
143. Li, S., Chen, Z., Sun, W., Li, S.: Experimental investigation on quasi-steady and unsteady self-excited aerodynamic forces on cable and rivulet. *J. Eng. Mech.* **142**, 06015004 (2015)
144. Jing, H., He, X., Wang, Z.: Numerical modeling of the wind load of a two-dimensional cable model in rain-wind-induced vibration. *J. Fluids Struct.* **82**, 121–133 (2018)
145. Miyata, Y., Yamada, H., Hojo, T.: Experimental study on aerodynamic characteristics of cables with patterned surface. *J. Struct. Eng. A.* **40**, 1065–1076 (1994)
146. Kleissl, K., Georgakis, C.T.T.: Comparison of the aerodynamics of bridge cables with helical fillets and a pattern-indented surface. *J. Wind Eng. Ind. Aerodyn.* **104–106**, 166–175 (2012)
147. Li, S., Deng, Y., Zhong, W., Chen, Z.: On the aerodynamic characteristics of stay cables attached with helical wires. *Adv. Struct. Eng.* **21**, 1262–1272 (2018)
148. Bi, J.H., Qiao, H.Y., Nikitas, N., Guan, J., Wang, J., Lu, P.: Numerical modelling for rain wind induced vibration of cables with longitudinal ribs. *J. Wind Eng. Ind. Aerodyn.* **178**, 69–79 (2018)
149. Nakamura, A., Kasuga, A., Arai, H.: The effects of mechanical dampers on stay cables with high-damping rubber. *Constr. Build. Mater.* **12**, 115–123 (1998)
150. Tabatabai, H., Mehrabi, A.B.: Design of mechanical viscous dampers for stay cables. *J. Bridge Eng.* **5**, 114–123 (2000)
151. Chen, Z.Q., Wang, X.Y., Ko, J.M., Ni, Y.Q., Spencer, B.F., Yang, G., Hu, J.H.: MR damping system for mitigating wind-rain induced vibration on Dongting Lake cable-stayed bridge. *Wind Struct. Int. J.* **7**, 293–304 (2004). <https://doi.org/10.12989/was.2004.7.5.293>
152. Li, S., Wu, T., Li, S., Gu, M.: Numerical study on the mitigation of rain-wind induced vibrations of stay cables with dampers. *Wind Struct.* **23**, 615–639 (2016). <https://doi.org/10.12989/was.2016.23.6.615>
153. Krarup, N.H., Zhang, Z., Kirkegaard, P.H.: Active modal control of rain-wind induced vibration of stay cables. *Procedia Eng.* **199**, 3158–3163 (2017)
154. Larsen, A., Larose, G.L.: Dynamic wind effects on suspension and cable-stayed bridges. *J. Sound Vib.* **334**, 2–28 (2015)
155. Honda, A., Yamanaka, T., Fujiwara, T., Saito, T.: Wind tunnel test on rain-induced vibration of the stay-cable. In: Proceedings of the International Symposium on Cable Dynamics, pp. 255–262 (1995)

156. Irwin, P.: Wind vibrations of cables on cable-stayed bridges. In: Proceedings of the Structure Congress, pp. 383–387 (1997)
157. Kumarasena, S., Jones, N., Irwin, P., Taylor, P.: Wind-induced vibration of stay cables. FHWA-HRT-05-083. U.S. Department of Transportation, Federal Highway Administration (2007)
158. Saito, T., Matsumoto, M., Kitazawa, M.: Rain-wind excitation of cables on cable-stayed Higashi-Kobe Bridge and cable vibration control. In: Proceedings of the International Conference on Cable-Stayed and Suspension Bridges, pp. 507–514 (1994)
159. Cheng, S., Larose, G.L., Savage, M.G., Tanaka, H., Irwin, P.A.: Experimental study on the wind-induced vibration of a dry inclined cable-Part I: phenomena. *J. Wind Eng. Ind. Aerodyn.* **96**, 2231–2253 (2008)
160. Cheng, S., Irwin, P., Tanaka, H.: Experimental study on the wind-induced vibration of a dry inclined cable-Part II: proposed mechanisms. *J. Wind Eng. Ind. Aerodyn.* **96**, 2254–2272 (2008)
161. Katsuchi, H., Yamada, H.: Wind-tunnel study on dry-galloping of indented-surface stay cable. In: 11th Americas Conference on Wind Engineering, Puerto Rico, pp. 22–26 (2009)
162. Duy, H.V., Katsuchi, H., Yamada, H., Nishio, M.: A wind tunnel study on control methods for cable dry-galloping. *Front. Struct. Civ. Eng.* **10**, 72–80 (2016)
163. Benidir, A., Flamand, O., Gaillet, L., Dimitriadis, G.: Impact of roughness and circularity-defect on bridge cables stability. *J. Wind Eng. Ind. Aerodyn.* **137**, 1–13 (2015)
164. Duy, H.V., Katsuchi, H., Yamada, H., Nishio, M.: Experimental study on dry-state galloping with various wind relative angles and its countermeasures. *J. Struct. Eng.* **60**, 428–436 (2014)
165. Larose, G.L., D'Auteuil: Wind Tunnel Investigations on an Inclined Stay Cable with a Helical Fillet Federal Highway Administration, McLean, VA, Report Number FHWA-HRT-14-070 (2014)
166. Zuo, D., Jones, N.P.: Wind tunnel testing of yawed and inclined circular cylinders in the context of field observations of stay-cable vibrations. *J. Wind Eng. Ind. Aerodyn.* **97**, 219–227 (2009)
167. Flamand, O., Boujard, O.: A comparison between dry cylinder galloping and rain-wind induced excitation. In: Proceeding of the 5th European & African Conference on Wind Engineering, Florence (2009)
168. Christiansen, H., Jakobsen, J.B., Macdonald, J.H.G., Larose, G.L., Bosch, H.R.: Aerodynamics of a stay cable with helical fillets - Part II: Fluctuating load and wake characteristics. *J. Wind Eng. Ind. Aerodyn.* **177**, 392–404 (2018)
169. Kimura, K., Kato, K., Kubo, Y.: Aeroelastic response of an inclined circular cylinder in smooth and turbulent flow. In: Proceedings of 7th International Colloquium on Bluff Body Aerodynamics and Applications, Shanghai (2012)
170. Matsumoto, M., Shiraiishi, N., Kitazawa, M., Knisely, C., Shirato, H., Kim, Y., Tsujii, M.: Aerodynamic behavior of inclined circular cylinders-cable aerodynamics. *J. Wind Eng. Ind. Aerodyn.* **33**, 63–72 (1990)
171. Zhou, T., Wang, H., Razali, S.F.M., Zhou, Y., Cheng, L.: Three-dimensional vorticity measurements in the wake of a yawed circular cylinder. *Phys. Fluids* **22**, 10–15 (2010)
172. McTavish, S., Raeesi, A., D'Auteuil, A., Yamauchi, K., Sato, H.: An investigation of the mechanisms causing large-amplitude wind-induced vibrations in stay cables using unsteady surface pressure measurements. *J. Wind Eng. Ind. Aerodyn.* **183**, 19–34 (2018)
173. Nikitas, N., MacDonald, J.H.G., Jakobsen, J.B., Andersen, T.L.: Critical Reynolds number and galloping instabilities: experiments on circular cylinders. *Exp. Fluids* **52**, 1295–1306 (2012)
174. Nikitas, N., Nikitas, N.: Aerodynamic forcing characteristics of dry cable galloping at critical Reynolds numbers. *Eur. J. Mech. B/Fluids* **49**, 243–249 (2015)
175. Nikitas, N., Macdonald, J.H.G.: Misconceptions and generalizations of the Den Hartog galloping criterion. *J. Eng. Mech.* **140**, 04013005 (2014)
176. Ma, W., Macdonald, J.H.G., Liu, Q., Nguyen, C.H., Liu, X.: Galloping of an elliptical cylinder at the critical Reynolds number and its quasi-steady prediction. *J. Wind Eng. Ind. Aerodyn.* **168**, 110–122 (2017)
177. Jubran, B.A., Hamdan, M.N., Al Bedoor, B.: Interference and turbulence intensity effects on the flow-induced vibration of smooth and rough cylinders. *J. Fluids Struct.* **7**(5), 457–470 (1993)
178. Bartoli, G., Cluni, F., Gusella, V., Procino, L.: Dynamics of cable under wind action: wind tunnel experimental analysis. *J. Wind Eng. Ind. Aerodyn.* **94**, 259–273 (2006)
179. Matteoni, G., Georgakis, C.T.: Effects of bridge cable surface roughness and cross-sectional distortion on aerodynamic force coefficients. *J. Wind Eng. Ind. Aerodyn.* **104**, 176–187 (2012)
180. Matteoni, G., Georgakis, C.T.: Effects of surface roughness and cross-sectional distortion on the wind-induced response of bridge cables in dry conditions. *J. Wind Eng. Ind. Aerodyn.* **136**, 89–100 (2015)
181. Macdonald, J.H.G., Larose, G.L.: A unified approach to aerodynamic damping and drag/lift instabilities, and its application to dry inclined cable galloping. *J. Fluids Struct.* **22**, 229–252 (2006)
182. Kleissl, K., Georgakis, C.T.: Aerodynamic control of bridge cables through shape modification: a preliminary study. *J. Fluids Struct.* **27**, 1006–1020 (2011)
183. Kleissl, K., Georgakis, C.T.: Comparison of the aerodynamics of bridge cables with helical fillets and a pattern-indented surface. *J. Wind Eng. Ind. Aerodyn.* **104–106**, 166–175 (2012)
184. Demartino, C., Ricciardelli, F.: Assessment of the structural damping required to prevent galloping of dry HDPE stay cables using the quasi-steady approach. *J. Bridge Eng.* **23**, 04018004 (2018)
185. Benidir, A., Flamand, O., Dimitriadis, G.: The impact of circularity defects on bridge stay cable dry galloping stability. *J. Wind Eng. Ind. Aerodyn.* **181**, 14–26 (2018)
186. Yeo, D., Jones, N.P.: Investigation on 3-D characteristics of flow around a yawed and inclined circular cylinder. *J. Wind Eng. Ind. Aerodyn.* **96**, 1947–1960 (2008)
187. Yeo, D., Jones, N.P.: A mechanism for large amplitude, wind-induced vibrations of stay cables. In: Proceedings of

- the Eleventh Americas Conference on Wind Engineering, San Juan, Puerto Rico (2009)
188. Wu, X., Sharma, A., Jafari, M., Sarkar, P.: Towards predicting dry cable galloping using detached eddy simulations. 55th AIAA Aerospace Science, pp. 1–15 (2017)
 189. Hoftzyer, M., Dragomirescu, E.: Numerical investigation of flow behaviour around inclined circular cylinders. In: The Fifth International Symposium on Computational Wind Engineering, Chapel Hill, North Carolina, USA (2010)
 190. Hayashi, T., Kawamura, T.: Non-uniformity in a flow around a yawed circular cylinder. *Flow Meas. Instrum.* **6**, 33–39 (1995)
 191. Macdonald, J.H.G., Larose, G.L.: Two-degree-of-freedom inclined cable galloping-Part I: general formulation and solution for perfectly tuned system. *J. Wind Eng. Ind. Aerodyn.* **96**, 291–307 (2008)
 192. Macdonald, J.H.G., Larose, G.L.: Two-degree-of-freedom inclined cable galloping-Part 2: analysis and prevention for arbitrary frequency ratio. *J. Wind Eng. Ind. Aerodyn.* **96**, 308–326 (2008)
 193. Raeesi, A., Cheng, S., Ting, D.S.K.: Aerodynamic damping of an inclined circular cylinder in unsteady flow and its application to the prediction of dry inclined cable galloping. *J. Wind Eng. Ind. Aerodyn.* **113**, 12–28 (2013)
 194. Raeesi, A., Cheng, S., Ting, D.S.K.: Application of a three-dimensional aeroelastic model to study the wind-induced response of bridge stay cables in unsteady wind conditions. *J. Sound Vib.* **375**, 217–236 (2016)
 195. Raeesi, A., Cheng, S., Ting, D.S.K.: A two-degree-of-freedom aeroelastic model for the vibration of dry cylindrical body along unsteady air flow and its application to aerodynamic response of dry inclined cables. *J. Wind Eng. Ind. Aerodyn.* **130**, 108–124 (2014)
 196. Luongo, A., Zulli, D.: Dynamic instability of inclined cables under combined wind flow and support motion. *Nonlinear Dyn.* **67**, 71–87 (2012)
 197. Carassale, L., Freda, A., Piccardo, G.: Aeroelastic forces on yawed circular cylinders: Quasi-steady modeling and aerodynamic instability. *Wind Struct. Int. J.* **8**, 373–388 (2005)
 198. Macdonald, J.H.G.: Separation of the contributions of aerodynamic and structural damping in vibrations of inclined cables. *J. Wind Eng. Ind. Aerodyn.* **90**, 19–39 (2002)
 199. Piccardo, G., Pagnini, L.C., Tubino, F.: Some research perspectives in galloping phenomena: critical conditions and post-critical behavior. *Contin. Mech. Thermodyn.* **27**, 261–285 (2015)
 200. Piccardo, G., Zulli, D., Luongo, A.: Dry galloping in inclined cables: linear stability analysis. *Procedia Eng.* **199**, 3164–3169 (2017)
 201. Lee, J.: *Advanced Electrical and Electronics Engineering*. Springer, Berlin (2011)
 202. Xie, Q., Cai, Y., Xue, S.: Wind-induced vibration of UHV transmission tower line system: wind tunnel test on aeroelastic model. *J. Wind Eng. Ind. Aerodyn.* **171**, 219–229 (2017)
 203. Farzaneh, M.: *Atmospheric Icing of Power Networks*. Springer, New York (2008)
 204. Laforte, J.L., Allaire, M.A., Laflamme, J.: State-of-the-art on power line de-icing. *Atmos. Res.* **46**, 143–158 (1998)
 205. DEN HARTOG, J.P.: Transmission line vibration due to sleet. *Trans. Am. Inst. Electr. Eng.* **51**, 1074–1076 (1932)
 206. Parkinson, G.V.: Phenomena and modeling of flow-induced vibrations of bluff bodies. *Prog. Aerosp. Sci.* **26**, 169–224 (1989)
 207. Nigol, O., Buchan, P.G.: Conductor galloping-part II Torsional mechanism. In: *IEEE Transactions on Power Apparatus and Systems*, pp. 708–720 (1981)
 208. Richardson, A.S.: Dynamic analysis of lightly iced conductor galloping in two degrees of freedom. *IEE Proc. C Gener. Transm. Distrib.* **128**, 211–218 (1981)
 209. Edwards, A.T., Madeyski, A.: Progress report on the investigation of galloping of transmission line conductors. In: *Transactions of the American Institute of Electrical Engineers. Part III: Power Apparatus and Systems*, pp. 666–686 (1956)
 210. Blevins, R., Iwan, W.: The galloping response of a two-degree-of-freedom system. *J. Appl. Mech.* **41**, 1113–1118 (1974)
 211. Desai, Y.M., Shah, A.H., Popplewell, N.: Galloping analysis for two-degree-of-freedom oscillator. *J. Eng. Mech.* **116**, 2583–2602 (1990)
 212. Yu, P., Desai, Y.M., Shah, A.H., Popplewell, N.: Three-degree-of-freedom model for galloping. Part I: formulation. *J. Eng. Mech.* **119**, 2404–2425 (1993)
 213. Yu, P., Desai, Y.M., Popplewell, N., Shah, A.H.: Three-degree-of-freedom model for galloping. Part II: solutions. *J. Eng. Mech.* **119**, 2426–2448 (1993)
 214. Yu, B.: *Nonlinear dynamics of cable galloping via a two-degree-of-freedom nonlinear oscillator*. Ph.D. Dissertation, Southern Illinois University, Carbondale, IL (2016)
 215. Jiang, X., Shu, L., Sima, W., Xie, S., Hu, J., Zhang, Z.: Chinese transmission lines' icing characteristics and analysis of severe ice accidents. *Int. J. Offshore Polar Eng.* **14**, 196–201 (2004)
 216. Pohlman, J.C., Landers, P.: Present state-of-the-art of transmission line icing. In: *IEEE Transactions on Power Apparatus and Systems*, pp. 2443–2450 (1982)
 217. Dalle, B., Admirat, P.: Wet snow accretion on overhead lines with French report of experience. *Cold Reg. Sci. Technol.* **65**, 43–51 (2011)
 218. Baenziger, M.A., James, W.D., Wouters, B., Li, L.: Dynamic loads on transmission line structures due to galloping conductors. *IEEE Trans. Power Deliv.* **9**, 40–49 (1994)
 219. Owen, N.L.: Wind-induced vibration of overhead power transmission lines. *Sci. Prog.* **87**, 79–99 (2004)
 220. Van Dyke, P., Havard, D.G.: Effect of ice and snow on the dynamics of transmission line cables—part I: Aeolian vibration, wake-induced oscillation and galloping motions. In: *Proceedings of the 11 International Workshop Atmospheric Icing of Structure*, pp. 285–290 (2005)
 221. Nigol, O., Buchan, P.G.: Conductor galloping Part I—Den Hartog mechanism. In: *IEEE Transactions on Power Apparatus and Systems*, pp. 699–707 (1981)
 222. Kim, J.-W., Sohn, J.-H.: Galloping simulation of the power transmission line under the fluctuating wind. *Int. J. Precis. Eng. Manuf.* **19**, 1393–1398 (2018)
 223. Zdero, R., Turan, O.F.: The effect of surface strands, angle of attack, and ice accretion on the flow field around electric

- cal power cables. *J. Wind Eng. Ind. Aerodyn.* **98**, 672–678 (2010)
224. Xinmin, L., Kuanjun, Z., Bin, L.: Research of experimental simulation on aerodynamic character for typed iced conductor. *AASRI Procedia* **2**, 106–111 (2012)
 225. Van Dyke, P., Laneville, A.: Galloping of a single conductor covered with a D-section on a high-voltage overhead test line. *J. Wind Eng. Ind. Aerodyn.* **96**, 1141–1151 (2008)
 226. Chabart, O., Lilien, J.L.: Galloping of electrical lines in wind tunnel facilities. *J. Wind Eng. Ind. Aerodyn.* **74–76**, 967–976 (1998)
 227. Meng, X., Wang, L., Hou, L., Fu, G., Sun, B., MacAlpine, M., Hu, W., Chen, Y.: Dynamic characteristic of ice-shedding on UHV overhead transmission lines. *Cold Reg. Sci. Technol.* **66**, 44–52 (2011)
 228. Chadha, J., Jaster, W.: Influence of turbulence on the galloping instability of iced conductors. *IEEE Trans. Power Appar. Syst.* **94**, 1489–1499 (1975)
 229. Gurung, C.B., Yamaguchi, H., Yukino, T.: Identification of large amplitude wind-induced vibration of ice-accreted transmission lines based on field observed data. *Eng. Struct.* **24**, 179–188 (2002)
 230. Matsumiya, H., Nishihara, T., Yagi, T.: Aerodynamic modeling for large-amplitude galloping of four-bundled conductors. *J. Fluids Struct.* **82**, 559–576 (2018)
 231. Xin-min, L., Xiao-chun, N., Yong-kun, Z., Yi, Y., Zhi-tao, Y.: Wind tunnel tests on aerodynamic characteristics of ice-coated 4-bundled conductors. *Math. Probl. Eng.* (2017). <https://doi.org/10.1155/2017/1628173>
 232. Zhou, A., Liu, X., Zhang, S., Cui, F., Liu, P.: Wind tunnel test of the influence of an interphase spacer on the galloping control of iced eight-bundled conductors. *Cold Reg. Sci. Technol.* **155**, 354–366 (2018)
 233. Zhou, L., Yan, B., Zhang, L., Zhou, S.: Study on galloping behavior of iced eight bundle conductor transmission lines. *J. Sound Vib.* **362**, 85–110 (2016)
 234. Hu, J., Yan, B., Zhou, S., Zhang, H.: Numerical investigation on galloping of iced quad bundle conductors. *IEEE Trans. Power Deliv.* **27**, 784–792 (2012)
 235. Ma, W.Y., Liu, Q.K., Du, X.Q., Wei, Y.Y.: Effect of the Reynolds number on the aerodynamic forces and galloping instability of a cylinder with semi-elliptical cross sections. *J. Wind Eng. Ind. Aerodyn.* **146**, 71–80 (2015)
 236. Li, S., Wu, T., Huang, T., Chen, Z.: Aerodynamic stability of iced stay cables on cable-stayed bridge. *Wind Struct. An Int. J.* **23**, 253–273 (2016)
 237. Demartino, C., Koss, H.H., Georgakis, C.T., Ricciardelli, F.: Effects of ice accretion on the aerodynamics of bridge cables. *J. Wind Eng. Ind. Aerodyn.* **138**, 98–119 (2015)
 238. Zhang, J., Makkonen, L., He, Q.: A 2D numerical study on the effect of conductor shape on icing collision efficiency. *Cold Reg. Sci. Technol.* **143**, 52–58 (2017)
 239. McComber, P., Paradis, A.: A cable galloping model for thin ice accretions. *Atmos. Res.* **46**, 13–25 (1998)
 240. Foti, F., Martinelli, L., Perotti, F.: A finite element approach to model galloping vibrations of iced suspended cables. *Procedia Eng.* **199**, 3127–3132 (2017)
 241. Gjelstrup, H., Georgakis, C.T.: A quasi-steady 3 degree-of-freedom model for the determination of the onset of bluff body galloping instability. *J. Fluids Struct.* **27**, 1021–1034 (2011)
 242. Gjelstrup, H., Larsen, A., Georgakis, C., Koss, H.: A new general 3Dof quasi-steady aerodynamic instability model. In: 6th International Colloquium on Bluff Bodies Aerodynamics and Applications, Milan, Italy (2008)
 243. Richardson, A.S.: A study of galloping conductors on a 230 kV transmission line. *Electr. Power Syst. Res.* **21**, 43–55 (1991)
 244. On, S., Analysis, T.H.E., Galloping, O.F., Power, F.O.R., Line, T.: A study on the analysis of galloping for power transmission line. In: Industrial Electronics, Proceedings of the ISIE IEEE International Symposium, vol. 2, pp. 973–978 (2001)
 245. He, M., Macdonald, J.: Aeroelastic stability of a 3DOF system based on quasi-steady theory with reference to inertial coupling. *J. Wind Eng. Ind. Aerodyn.* **171**, 319–329 (2017)
 246. Mcdaniel, W.N.: An analysis of galloping electric transmission lines. *Trans. Am. Inst. Electr. Eng. III Power Appar. Syst.* **79**, 406–412 (1960)
 247. Foti, F., Martinelli, L.: Finite element modeling of cable galloping vibrations. Part II: application to an iced cable in 1:2 multiple internal resonance. *JVC J. Vib. Control* **24**, 1322–1340 (2018)
 248. Desai, Y.M., Yu, P., Popplewell, N., Shah, A.H.: Finite element modelling of transmission line galloping. *Comput. Struct.* **57**, 407–420 (1995)
 249. Zhang, Q., Popplewell, N., Shah, A.H.: Galloping of bundle conductor. *J. Sound Vib.* **234**, 115–134 (2000)
 250. Yan, Z., Li, Z., Savory, E., Lin, W.E.: Galloping of a single iced conductor based on curved-beam theory. *J. Wind Eng. Ind. Aerodyn.* **123**, 77–87 (2013)
 251. Yan, Z., Savory, E., Li, Z., Lin, W.E.: Galloping of iced quad-conductors bundles based on curved beam theory. *J. Sound Vib.* **333**, 1657–1670 (2014)
 252. Yan, Z., Yan, Z., Li, Z., Tan, T.: Nonlinear galloping of internally resonant iced transmission lines considering eccentricity. *J. Sound Vib.* **331**, 3599–3616 (2012)
 253. Yu, P., Shah, A.H., Popplewell, N.: Inertially coupled galloping of iced conductors. *J. Appl. Mech. Trans. ASME* **59**, 140–145 (1992)
 254. Wang, X., Lou, W.J.: Numerical approach to galloping of conductor. In: Proceedings of the 7th Asia-Pacific Conference on Wind Engineering, Taipei, Taiwan (2009)
 255. Wang, J., Lilien, J.L.: Overhead electrical transmission line galloping: a full multi-span 3DOF model, some applications and design recommendations. *IEEE Trans. Power Deliv.* **13**, 909–916 (1998)
 256. Kollár, L.E., Farzaneh, M., Van Dyke, P.: Modeling ice shedding propagation on transmission lines with or without interphase spacers. *IEEE Trans. Power Deliv.* **28**, 261–267 (2013)
 257. McClure, G., Lapointe, M.: Modeling the structural dynamic response of overhead transmission lines. *Comput. Struct.* **81**, 825–834 (2003)
 258. Kálmán, T., Farzaneh, M., McClure, G.: Numerical analysis of the dynamic effects of shock-load-induced ice shedding on overhead ground wires. *Comput. Struct.* **85**, 375–384 (2007)
 259. Zdravkovich, M.: The effects of interference between circular cylinders in cross-flow. *J. Fluids Struct.* **1**, 239–261 (1987)

260. Zdravkovich, M.M.: Review of flow interference between two circular cylinders in various arrangements. *J. Fluids Eng.* **99**, 618–633 (1977)
261. Sumner, D.: Two circular cylinders in cross-flow: a review. *J. Fluids Struct.* **26**, 849–899 (2010)
262. Bearman, P.W.: Circular cylinder wakes and vortex-induced vibrations. *J. Fluids Struct.* **27**, 648–658 (2011)
263. Zhou, Y., Alam, M.: Wake of two interacting circular cylinders: a review. *Int. J. Heat Fluid Flow* **62**, 510–537 (2016)
264. He, X., Cai, C., Wang, Z., Jing, H., Qin, C.: Experimental verification of the effectiveness of elastic cross-ties in suppressing wake-induced vibrations of staggered stay cables. *Eng. Struct.* **167**, 151–165 (2018)
265. Zdravkovich, M.M.: Flow induced oscillations of two interfering circular cylinders. *J. Sound Vib.* **101**, 511–521 (1985)
266. Yoshimura, T., Savage, M.G., Tanaka, H., Wakasa, T.: A device for suppressing wake galloping of stay-cables for cable-stayed bridges. *J. Wind Eng. Ind. Aerodyn.* **49**, 497–505 (1993)
267. Mattiello, E., Eriksen, M.B., Georgakis, C.T.: Determination of aerodynamic damping of twin cables in wet conditions through passive-dynamic wind tunnel tests. In: 6th European and African Conference on Wind Engineering (2013)
268. Acampora, A., Macdonald, J.H.G., Georgakis, C.T., Nikitas, N.: Identification of aeroelastic forces and static drag coefficients of a twin cable bridge stay from full-scale ambient vibration measurements. *J. Wind Eng. Ind. Aerodyn.* **124**, 90–98 (2014)
269. Li, Y., Wu, M., Chen, X., Wang, T., Liao, H.: Wind-tunnel study of wake galloping of parallel cables on cable-stayed bridges and its suppression. *Wind Struct.* **16**, 249–261 (2013)
270. Kim, S., Kim, H.K., Lee, H.: An experimental investigation on characteristics of flow field of wake galloping. In: International Association for Bridge and Structural Engineering, pp. 757–764 (2012)
271. Gawronski, K.E.: Effect of conductor geometry on bundle conductor galloping. *Electr. Power Syst. Res.* **1**, 181–188 (1978)
272. Cigada, A., Diana, G., Falco, M., Fossati, F., Manenti, A.: Vortex shedding and wake-induced vibrations in single and bundle cables. *J. Wind Eng. Ind. Aerodyn.* **72**, 253–263 (1997)
273. Liu, X., Levitan, M., Nikitopoulos, D.: Wind tunnel tests for mean drag and lift coefficients on multiple circular cylinders arranged in-line. *J. Wind Eng. Ind. Aerodyn.* **96**, 831–839 (2008)
274. Assi, G.R.S.: Wake-induced vibration of tandem and staggered cylinders with two degrees of freedom. *J. Fluids Struct.* **50**, 340–357 (2014)
275. Assi, G.R.S., Bearman, P.W., Kitney, N., Tognarelli, M.A.: Suppression of wake-induced vibration of tandem cylinders with free-to-rotate control plates. *J. Fluids Struct.* **26**, 1045–1057 (2010)
276. Arie, M., Kiya, M., Moriya, M., Mori, H.: Pressure fluctuations on the surface of two circular cylinders in tandem arrangement. *J. Fluids Eng.* **105**, 161–166 (1983)
277. Jenkins, L., Neuhart, D., McGinley, C., Khorrami, M., Choudhari, M.: Measurements of unsteady wake interference between tandem cylinders. In: 36th AIAA Fluid Dynamics Conference and Exhibit, pp. 1–18 (2006)
278. Sun, T.F., Gu, Z.F., He, D.X., Zhang, L.L.: Fluctuating pressure on two circular cylinders at high Reynolds numbers. *J. Wind Eng. Ind. Aerodyn.* **41**, 577–588 (1992)
279. Kim, S., Alam, M., Sakamoto, H., Zhou, Y.: Flow-induced vibration of two circular cylinders in tandem arrangement. Part 2: suppression of vibrations. *J. Wind Eng. Ind. Aerodyn.* **2(97)**, 312–319 (2009)
280. Kim, S., Alam, M.M., Sakamoto, H., Zhou, Y.: Flow-induced vibrations of two circular cylinders in tandem arrangement. Part 1: characteristics of vibration. *J. Wind Eng. Ind. Aerodyn.* **97**, 304–311 (2009)
281. Lin, J.C., Yang, Y., Rockwell, D.: Flow past two cylinders in tandem: instantaneous and averaged flow structure. *J. Fluids Struct.* **16**, 1059–1071 (2002)
282. Alam, M.M., Meyer, J.P.: Global aerodynamic instability of twin cylinders in cross flow. *J. Fluids Struct.* **41**, 135–145 (2013)
283. Palau-Salvador, G., Stoesser, T., Rodi, W.: LES of the flow around two cylinders in tandem. *J. Fluids Struct.* **24**, 1304–1312 (2008)
284. Braun, A.L., Awruch, A.M.: Aerodynamic and aeroelastic analysis of bundled cables by numerical simulation. *J. Sound Vib.* **284**, 51–73 (2005)
285. Wu, C., Yan, B., Huang, G., Zhang, B., Lv, Z., Li, Q.: Wake-induced oscillation behaviour of twin bundle conductor transmission lines. *R. Soc. Open Sci.* **5**, 180011 (2018)
286. Brzozowski, V.J., Hawks, R.J.: Wake-induced full span instability of bundle conductor transmission lines. *AIAA J.* **14**, 179–184 (1976)
287. Hoover, A.N., Hawkst, R.J.: Role of turbulence in wake-induced galloping of transmission lines. *AIAA J.* **15**, 66–70 (1977)
288. Bokaian, A.: Galloping of a circular cylinder in the wake of another. *J. Sound Vib.* **128**, 71–85 (1989)
289. Nguyen, V.-T., Ronald Chan, W.H., Nguyen, H.H.: Numerical investigation of wake induced vibrations of cylinders in tandem arrangement at subcritical Reynolds numbers. *Ocean Eng.* **154**, 341–356 (2018)
290. Abdulhadi, M.: Aerodynamic forces on bluff structures in a wake. *J. Wind Eng. Ind. Aerodyn.* **21**, 101–115 (1985)
291. Akosile, O.O., Sumner, D.: Staggered circular cylinders immersed in a uniform planar shear flow. *J. Fluids Struct.* **18**, 613–633 (2003)
292. Alam, M.M., Sakamoto, H.: Investigation of Strouhal frequencies of two staggered bluff bodies and detection of multistable flow by wavelets. *J. Fluids Struct.* **20**, 425–449 (2005)
293. Alam, M.M., Sakamoto, H., Zhou, Y.: Determination of flow configurations and fluid forces acting on two staggered circular cylinders of equal diameter in cross-flow. *J. Fluids Struct.* **21**, 363–394 (2005)
294. Alam, M.M., Moriya, M., Takai, K., Sakamoto, H.: Fluctuating fluid forces acting on two circular cylinders in a tandem arrangement at a subcritical Reynolds number. *J. Wind Eng. Ind. Aerodyn.* **91**, 139–154 (2003)
295. Alam, M.M., Moriya, M., Sakamoto, H.: Aerodynamic characteristics of two side-by-side circular cylinders and

- application of wavelet analysis on the switching phenomenon. *J. Fluids Struct.* **18**, 325–346 (2003)
296. Alam, M.M., Sakamoto, H., Moriya, M.: Reduction of fluid forces acting on a single circular cylinder and two circular cylinders by using tripping rods. *J. Fluids Struct.* **18**, 347–366 (2003)
 297. Alam, M.M., Zhou, Y.: Flow around two side-by-side closely spaced circular cylinders. *J. Fluids Struct.* **23**, 799–805 (2007)
 298. Alam, M.M., Zhou, Y.: Phase lag between vortex shedding from two tandem bluff bodies. *J. Fluids Struct.* **23**, 339–347 (2007)
 299. Alam, M.M., Meyer, J.P.: Two interacting cylinders in cross flow. *Phys. Rev. E Stat. Nonlinear Soft Matter Phys.* **84**, 056304 (2011)
 300. Alam, M.M.: The aerodynamics of a cylinder submerged in the wake of another. *J. Fluids Struct.* **51**, 393–400 (2014)
 301. Bearman, P.W., Wadcock, A.J.: The interaction between a pair of circular cylinders normal to a stream. *J. Fluid Mech.* **61**, 499–511 (1973)
 302. Biermann, D., Herrnstein, W.H.: The interference between struts in various combinations. National Advisory Committee for Aeronautics. Technical report 468 (1934)
 303. Brun, C., Tenchine, D., Hopfinger, E.J.: Role of the shear layer instability in the near wake behavior of two side-by-side circular cylinders. *Exp. Fluids.* **36**, 334–343 (2004)
 304. Cooper, K.R.: Wind tunnel measurements of the steady aerodynamics forces on a smooth circular cylinder immersed in the wake of an identical cylinder. National Research Council of Canada LTR-LA-119 (1974)
 305. Gu, Z., Sun, T.: On interference between two circular cylinders in staggered arrangement at high subcritical Reynolds numbers. *J. Wind Eng. Ind. Aerodyn.* **80**, 287–309 (1999)
 306. Gu, Z.F., Sun, T.F., He, D.X., Zhang, L.L.: Two circular cylinders in high-turbulence flow at supercritical Reynolds number. *J. Wind Eng. Ind. Aerodyn.* **49**, 379–388 (1993)
 307. Hiwada, M., Mabuchi, I., Yanagihara, H.: Fluid flow and heat transfer around two circular cylinders. *Bull. JSME* **25**, 1737–1745 (1982)
 308. Hori, E.: Experiments on flow around a pair of parallel circular cylinders. In: Proceedings of the 9th Japan National Congress for Applied Mechanics, Tokyo, pp. 231–234 (1959)
 309. Igarashi, T.: Characteristics of the flow around two circular cylinders arranged in tandem: 1st report. *Bull. JSME* **24**, 323–331 (1981)
 310. Igarashi, T.: Characteristics of the flow around two circular cylinders arranged in tandem: 2nd report, unique phenomenon at small spacing. *Bull. JSME* **27**, 2380–2387 (1984)
 311. Ishigai, S., Nishikawa, E., Nishimura, K., Cho, K.: Experimental study on structure of gas flow in tube banks with tube Axes Normal to Flow: part I, karman vortex flow from Two tubes at various spacings. *Bull. JSME* **86**, 949–956 (1972)
 312. Ishigai, S., Nishikawa, E., Yagi, E.: Structure of gas flow and vibration in tube banks with tube axes normal to flow. In: Proceedings of the International Symposium on Marine Engineering, Tokyo, Japan, pp. 15–33 (1973)
 313. Jendrzeycyk, J.A., Chen, S.S.: Fluid forces on two circular cylinders in crossflow. Technical report No. ANL-85-35. Argonne National Lab., IL (USA) (1985)
 314. Kamemoto, K.: Formation and interaction of two parallel vortex streets. In: Bulletin of JSME, pp. 283–90 (1976)
 315. Kiya, M., Arie, M., Tamura, H., Mori, H.: Vortex shedding from two circular cylinders in staggered arrangement. *J. Fluids Eng. Trans. ASME* **102**, 166–173 (1980)
 316. Kiya, M., Mochizuki, O., Ido, Y., Suzuki, T., Arai, T.: Flip-flopping flow around two bluff bodies in tandem arrangement. In: Eckelmann, H., Michael, J., Graham, R., Huerre, P., Monkewitz, P.A. (eds.) *Bluff-Body Wakes, Dynamics and Instabilities*, pp. 15–18. Springer, Berlin (1993)
 317. Kobayashi, T.: Characteristics of fluid-dynamics acting on circular or square cylinders in close proximity. *Trans. JSME* **42**, 1452–1461 (1976). (in Japanese)
 318. Kostic, Z.G., Oka, S.N.: Fluid flow and heat transfer with two cylinders in cross flow. *Int. J. Heat Mass Transf.* **15**, 279–299 (1972). [https://doi.org/10.1016/0017-9310\(72\)90075-0](https://doi.org/10.1016/0017-9310(72)90075-0)
 319. Kwon, S.H., Park, J., Ha, D.D., Lee, Y.H.: Experimental study of flow fields around cylinder arrays using PIV. In: Proceedings of the Sixth International Offshore and Polar Engineering Conference, Los Angeles, USA, pp. 145–150 (1996)
 320. Lee, T., Basu, S.: Nonintrusive measurements of the boundary layer developing on a single and two circular cylinders. *Exp. Fluids* **23**, 187–192 (1997)
 321. Lee, T., Panagakos, A.: Investigation of boundary layer behaviour on single and tandem cylinders. In: International Symposium on Fluid-Structure Interactions, Aeroelasticity, Flow-Induced Vibration and Noise, Dallas, TX, pp. 103–112 (1997)
 322. Ljungkrona, L., Sundén, B.: Flow visualization and surface pressure measurement on two tubes in an inline arrangement. *Exp. Therm. Fluid Sci.* **6**, 15–27 (1993)
 323. Ljungkrona, L., Norberg, C.H., Sundén, B.: Free-stream turbulence and tube spacing effects on surface pressure fluctuations for two tubes in an in-line arrangement. *J. Fluids Struct.* **5**, 701–727 (1991)
 324. Maekawa, T.: Study on wind pressure against ACSR double conductor. *Electr. Eng. Jpn.* **84**, 169–178 (1964)
 325. Moriya, M., Sakamoto, H.: Fluctuating fluid forces acting on a downstream circular cylinder in the staggered arrangement. *Trans. JSME* **51**, 2098–2104 (1985)
 326. Ng, C.W., Cheng, V.S.Y., Ko, N.W.M.: Numerical study of vortex interactions behind two circular cylinders in bistable flow regime. *Fluid Dyn. Res.* **19**, 379–409 (1997)
 327. Nishimura, T., Ohori, Y., Kawamura, Y.: Flow pattern and rate of mass transfer around two cylinders in tandem. *Int. Chem. Eng.* **26**, 123–129 (1986)
 328. Novak, J.: Strouhal number of a quadrangular prism, angle iron and two circular cylinders arranged in tandem. *Acta Tech. CSAV* **19**, 361–73 (1974)
 329. Okajima, A.: Flows around two tandem circular cylinders at very high Reynolds numbers. *Bull. JSME* **22**, 504–511 (1979)
 330. Ozono, S., Oda, J., Yoshida, Y., Wakasugi, Y.: Critical nature of the base pressure of the upstream circular cylinder in two staggered ones in cross-flow. *Theor. Appl. Mech.* **50**, 335–340 (2001)

331. Price, S.J.: The origin and nature of the lift force on the leeward of two bluff bodies. *Aeronaut. Q.* **27**, 154–168 (1976)
332. Price, S.J., Paidoussis, M.P.: The aerodynamic forces acting on groups of two and three circular cylinders when subject to a cross-flow. *J. Wind Eng. Ind. Aerodyn.* **17**, 329–347 (1984)
333. Spivack, H.M.: Vortex frequency and flow pattern in the wake of two parallel cylinders at varied spacing normal to an air stream. *J. Aeronaut. Sci.* **13**, 289–301 (1946)
334. Sumner, D., Richards, M.D.: Some vortex-shedding characteristics of the staggered configuration of circular cylinders. *J. Fluids Struct.* **17**, 345–350 (2003)
335. Sumner, D.: Closely spaced circular cylinders in cross-flow and a universal wake number. *J. Fluids Eng.* **126**, 245 (2004)
336. Sumner, D., Richards, M.D., Akosile, O.O.: Two staggered circular cylinders of equal diameter in cross-flow. *J. Fluids Struct.* **20**, 255–276 (2005)
337. Sumner, D., Schenstead, A.J.: Moderately and widely spaced circular cylinders in crossflow and a universal wake number. *J. Fluids Eng.* **128**, 1122 (2006)
338. Suzuki, N.: Aerodynamic forces acting on circular cylinders arranged in a longitudinal row. In: *Proceedings of the International Symposium on Wind Effects on Buildings and Structure*, pp. 377–386 (1971)
339. Ting, D.S.K., Wang, D.J., Price, S.J., Paidoussis, M.P.: An experimental study on the fluidelastic forces for two staggered circular cylinders in cross-flow. *J. Fluids Struct.* **12**, 259–294 (1998)
340. Wardlaw, R.L., Cooper, K.R.: A wind tunnel investigation of the steady aerodynamic forces on smooth and stranded twin bundled power conductors for the Aluminum Company of America. In: *National Research Council of Canada, LTR-LA-117* (1973)
341. Wong, C.W., Zhou, Y., Alam, M.M., Zhou, T.M.: Dependence of flow classification on the Reynolds number for a two-cylinder wake. *J. Fluids Struct.* **49**, 485–497 (2014)
342. Wu, J., Welch, L.W., Welsh, M.C., Sheridan, J., Walker, G.J.: Spanwise wake structures of a circular cylinder and two circular cylinders in tandem. *Exp. Therm. Fluid Sci.* **9**, 299–308 (1994)
343. Xu, S.J., Zhou, Y., So, R.M.C.: Reynolds number effects on the flow structure behind two side-by-side cylinders. *Phys. Fluids* **15**, 1214–1219 (2003)
344. Xu, G., Zhou, Y.: Strouhal numbers in the wake of two inline cylinders. *Exp. Fluids* **37**, 248–256 (2004)
345. Zdravkovich, M.M., Pridden, D.L.: Interference between two circular cylinders; series of unexpected discontinuities. *J. Wind Eng. Ind. Aerodyn.* **2**, 255–270 (1977)
346. Zhang, H., Melbourne, W.H.: Interference between two circular cylinders in tandem in turbulent flow. *J. Wind Eng. Ind. Aerodyn.* **41**, 589–600 (1992)
347. Zhou, Y., Feng, S.X., Alam, M.M., Bai, H.L.: Reynolds number effect on the wake of two staggered cylinders. *Phys. Fluids* **21**, 1–14 (2009)
348. Gu, Z.: On interference between two circular cylinders at supercritical Reynolds number. *J. Wind Eng. Ind. Aerodyn.* **62**, 175–190 (1996)
349. Irvine, H.M., Caughey, T.K.: The linear theory of free vibrations of a suspended cable. *Proc. R. Soc. Lond. A Math. Phys. Sci.* **341**, 299–315 (1974)
350. Martinelli, L., Perotti, F.: Numerical analysis of the non-linear dynamic behaviour of suspended cables under turbulent wind excitation. *Int. J. Struct. Stab. Dyn.* **1**, 207–233 (2001)
351. Paola, D.M., Muscolino, G., Sofi, A.: Monte Carlo simulation for the response analysis of long-span suspended cables under wind loads. *Wind Struct.* **7**, 107–130 (2004)
352. Luongo, A., Piccardo, G.: Non-linear galloping of sagged cables in 1:2 internal resonance. *J. Sound Vib.* **214**, 915–940 (1998)
353. Gattulli, V., Martinelli, L., Perotti, F.: Dynamics of suspended cables under turbulence loading: reduced models of wind field and mechanical system. *J. Wind Eng. Ind. Aerodyn.* **95**, 183–207 (2007)
354. Luongo, A., Zulli, D., Piccardo, G.: A linear curved-beam model for the analysis of galloping in suspended cables. *J. Mech. Mater. Struct.* **2**, 675–694 (2007)
355. Hagedorn, P., Schäfer, B.: On non-linear free vibrations of an elastic cable. *Int. J. Nonlinear Mech.* **15**, 333–340 (1980)
356. Luongo, A., Rega, G., Vestroni, F.: Monofrequent oscillations of a non-linear model of a suspended cable. *J. Sound Vib.* **82**, 247–259 (1982)
357. Benedettini, F., Rega, G., Vestroni, F.: Modal coupling in the free nonplanar finite motion of an elastic cable. *Mechanica* **21**, 38–46 (1986)
358. Rega, G.: Nonlinear vibrations of suspended cables—part I: modeling and analysis. *Appl. Mech. Rev.* **57**, 443–478 (2004)
359. Visweswara Rao, G., Iyengar, R.N.: Internal resonance and non-linear response of a cable under periodic excitation. *J. Sound Vib.* **149**, 25–41 (1991)
360. Benedettini, F., Rega, G.: Numerical simulations of chaotic dynamics in a model of an elastic cable. *Nonlinear Dyn.* **1**, 23–38 (1990)
361. Lee, C.L., Perkins, N.C.: Nonlinear oscillations of suspended cables containing a two-to-one internal resonance. *Nonlinear Dyn.* **3**, 465–490 (1992)
362. Rega, G.: Nonlinear vibrations of suspended cables—part II: deterministic phenomena. *Appl. Mech. Rev.* **57**, 479–514 (2004)
363. Ibrahim, R.A.: Nonlinear vibrations of suspended cables—Part III: random excitation and interaction with fluid flow. *Appl. Mech. Rev.* **57**, 515–549 (2004)
364. Srinil, N., Rega, G.: Space–time numerical simulation and validation of analytical predictions for nonlinear forced dynamics of suspended cables. *J. Sound Vib.* **315**, 394–413 (2008)
365. Rega, G., Srinil, N.: Nonlinear hybrid-mode resonant forced oscillations of sagged inclined cables at avoidances. *J. Comput. Nonlinear Dyn.* **2**, 324–336 (2007)
366. Srinil, N., Rega, G.: Two-to-one resonant multi-modal dynamics of horizontal/inclined cables. Part I: theoretical formulation and model validation. *Nonlinear Dyn.* **48**, 231–252 (2007)
367. Srinil, N., Rega, G., Chucheepsakul, S.: Large amplitude three-dimensional free vibrations of inclined sagged elastic cables. *Nonlinear Dyn.* **33**, 129–154 (2003)

368. Rega, G., Srinil, N., Alaggio, R.: Experimental and numerical studies of inclined cables: free and parametrically-forced vibrations. *J. Theor. Appl. Mech.* **46**, 621–640 (2008)
369. Karoumi, R.: Some modeling aspects in the nonlinear finite element analysis of cable supported bridges. *Comput. Struct.* **71**, 16 (1999)
370. Faravelli, L., Ubertini, F.: Nonlinear state observation for cable dynamics. *J. Vib. Control* **15**, 1049–1077 (2009)
371. Georgakis, C.T.Ā., Taylor, C.A.: Nonlinear dynamics of cable stays. Part 1: sinusoidal cable support excitation. *J. Sound Vib.* **281**, 537–564 (2005)
372. Georgakis, C.T.Ā., Taylor, C.A.: Nonlinear dynamics of cable stays. Part 2: stochastic cable support excitation. *J. Sound Vib.* **281**, 565–591 (2005)
373. Gattulli, V., Lepidi, M.: Nonlinear interactions in the planar dynamics of cable-stayed beam. *Int. J. Solids Struct.* **40**, 4729–4748 (2003)
374. Luongo, A., Zulli, D., Piccardo, G.: Analytical and numerical approaches to nonlinear galloping of internally resonant suspended cables. *J. Sound Vib.* **315**, 375–393 (2008)
375. Luongo, A., Piccardo, G.: Non-linear galloping of iced suspended cables with two-to-one internal resonance. In: *International Symposium on Cable Dynamics* (1995)
376. Luongo, A., Paolone, A., Piccardo, G.: Postcritical behavior of cables undergoing two simultaneous galloping modes. *Meccanica* **33**, 229–242 (1998)
377. Luongo, A., Zulli, D., Piccardo, G.: On the effect of twist angle on nonlinear galloping of suspended cables. *Comput. Struct.* **87**, 1003–1014 (2009)
378. Van der Burgh, A.H.P.: Rain-wind-induced vibrations of a simple oscillator. *Int. J. Nonlinear Mech.* **39**, 93–100 (2004)
379. Marsico, M.R., Wagg, D.J., Neild, S.A., Macdonald, J.H.G.: Nonlinear cable vibrations: experimental tests on an inclined cable. In: *Proceedings of the 8th International Conference on Structural Dynamics*, pp. 4–6 (2011)
380. Liu, X., Huo, B., Zhang, S.: Nonlinear dynamic analysis on the rain-wind-induced vibration of cable considering the equilibrium position of rivulet. *Abstr. Appl. Anal.* **52**, 1327–1346 (2013)
381. Abdel-rohman, M., Spencer, B.F.: Control of wind-induced nonlinear oscillations in suspended cables. *Nonlinear Dyn.* **37**, 341–355 (2004)
382. Chang, W.K., Pilipchuk, V., Ibrahim, R.A.: Fluid flow-induced nonlinear vibration of suspended cables. *Nonlinear Dyn.* **14**, 377–406 (1997)
383. Xie, X., Zhang, H., Zhang, Z.: Nonlinear dynamic response of stay cables under axial harmonic excitation. *J. Zhejiang Univ. A* **9**, 1193–1200 (2008)
384. Xie, X., Li, X., Shen, Y.: Static and dynamic characteristics of a long-span cable-stayed bridge with CFRP cables. *Materials (Basel)* **7**, 4854–4877 (2014)
385. Guo, H., Liu, B., Yu, Y.: Galloping suppression of a suspended cable with wind loading by a nonlinear energy sink. *Arch. Appl. Mech.* **87**, 1007–1018 (2017). <https://doi.org/10.1007/s00419-017-1227-z>
386. Lacarbonara, W., Paolone, A., Vestroni, F.: Galloping instabilities of geometrically nonlinear nonshallow cables under steady wind flows. In: *ASME International Design Engineering Technical Conferences and Computers and Information in Engineering Conference*, pp. 1565–1574 (2005)
387. Pasca, M., Vestroni, F., Gattulli, V.: Active longitudinal control of wind-induced oscillations of a suspended cable. *Meccanica* **1**, 255–266 (1998)
388. Feng, R., Wu, Y., Shen, S.: A simplified calculating method of nonlinear frequency of cable net under mean wind load. *Acta Mech. Solida Sin.* **19**, 248–254 (2006)
389. Kang, H.J., Zhu, H.P., Zhao, Y.Y., Yi, Z.P.: In-plane nonlinear dynamics of the stay cables. *Nonlinear Dyn.* **73**, 1385–1398 (2013)
390. Taylor, I.J., Robertson, A.C.: Numerical simulation of the airflow–rivulet interaction associated with the rain-wind induced vibration phenomenon. *J. Wind Eng. Ind. Aerodyn.* **99**, 931–944 (2011)
391. Wu, T., Kareem, A., Li, S.: Excitation mechanism of rain-wind induced vibration of cables: unsteady and nonlinear aspects. In: *Proceedings of the BBAAVII, Shanghai, China*, pp. 654–663 (2012)
392. Li, H., Chen, W., Xu, F., Li, F., Ou, J.: A numerical and experimental hybrid approach for the investigation of aerodynamic forces on stay cables suffering from rain-wind induced vibration. *J. Fluids Struct.* **26**, 1195–1215 (2010)
393. Felice, G., Caracoglia, L.: Generalized power-law stiffness model for nonlinear dynamics of in-plane cable networks. *J. Sound Vib.* **332**, 1961–1981 (2013)
394. Felice, G., Barbiellini, B., Caracoglia, L.: Stochastic unilateral free vibration of an in-plane cable network. *J. Sound Vib.* **340**, 95–111 (2015)
395. Casciati, F., Ubertini, F.: Nonlinear vibration of shallow cables with semiactive tuned mass damper. *Nonlinear Dyn.* **53**, 89–106 (2008)
396. Caracoglia, L., Giaccu, G.F., Barbiellini, B.: Estimating the standard deviation of eigenvalue distributions for the nonlinear free-vibration stochastic dynamics of cable networks. *Meccanica* **52**, 197–211 (2017)
397. Yu, Z., Xu, Y.L.: Non-linear vibration of cable-damper systems part I: formulation. *J. Sound Vib.* **225**, 447–463 (1999)
398. Xu, Y.L., Yu, Z.: Non-linear vibration of cable-damper systems part II: application and verification. *J. Sound Vib.* **225**, 465–481 (1999)
399. Ni, Y.Q., Chen, Y., Ko, J.M., Cao, D.Q.: Neuro-control of cable vibration using semi-active magneto-rheological dampers. *Eng. Struct.* **24**, 295–307 (2002)
400. Cai, C.S., Wu, W.J., Shi, X.M.: Cable vibration reduction with a Hung-on TMD system. Part I: theoretical study. *J. Vib. Control* **12**, 801–814 (2006)
401. Wu, W.J., Cai, C.S.: Cable vibration reduction with a Hung-on TMD system. Part II: parametric study. *J. Vib. Control* **12**, 881–899 (2006). <https://doi.org/10.1177/1077546306065858>
402. Casciati, F., Ubertini, F.: Control of cables nonlinear vibrations under turbulent wind action. In: *5th International Conference on Computational Stochastic Mechanics*, Rhodes, Greece, pp. 169–178 (2006)
403. Chen, J.-C.: Response of large space structures with stiffness control. *J. Spacecr. Rockets* **21**, 463–467 (1984)
404. Fujino, Y., Warnitchai, P., Pacheco, B.M.: Active stiffness control of cable vibration. *J. Appl. Mech.* **60**, 948–953 (1993)
405. Susumpow, T., Fujino, Y.: Active control of multimodal cable vibrations by axial support motion. *J. Eng. Mech.* **121**, 964–972 (1995)

406. Doocy, E.S., Hard, A.R., Ikegami, R., Rawlins, C.B.: Transmission Line Reference Book, Wind Induced Conductor Motion. Electrical Power Research Institute, Palo Alto (1979)
407. Chowdhury, A.G., Sarkar, P.P.: A new technique for identification of eighteen flutter derivatives using a three-degree-of-freedom section model. *Eng. Struct.* **25**, 1763–1772 (2003)

Publisher's Note Springer Nature remains neutral with regard to jurisdictional claims in published maps and institutional affiliations.